Functional Organization of the Ventral Temporal Cortex

Jason M. Webster

A dissertation

Submitted in partial fulfillment of the

Requirements for the degree of

Doctor of Philosophy

University of Washington

2018

Reading Committee:

Ione Fine, Chair

Thomas Grabowski

Andrea Stocco

Program Authorized to Offer Degree:

Psychology

University of Washington

Abstract

Functional Organization of the Ventral Temporal Cortex

Jason M. Webster

Chair of the Supervisory Committee:

Ione Fine

Department of Psychology

Many complex aspects of human visual perception and recognition take place in the ventral temporal cortex; however, the functional organization of this region remains unknown. Much of the brain has been found to consist of discrete cortical areas which are distinguishable by various aspects of cortical organization, including functional properties. In the ventral temporal cortex, only a handful of visual category-selective areas have been found which collectively constitute a minority of the region. This thesis addresses two issues regarding the ventral temporal cortex. The first is an investigation of the development of known category-selective regions through a review of neural plasticity and an empirical study of a subject with a unique developmental history. The second is an approach to functionally parcellating the ventral temporal cortex, which surveys other approaches to parcellating the ventral temporal cortex and then introduces a novel data-driven method for identifying cortical functional organization.

TABLE OF CONTENTS

LIST OF FIGURES

LIST OF TABLES

INTRODUCTION

This dissertation addresses two aspects of the functional organization of the ventral temporal cortex (VTC). The first is the role of plasticity in the development of category-selective functional regions Chapters 2 and 3. The second is the introduction of a data-driven method for investigating the functional organization of the ventral temporal cortex Chapters 4 and 5. The dissertation concludes with an overall summary. The paragraphs below briefly describe the contents of each chapter.

Chapter 1 describes current perspectives on the functional organization of the VTC. After discussing distributed and large-scale organizations, the remainder of the chapter addresses parcellation into distinct areas. Aspects of neural organization are introduced and criteria for a region to be considered a cortical area are proposed. Evidence for category-selective areas are discussed and the chapter closes with considerations for fMRI investigations of functional organization.

Chapter 2 describes the role of neural plasticity in the visual system, with a focus on implications for subject M.M., who is the subject the research reported in Chapter 3. Developmental and adult plasticity, as well as cortical reorganization, are discussed. This chapter closes with a discussion of dynamic localizers, an approach to identifying category-selective regions, which is uniquely suited to studying M.M.'s recovered vision.

Chapter 3 explores the extent of experience-dependent plasticity which occurred in more than a decade after recovered sight for M.M, who was blinded at 3.5 years of age3 and had sight restored at age 46. Tests shortly after sight restoration revealed intact color and motion processing, but striking visual impairments in including 3D form and face processing. These capacities are thought to be primarily mediated by category-selective region in the ventral temporal cortex. Behavioral and fMRI results more than 10 years after sight restoration are reported which suggest that while these regions require experience to develop normally, though maintain only limited plasticity in adulthood.

Chapter 4 reviews cortical parcellation methods based on different aspects of cortical organization, with a focus on applications to the ventral temporal cortex. Methods addressed include gross anatomy, long-range connectivity, myeloarchitecture, cytoarchitecture, receptor-architecture, resting-state functional-connectivity MRI, stimulus-driven response, and topographic parcellations.

Chapter 5 introduces a novel data-driven method for exploring cortical functional organization called Grouping by Response Similarity. When applied to the ventral temporal cortex, this method reveals a parcellation of functionally coherent regions, a subset of which corresponding to the known category-selective regions. Importantly, this method does not require the experimenter to code anything about stimuli or their relationships. Thus, unlike traditional methods, it is amenable to naturalistic stimuli and well suited to exploratory analysis.

Additionally, GRS has no information about spatial information, so any clustering observed is as a consequence of similarities in functional responses. The method is evaluated against two conservative null models. A simulation demonstrates the effectiveness of the method while providing potential insights into the nature of the clusters observed in the fMRI data. The results of an initial investigation of the coding in face-selective regions as well as some of the novel regions are reported.

ToC

Chapter 1 : Current Perspectives on Functional Organization of the Ventral Temporal Cortex

While historically contentious, the notion of cortical localization of function has now gained widespread acceptance, though the nature of the cortical organization for the ventral temporal cortex (VTC) remains unsettled.

The first revolution in the understanding the localization of psychological function was recognizing the brain as the organ of thought and perception. The ancient Egyptian ritual of mummification (~2000 B.C.E) involved the indiscriminate removal of the brain to be left in the torso while other organs, imbued with particular significance, were carefully preserved in ceremonial jars. It would be centuries before the significance of the brain was documented, but two notable physicians of antiquity would eventually provide a surprisingly modern account of the function of the brain. Hippocrates (~460-370 B.C.E.) believed that all human experience and mental function was the province of the brain, and the brain alone. Much later Aelius Galenus (129-~200 C.E.), commonly known as Galen of Pergamon, would also associate higher cognitive functions with the brain. Interestingly, both served as physicians to individuals injured in combat, Hippocrates as a field medic to the Greek army and Galen as physician to the gladiatorial school (Gross, 2013). Given the weaponry of the times, they likely encountered a range of head trauma victims who suffered from distinct cognitive and perceptual deficits. The opportunity to observe a large number of patients with head trauma may explain why these particular individuals would have been among the first to identify the mind with the brain.

The second revolution was associating specific portions of cortex with particular functions. The modern origin of this idea is often attributed to Franz Joseph Gall (1748-1828), who advocated viewing the cortex as a set of 'organs' that performed distinct intellectual, perceptual, or affective functions. Moreover, Gall proposed that individual differences in these structure 'organs' would manifest in differences in behavior (Gross, 2013; Zola-Morgan, 1995). While he was incorrect about the nature of these functions, their influence on skull morphology, and pursued this theory in a manner that we would now recognize as pseudoscientific (i.e., an exclusive focus on seeking confirmatory evidence), the notion that cortical regions could have distinct functional roles whose

idiosyncratic differences between individuals would correlate with behavior had a significant influence on the development of modern neuroscience. That his ideas gained such traction was likely significantly influenced by the emergence of neuropsychology and the classic case studies of Paul Broca (1824-1880) and Karl Wernicke (1848-1905). Later developments would include experiments that demonstrated that electrical stimulation of particular regions of the cortex would evoke distinct behaviors or experiences and the advent of modern neuroimaging techniques.

Currently, there is a consensus that 'low-level' sensory and motor regions of the cortex are divided into discrete cortical areas, while there is less agreement about whether 'high-level' association regions in the temporal, parietal, and frontal cortex contain distinct functional areas which tessellate the cortical surface. The work that follows will address these issues for the ventral visual pathway, which constitutes the majority of the ventral temporal cortex. The next three sections will discuss three proposals for how the ventral temporal cortex might be organized: distributed organization, large-scale organization, and parcellation into distinct functional areas. Afterward, I will put forth a tentative set of criteria for a region* of cortex should satisfy to be considered a cortical area. The remainder of the chapter will examine the evidence for such cortical areas in the ventral temporal cortex.

1.1 Distributed Organizations

Neuropsychologists and neurologists have long debated the extent to which the specific areas of the brain perform distinct functions. Lesions to the cortex often seemed to result in diffuse degradations of performance across a range of tasks rather than circumscribed losses of categories of memory, behavioral capacities, or perceptual abilities (Pribram, 1961). However, this conflicted with results which clearly demonstrated systematic symptoms for particular brain lesions. It was in light of the remarkable specificity of certain lesions that the most influential proposals of distributed localization developed. Systematic research programs searched for the localization of distinct memory traces linking sensory input to motor outputs, but despite coming at times tantalizingly close, for example narrowing the search to a comparatively small region of cortex, the information seemed to be disturbed throughout the region. The summary of this work by Karl Lashley was highly influential

*I am adopting the convention of using 'region' to mean an arbitrary portion of cortex, as it is often used in 'region of interest'.

and set the stage for much of the future research of distributed representations in neurophysiology and computational modelling (D. Bruce, 2001; Grossberg, 1974; Pribram, 1982).

In turn, research on neural modelling has played a prominent role in theories which propose distributed functional organizations. Connectionist architectures, an early form of neural network model loosely inspired by knowledge about the nervous system, suggested that information is stored across a widely distributed pattern of synaptic weights between 'layers' of neurons (Hinton, McClelland, & Rumelhart, 1986). An even earlier line of more biologically-motivated neural models result in a similarly distributed architecture (Grossberg, 1968). More recently, there has been considerable research interest in the potential parallels between large-scale neural network models and particular regions of the brain, although demonstrable correspondences remain elusive (Naselaris et al., 2018). These models have gone under a range of names including deep networks, deep neural nets, convolutional networks, and hierarchical convolutional neural networks (Yamins & DiCarlo, 2016a). This renewal of interest began in 2012 with a demonstration of a deep convolutional neural network, AlexNet, which outperformed all existing algorithms on object categorization tasks, and approached that of human research participants (Krizhevsky, Sutskever, & Hinton, 2012). Subsequently, it was found that the lower layers of these networks displayed 'gabor-like' weights which resembled those found in V1 (Zeiler & Fergus, 2013) and that the activity in the highest layers had Representational Dissimilarity Matrices (Kriegeskorte, Mur, & Bandettini, 2008) similar to those found in the most active voxels of the human ventral temporal cortex (Kriegeskorte, 2015). Combinations of units from the top level could be combined into a synthetic 'neuron' whose response properties closely mirrored those of IT neurons in the macaque (Khaligh-Razavi & Kriegeskorte, 2014). However, to date, these models have failed to demonstrate the kinds of spatial organization of response properties observed in humans and macaques (Yamins & DiCarlo, 2016a). While successively more anterior regions of the visual system correspond to increasingly complex stimulus features, it is unclear what properties are represented throughout much of the ventral temporal cortex. A comparison of the properties of successive stages of an eight layer DNN demonstrated that more anterior regions of the visual system corresponded to higher layers of the network, however, the highest stages seemed to correspond to regions just beyond LO (Guclu & van Gerven, 2015).

A related line of thought about distributed organizations developed in response to the results of vision research using fMRI. In this view, sets of stimuli that share specific features may evoke relatively similar patterns across the cortex but have highly non-local representations. One proposal suggests that the ventral temporal cortex contains distributed representations, with the high-level representation of the object corresponding to the pattern of activity across the entire ventral temporal cortex. While also putting forth models for the organization of the face processing network (Haxby, Hoffman, & Gobbini, 2000), members of the Haxby lab have also been the most prominent advocates for functionally distributed architectures. In particular, they proffer category-specific information outside of the purported category-selective areas (i.e., face-related information outside the face areas)

(Ishai, Ungerleider, Martin, Schouten, & Haxby, 1999) and information about categorical distinctions for non-preferred categories in category-selective regions (e.g. scenes vs bodies in the FFA) (Haxby et al., 2001).

1.2 Large-Scale Organizational Principles

Several proposals have been made for patterns of functional organization that cover all or most of the ventral temporal cortex. The characteristics of the organizing principles for these large-scale functional organizations range from proposals based on neuroanatomy to relatively abstract stimulus response properties.

Modal/Transmodal. One potential organizing principle for such a cortical structure is the large-scale gradient from sensorimotor areas to transmodal areas (Huntenburg, Bazin, & Margulies, 2018). Both within and across modalities, the functional role of an area in the processing hierarchy is associated with cortical distance from primary areas. Across modalities, areas display similarities in their microstructural properties and patterns of connectivity to the extent they are situated similarly along this gradient (Huntenburg et al., 2018).

Neuron Density. A series of systematic analyses of neuron cell densities across the cortex found that neurons are most numerous in primary sensory areas and that there is an overall gradient of decreasing neuron density that proceeds caudal to rostral (C. E. Collins, Airey, Young, Leitch, & Kaas, 2010). This pattern is found across a range of species, so is likely a result of evolutionarily conserved processes in which neurogenesis ends earlier in more anterior regions, resulting in cells that are not only less numerous, but have larger cell bodies and longer processes. The resulting morphological differences may serve to predispose increasingly anterior areas to perform processes akin to dimensionality reduction (Cahalane, Charvet, & Finlay, 2012).

Gene Expression Gradients. Another line of research which is still in its nascent stages is the analysis of gene expression gradients. Each of an organism's cells has the same genetic information, but the differential genetic expression across the various tissue types results in cells becoming either skin, liver, muscle, or neural cells. Gradients of gene expression in the brain contribute to brain structure, connectivity, and neural specialization. One such gradient that may be particularly relevant to the organization of the ventral visual pathway is a gradient in opioid receptors which increases anteriorly throughout the ventral temporal cortex (Biederman & Vessel, 2006).

Eccentricity. The ventral temporal cortex may at least partially be organized by eccentricity, similar to the retinotopic organization of the early visual cortex. While the reversing pattern of polar angle preferences identifies borders within the early visual areas, they share an eccentricity organization where foveal regions are represented posteriorly, in and around the occipital pole, and increasingly eccentric portions of the visual field are represented increasingly anteriorly (Wandell, Dumoulin, & Brewer, 2007). More recently, the observation that mid-level visual areas may also be organized along representations of increasing eccentricity (Wandell,

Dumoulin, & Brewer, 2009) suggested that the clustering of organizational properties may be more common than initially believed. At least one group has proposed the existence of an additional eccentricity gradient that spans the ventral temporal cortex (I. Levy, Hasson, Avidan, Hendler, & Malach, 2001). Specifically, foveal regions are represented laterally while peripheral regions are represented medially along the surface of the ventral temporal cortex. Comparing data from the same subjects, they found that face and letter preferring regions were within foveally biased cortex, while the parahippocampal place area, a scene-selective region, was found in the peripherally biased regions of cortex (Hasson, Levy, Behrmann, Hendler, & Malach, 2002). Importantly, this account may provide cues to the development of functionally specialized regions since the eccentricity information would become available prenatally, potentially providing the correlated neural activity for the initial refinement of long-range axonal pathways in the VTC. Subsequently, differential acuity demands for processing different categories of stimuli (Malach, Levy, & Hasson, 2002), along with stereotyped saccade patterns (Itti & Koch, 2001; Smith, 2013; Tatler, Hayhoe, Land, & Ballard, 2011), could predispose regions with a particular eccentricity bias to selectively undergo the learning, which would, in turn, drive the patterning of local connectivity.

Shape, Spatial Frequency, or Curvature. Shape, spatial frequency, and curvature are image-level properties which are highly correlated in natural images. While evidence for each of these properties has been put forth, a more definitive account awaits a series of systematic analyses. Averaged responses of electrophysiologically recorded neurons in the inferotemporal cortices of macaques demonstrated a primary functional division by low-level properties, followed by a somewhat finer scale separation by shape (Baldassi et al., 2013). However, other studies examining activity averaged over populations of neurons found that the primary functional distinctions were categorical (Kiani, Esteky, Mirpour, & Tanaka, 2007). Analyses of fMRI responses have led to similarly conflicting accounts. While some groups find that stimulus similarity alone is sufficient to account for the pattern of VTC responses (O'Toole, Jiang, Abdi, & Haxby, 2005), others report a posterior to anterior gradient of increasing category-selectivity independent of stimulus similarity (Bracci & Op de Beeck, 2016). These studies primarily focused on functional clustering, but there is also evidence for some spatial segregation of shape selectivity across the VTC. Specifically, the medial regions of cortex (including the parahippocampal place area) seem particularly sensitive to high spatial frequency content (Rajimehr, Devaney, Bilenko, Young, & Tootell, 2011). However, there seemed to be no VTC regions preferring low spatial frequency content. One particularly interesting line of research examined the emergence of 'category-selectivity' for novel stimulus sets in juvenile macaques. These regions developed in consistent cortical locations across individuals regardless of the order in which they were trained. While there was no evidence of spatial frequency (or eccentricity) as an organizing principle, however, there was an inverse association between increasing curvature and eccentricity, with increasingly face like stimuli being found closer to areas that preferred foveal, curvy stimuli (Srihasam, Vincent, & Livingstone, 2014).

Animate/Inanimate. A study analyzing the fMRI response to animate and inanimate objects found a preference for inanimate along the medial ventral temporal cortex, a preference for animate on and around the fusiform gyrus, and another region preferring inanimate lateral to the fusiform gyrus (Sha et al., 2015). A more data-driven approach also found segregation of preferences for animate and inanimate visual stimuli. However, their results were more suggestive of a complex topography than the single large-scale medial-lateral gradient, and the amount of cortex that preferentially responded to inanimate stimuli was comparatively quite small (Naselaris, Stansbury, & Gallant, 2012). Some evidence suggests that the animate/inanimate distinction is not based on low-level properties, but rather the ethological role they play in virtue of their connectivity to other brain areas; early blind subjects show similar patterns of preference for animate and inanimate in response to object names (Mahon, Anzellotti, Schwarzbach, Zampini, & Caramazza, 2009). There have also been suggestions that this distinction would be better characterized as a continuum (Sha et al., 2015). A recent line of research extended the observations about the animate/inanimate division along with the observation that there are large regions that alternatingly prefer objects of small and large real-world size (Konkle & Oliva, 2012). Specifically, this account proposes that the ventral temporal cortex is one of two pathways which have a mirroring tripartite division consisting of big objects, all animals, and small objects (Konkle & Caramazza, 2013).

The presence of large-scale gradients is not mutually exclusive with the possibility that the cortex is further subdivided into discrete functional areas. These large-scale gradients may play a role in arealization. Indeed, these gradients may partially explain how particular regions of cortex come to be specialized for particular functions, as well as provide an explanatory framework for the relationship between the functional roles of particular areas and their spatial arrangement across the cortical surface (Huntenburg et al., 2018). This is particularly relevant for experience-dependent functional areas such as the WVFA (Baker et al., 2007) and regions that specialize for the processing of arbitrary symbol sets.

1.3 Distinct Areas

The neuroscientific literature is replete with terms for specialized regions of cortex: zones, fields, globs, blobs, clusters, modules, regions, and areas. In part, this heterogeneity of terminology reflects the siloing of researchers from different subfields (e.g., anatomy vs. physiology) and even from different methodological backgrounds (e.g., immunohistochemistry vs. myeloarchitectonics). Before attempting to propose a set of criteria that a region of cortex must satisfy to be designated a cortical area, the remainder of this section will describe aspects of cortical organization based on cytoarchitecture, myeloarchitecture, structural connectivity, functional connectivity, response properties, topography, and gross anatomy. Chapter 4 (see below) will address the application of each of these approaches to parcellating the cortex in more detail.

1.3.1 Cytoarchitecture

Cytoarchitecture is the analysis of the laminar density and size distributions of neurons as seen through histological preparation, that is, by thinly slicing the cortex and staining cell bodies. By far the most well-known cytoarchitectural atlases was published by Korbinian Brodmann in 1909, although there have been several attempts to develop cytoarchitectonic parcellations of the cortex.

Modern cytoarchitectural analysis has developed substantially more advanced techniques. A recent development is the ability to do unbiased, automated analysis with observer-independent quantitative cytoarchitectural mapping (Schleicher, Morosan, Amunts, & Zilles, 2009).

1.3.2 Myeloarchitecture

Similar to cytoarchitecture, myeloarchitecture can be observed through the serial section and staining of slices, but the particular stains label myelin, thus enabling the visualization of a subset of axonal pathways. Regions of cortex have been noted to differ in the pattern of myeloarchitecture since around 1920, and many groups have characterized the myeloarchitectonic properties of different cortical regions. Perhaps the best known such feature is the stria of Gennari, which corresponds to the arrival of projections from the Lateral Geniculate Nucleus to layer IV of the primary visual cortex (area V1).

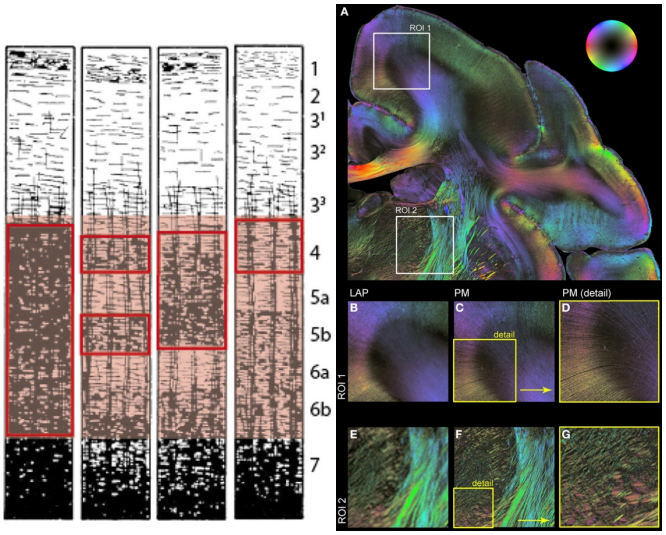

Figure 1.1. Differences in myelin staining

Panel 1: Four regions of cortex along with the laminar depth labels. Layer 7 corresponds to the white matter. Red boxes highlight distinctive patterns in each slice. Adapted from (Dinse et al., 2015). **Panel 2**: Polarized Light imaging of vervet monkey cortex. Adapted from (Reckfort et al., 2015).

While the lack of available quantitative methods and the rising popularity of cytoarchitectonic analysis contributed to relatively slow growth in the study of myeloarchitecture, recent developments in polarized light imaging may bring about a resurgence of interest. The subfigures (B,E) and (C,D,F,G) in the right panel of Figure 1.1 illustrates two developing methods that allow for detailed analysis of interregional connectivity (Reckfort et al., 2015) as well as regional differences in myeloarchitecture. Currently, there are no methods for generating cyto- or myeloarchitecture maps in living individuals, however, several groups are working on techniques for estimating myelin concentration group averaged data from living subjects (Dinse et al., 2015; Glasser & Van Essen, 2011).

1.3.3 Receptor Architecture

Cortical neurons typically contain distinct receptors for different types of neurotransmitters, with the highest concentration of binding sites occurring in the dendrites. Different types of neurons tend to express distinct subsets of receptor types, though the particular concentration may differ between regions of cortex. Additionally, cortical regions differ in the laminar composition by particular neuron types. As a result, the distribution of receptors provides a structural property that is closely linked to cortical function. There are currently two methods for determining receptor architecture. The first is through transcriptomics, the analysis of gene expression through RNA analysis in tissue microarrays (Hawrylycz et al., 2012). To the extent the diagnostic RNA sequences are known, this method can provide a synoptic readout of the receptor distributions for each tissue sample. The second method is receptor autoradiography, which entails binding a radiolabeled receptor ligand to a tissue slice (Geary & Wooten, 1989). This method can provide a high-resolution image of receptor distribution over an entire tissue slice, but each receptor must be separately labelled, and a combination of the difficulty of repeatedly labelling and cleaning a slice and the limited number available ligands (Zilles & Palomero-Gallagher, 2017) results in a sparser picture of the receptors present.

1.3.3 Structural Connectivity

The analysis of long-range structural connections began with the visual inspection of white matter bundles during dissections but was revolutionized with the advent of recombinant adeno-associated retrovirus tracers (rAAV), which label efferent regions (anterograde tracers), and pseudorabies virus tracers (PRV), which label afferent regions (retrograde tracers). These methods have been used in detailed studies of connectivity in several non-human animals and revealed much of what is known about corticocortical and cortico-subcortical connectivity. These techniques are still in use and are being most notably used by the Allen Institute to create a relatively thorough and systematic connectivity atlas for the mouse. Axonal tracing requires labeling in a living animal and ex-vivo serial sectioning of the brain, so data at this resolution for human connectivity is not available. However, there are MR methodologies being developed for in-vivo analysis of connectivity patterns, including several variants of Diffusion Tensor Imaging (DTI) and Diffusion Spectrum Imaging (DSI). The ongoing NIH Human Connectome Project, which seeks to provide connectivity data for a large number of healthy adults to the scientific community, has spurred a wave of innovation in these techniques, including prompting MR scanner manufactures to create optimized versions of their scanning platforms and software to generate high-quality diffusion data.

1.3.4 Functional Connectivity

The analysis of fMRI data from subjects who are receiving no experimental stimuli and performing no explicit task has been used by many groups to study patterns of brain activity. These studies have been called resting state fMRI (rs-fMRI) and functional connectivity fMRI (fc-MRI). The common feature of these methods is the

evaluation of the correlational structure of the fMRI time courses. Numerous methodological studies in this line of research have highlighted the importance of removing components of the fMRI signal that relate to motion or physiological processes such as respiration and heartbeat, however, there remain concerns that systemic blood flow purely due to characteristics of the circulatory system may be a driving factor in some aspects of the resting state signal (Tong, Hocke, Fan, Janes, & Frederick, 2015; Tong et al., 2013).

1.3.5 Neural Response Properties

Electrophysiological recording of single cells within nearby regions of the cortex often share a number of response characteristics (only a subset of these properties is available through noninvasive methods such as fMRI). However, when making systematic recordings along the extent of the cortex, abrupt transitions in the response characteristics were sometimes noticed. An example of an abrupt transition which is indicative of an area boundary is change in response properties from cells measured in V1, compared with nearby cells in V2. The former would have smaller receptive fields and respond to simpler features. However, abrupt transitions are not always indicative of areal boundaries. For example, if making systematic recordings just across the V2 border and running parallel to it, cells would be alternately sampled from the thick, thin, and pale stripe regions, and thus vary in properties such as their response to achromatic or moving gratings, yet all the cells would be within a single area. As a result, this criterion for establishing regional boundaries is often only taken into account when a sufficiently large region has been systematically sampled to provide information about the diversity of cell responses within an area.

1.3.6 Topographic Organization

One potential way to overcome the problem of locally heterogeneous differences in response characteristics within an area is to regard variation within a topographic map as characteristic of an area. For example, V1 has cells nearby that differ in properties such as ocular dominance, orientation preference, and chromatic preference, however, at a larger scale, all of these variations occur repeatedly at each location throughout the larger retinotopic map. Complete topographic maps have been identified in a number of visual, auditory, somatosensory, and motor regions of cortex. Similar maps have been identified in subcortical structures. Such maps are perhaps the strongest candidates indicating that a portion of cortex performs a distinct functional role.

1.3.7 Cortical Folding: a potential link between different methods

While cortical folding patterns have not directly been used to argue for functional boundaries in the cortex, a number of cortical parcellation schemes have been proposed based on sulcal and gyral patterns. Since the discovery of motor cortex, one of the first discoveries of a functional map (Gross, 2013), it has been noted that portions of cortex with certain response properties were reliably located relative to certain sulci or gyri, when the motor region was described as being anterior to the central sulcus. More recently, it has been established

that cortical folding patterns were highly predictive of the location of certain cytoarchitectural areas (Fischl et al., 2008), that the extent of V1 can be predicted from the cortical folding pattern as reliably as hand labeling fMRI retinotopic maps from living subjects. The validity of the result was also supported through comparison to the myeloarchitectonic signature of the stria of Gennari with extensive high-resolution imaging in ex-vivo subjects (Hinds et al., 2009). Additionally, it has been shown that the border between auditory regions A1 and R is reliably tied to the anatomy of individuals with a spectrum of single to duplicated Herschel's gyri (Da Costa et al., 2011). Most recently, it was argued that the mid-fusiform sulcus, a hominid-specific structure (Weiner & Zilles, 2015) that also has a number of anatomical variants, is reliably located with respect to divisions between areas that differ in cytoarchitecture and functional properties (Weiner et al., 2014). The same group later argued that this sulcus is also aligned with the division between several other previously described functional properties, receptor architectonic regions, and MRI estimates of myeloarchitecture (Grill-Spector & Weiner, 2014). The close correspondence that they reported for cortical folding and cytoarchitecture is only one of a series of such discoveries and may be common throughout the brain (Weiner & Zilles, 2015). As understanding of the developmental coevolution of gyrification and arealization increases, it is likely that the number of properties that will be reliably estimated by examining cortical folding will increase, which is highly desirable since the pattern of cortical folding can be quickly and reliably estimated with around a four-minute T1 scan using MRI.

1.4 Proposed criteria for cortical areas

While many of the approaches described in the preceding section has sought to describe areas as regions bounded by abrupt transitions in the measured properties, the proposal I find most compelling requires multiple criteria to be met. This approach was widely popularized by one of the most influential studies on cortical organization, which synthesized several large bodies of evidence regarding the macaque visual system (Felleman & Van Essen, 1991). To be considered an area, this study proposed a number of criteria spanning many different methodologies that needed to be met.

The consilience of multiple methods provides the most reasonable standard for what criteria a region of cortex should possess to be considered an area. In particular, Van Essen (2004) suggests that four criteria: the agreement of borders defined by

- Cytoarchitecture and/or myeloarchitecture
- Structural connectivity
- Response properties
- Topographic organization

While any region meeting all the criteria would clearly constitute an area, in practice areas have often been designated when a region was found to meet some subset of the criteria. By combining different methodologies

for segmenting the cortex, this approach not only provides a significant impetus for affording a region of cortex status as a distinct theoretical entity, while also motivating interdisciplinary collaboration and tracking explicit information about individual differences. Interestingly, this approach also allows for the description of areas which are species-specific, which is consequential since there has been extensive cortical expansion in the human cortex relative to other primates (Orban, Van Essen, & Vanduffel, 2004). However, evolutionarily, once an area emerges, it tends to be found in phylogenetically related species (Krubitzer, 2009).

As an aside, this list of criteria seems to be a variant of an earlier proposal by Zeki, although Zeki included the further requirement that the region have distinct callosal connections (S. M. Zeki, 1978). While this additional criterion is intriguing, the presence of areas with seemingly full-field representations in the ventral temporal cortex may mitigate the motivation for this assumption.

The identification of borders defined by receptor architecture is a seemingly crucial omission. An area with neural circuits having identical structure and connectivity would process information differently to the extent that they differed in receptor architecture. Differences in receptor architecture would alter the response characteristics of the cells and, thus, also likely the topographic properties throughout such an area. In this way, a region meeting the Van Essen criteria could be inferred to also differ in receptor architecture. However, the receptor architecture is a more essential characteristic: given a particular cytoarchitecture and connectivity, two areas *could not* differ in their functional properties without differing in their receptor architecture, but two areas *could* differ in their receptor architecture and yet have the same functional properties.

Three obstacles to applying these criteria are the relatively large number of variants of each method, the substantial individual differences in VTC anatomy, and experience-dependent variation (Behrmann & Plaut, 2015). As a result, it is difficult to determine whether these constraints are simultaneously met. Ideally, multiple methodologies would be applied within the same individual to determine if the boundaries suggested by each method are actually coextensive. This goal has not been achieved due to the current lack of available non-invasive methods for examining cytoarchitecture, myeloarchitecture, and receptor architecture, and the lack of systematic methods for assessing the functional roles and topographic organization of high-level visual areas.

Fortunately, a shift is already in progress, toward objective, automated analyses that can be co-registered (along with information about the spatial distribution of uncertainty) onto models of the cortical surface (Van Essen, 2005). Additionally, metrics have been developed to compare the spatial agreement of brain parcellations on the surface (Bohland, Bokil, Allen, & Mitra, 2009). Advances in methodology are approaching the ability to perform *in vivo* individual subject analysis for anatomical properties. Chapter 5 will describe a method I have been developing which uses a data-driven approach to identify functionally coherent regions in the VTC, which is a substantial step towards the functional characterization of these regions.

1.5 How much of cortex is arealized?

By the criteria listed above, a substantial amount of the cortex has been demonstrated to contain cortical areas including multiple early visual, auditory, somatosensory, and motor areas. For some regions near these areas, a subset of the criteria has been met or there exists disagreement about whether they have been met. These areas include human V4 and the parabelt auditory regions. For the most part, these regions have not failed to meet the other criteria; rather, they have not been evaluated.

For substantial regions of the temporal, parietal, and frontal cortices, it is not clear whether or not parcellation into areas will be possible. Constructing parcellations based on certain criteria seems relatively straightforward (e.g., cytoarchitecture, connectivity). It is currently unclear how parcellation based on response properties, particularly topographically organized properties, can be performed for these regions. No current experimental manipulations or analysis methods gave been shown to be diagnostic of such patterns, consequently, the absence of evidence should not be considered as evidence of absence.

The method described in Chapter 5 below is intended to partially address this challenge by identifying regions with coherent response properties without requiring knowledge of the functional properties of the target regions. Preliminary results from simulations suggest that not only does the method identify coherent functional regions, but the internal topology of these regions is also recovered (at least in the cases we have tested). Future extensions of this method may allow us to identify topographic organization by mapping these functional gradients onto the cortical surface.

In principle, it seems possible that some regions of association cortex do not contain areas that would meet all of the above constraints. There is evidence to suggest that parts of the entorhinal cortex may be receiving patterns of input that may not be consistent with a topographical organization (Jbabdi, Sotiropoulos, & Behrens, 2013). It has also been suggested that piriform cortex is not only not topographically organized, but is characterized by an 'anti-map' (Chuck Stevens, presentation at ISB 2013). However, considering the developmental principles that govern brain development and plasticity such as gene expression gradients, dendritic field arborization & pruning, and Hebbian synaptic modification, it seems entirely possible that arealization is the natural consequence of the dynamics of cortical organization.

1.6 Evidence for functional areas in the VTC

1.6.1 Face Areas

An influential early model for face perception described several different types of information available from faces and proposed that these could be separated into distinct processing streams for the changeable aspects of faces, including emotion recognition, and structural aspects of faces, including identification (V. Bruce & Young, 1986). These distinctions were later supported by research in both humans and macaque monkeys (Haxby et al., 2000).

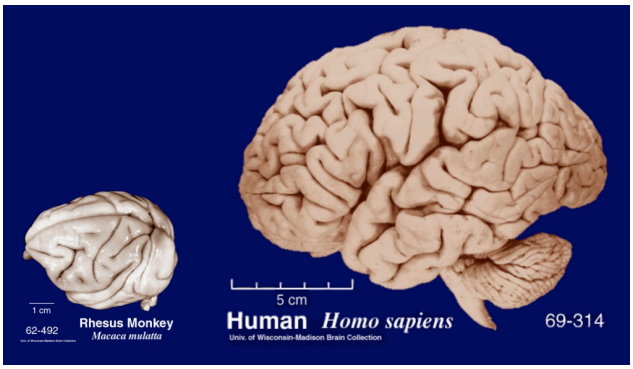

Figure 1.2. The relative size of human and macaque brains

Adapted from the Comparative Mammalian Brain Collections (http://www.brainmuseum.org)

Faces are informationally dense visual stimuli that convey socially relevant information including species, age, sex, state of health, emotion, intent, and identity. Primates, with few exceptions, are highly social creatures (Kappeler & van Schaik, 2002). Psychophysical studies have demonstrated that humans display characteristic patterns of behavioral responses across a range of experimental paradigms that are unique to faces. Macaques are another highly social primate genus that genetically diverged from the human lineage about 25 million years ago (Gibbs et al., 2007). Rhesus macaques (*Macaca Mulatta*), which have become the most commonly used model species for the human visual system, were the first species where the face-selective cells that might underlie these face-specific psychophysical patterns were identified (Desimone, Albright, Gross, & Bruce, 1984). See Figure 1.2 for a comparison of the brain size of the two species. The earliest reports of face-selective cells suggested a surprising amount of spatial clustering and even presented evidence for populations of cells with different spatial frequency selectivity (Rolls, 1984). Subsequent studies from various labs replicated the findings and also identified other regions of the occipital and temporal lobes containing face-selective neurons. Research into the details of the location, connectivity, development, and functional roles of these regions is ongoing. The remainder of this section will review this work, particularly as it relates to the human face-selective regions known as the Fusiform Face Area (FFA)/mFus-faces (Kanwisher, McDermott, & Chun, 1997) and the anterior face patch (AFP) (Rajimehr, Young, & Tootell, 2009), and their likely homologues AL and AM in the macaque (Tsao, Moeller, & Freiwald, 2008).

1.6.1.1 Location

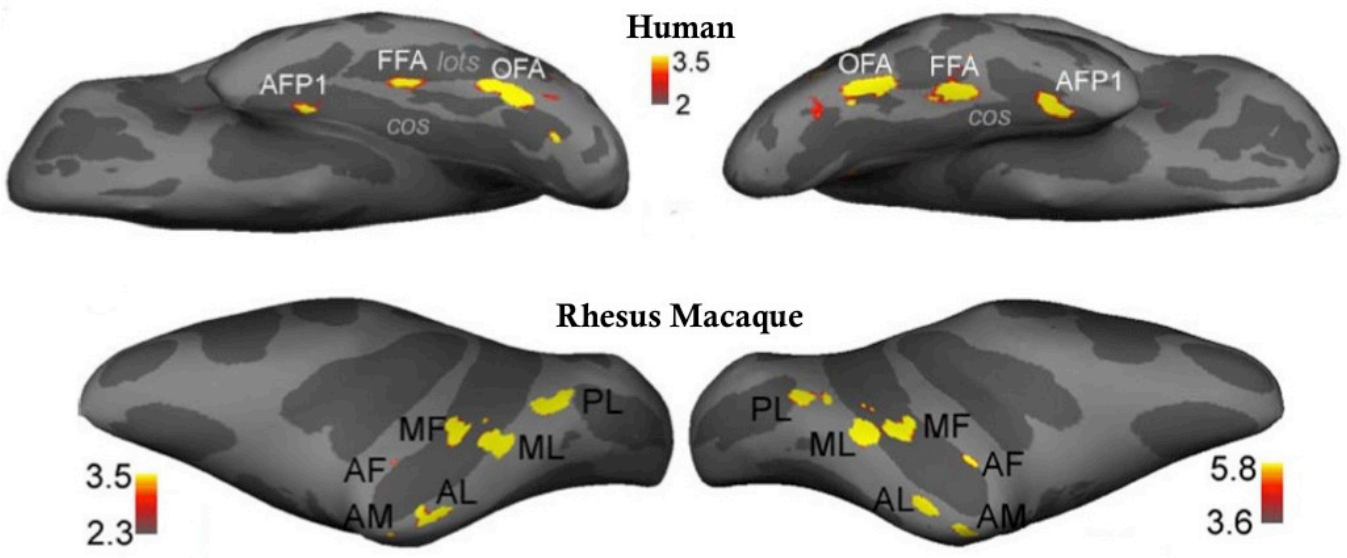

Figure 1.3. Face-selective regions in the human and macaque

Inflated hemispheres of the human and macaque scaled to equate the size of face-selective regions identified by the statistical contrast of faces-objects, legends indicate the value of $-log_{10}(p)$. Macaque brains are in the lateral view. Human brains are in the inferior view. Note that human STS face-selective regions are not visible. Face-selective regions in the frontal cortex of both species are not shown. AFP1: anterior face patch one, FFA: fusiform face area, OFA: occipital face area, cos: collateral sulcus, lots: lateral occipito-temporal sulcus, AM: anterior medial, AL: anterior lateral, AF: anterior fundus, MF: medial fundus, ML: medial lateral, PL: posterior lateral.

With the introduction of neuroimaging, the finding of face-selective cells in the macaque was paralleled by the discovery of face-selective regions in the human. While some systematic reviews of the correspondence between macaque and human high-level visual areas make no mention of face selectivity (Orban et al., 2004), others have revealed that both species have a network of several face-selective regions that can be reliably identified with functional magnetic resonance imaging (fMRI) by contrasting the blood-oxygen-level-dependent (BOLD) signal response of faces to objects (Tsao et al., 2008). Figure 1.3 shows fMRI face contrasts from representative individuals of both species. Given the anatomical information provided in the Rolls study that first identified face-selective cells, the neurons most likely corresponded to the face patch AL.

Understanding the relationship between the face networks of humans and macaques relies upon having established homologies. The mapping between the human and macaque temporal cortices is additionally complicated by the immense cortical expansion that has taken place in the human genetic line (Rilling, 2014; D. C. Van Essen & Dierker, 2007), as illustrated in Figure 1.4. However, based on the layout of the face networks, it is likely that the FFA corresponds to the face patch AL and the human AFP to macaque AM. The FFA is located on the posterior portion of the fusiform gyrus, just lateral to the mid-fusiform sulcus (Weiner et al., 2014), and the anterior face patch is located in the anterior terminus of the collateral sulcus (Nasr & Tootell, 2012; Rajimehr et al., 2009).

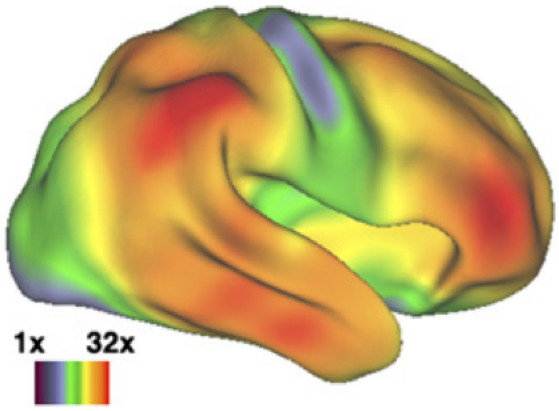

Figure 1.4. Relative expansion from macaque to human
Adapted from (D. C. Van Essen & Dierker, 2007)

In macaques, the AL is located on the lower lip of the STS and extending into the medial temporal gyrus in TEad. The location of AM is anterior and lateral to the end of the anterior middle temporal sulcus (AMTS) in perirhinal cortex (PRh) (anatomical and functional evidence for the homology of these pairs of areas are reviewed in J. A. Collins & Olson, 2014). There is general census that visual processing proceeds through a hierarchy of richly interconnected regions from lower-level representations in V1 in the occipital lobe through higher-level regions in the anterior temporal lobes (DiCarlo, Zoccolan, & Rust, 2012; Felleman & Van Essen, 1991; Rust & Dicarlo, 2010). Results from human and macaque studies suggest that the faces areas fit into this framework (Duchaine & Yovel, 2015; Moeller, Freiwald, & Tsao, 2008).

1.6.1.2 Connectivity

At least one group has studied the face processing system using resting-state functional connectivity MRI (rs-fcMRI). After localizing the face areas, rs-fcMRI partial correlations were estimated for the functional connectivity between each region (O'Neil et al., 2014). The results are shown in Figure 1.5. Interestingly, the 'unique' correlation between the AFP and the FFA was correlated with behavior on a separate face memory task, although it is not clear whether this was a planned comparison. Overall, the results of this study are questionable due to particular methodological choices made by the experimenters. First, the 'uniqueness' of the connectivity to the AFP cannot be concluded since they only evaluated the connections from a predetermined set of regions of interest (ROIs). Second, the functional contrast used to

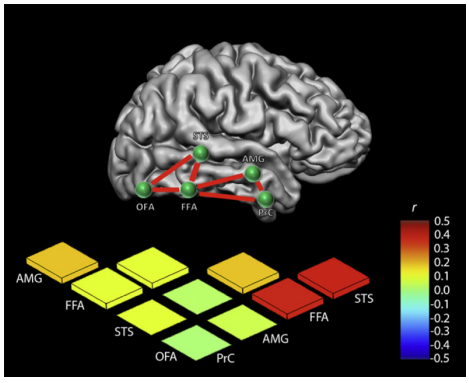

Figure 1.5 rs-fcMRI of the human face network
Adapted from (O'Neil, Hutchison, McLean, & Kohler, 2014)

define the regions was faces – places (as opposed to faces – objects), which is likely to have included regions that were not highly face-selective. Lastly, and most importantly, the experimenters smoothed the data (apparently in the volume) and normalized the data to an anatomical template. Both of these steps are likely to have contaminated the data with signal that did not belong to the ROIs, including sources not even within the grey matter.

Another line of research examined the relationship between structural connectivity and face-selective responses in human subjects. White matter pathways discernable through DTI was shown to be associated with activity in face-selective regions, and a classifier trained on group data was able to predict the location of face-selective activity in the location of the FFA in individual subjects based solely on DTI from that subject (Saygin et al., 2012). The anterior face patch was not consistently predicted in this line of research (Osher et al., 2015; Saygin et al., 2012), most likely because the particular stimuli, task, and scanning sequences did not consistently elicit activity in the AFP (Axelrod & Yovel, 2013). However, the results do provide impressive evidence of the link between structural connectivity patterns and cortical function for at least some 'category-selective' regions.

The most compelling case for distinctive connectivity within the face network comes from research that combined simultaneous electrical microstimulation with fMRI (Freiwald, Tsao, & Livingstone, 2009). Figure 1.6 illustrates the pattern of findings. Microstimulation of each face patch selectively drove responses in a distinct subset of the other face patches (elicited activity was also seen within the amygdala, claustrum, and pulvinar). The patterns of elicited activity were highly reproducible across sessions occurring on different days. Importantly, stimulation outside, but nearby the face patches drove activity in other regions, but selectively spared the face patches. Interestingly, the face patches appear not to be differentiated from neighboring regions in terms of cytoarchitecture, yet the patches form a functionally interconnected network with strong connections between face patches and little connectivity to other regions of IT (Grimaldi, Saleem, & Tsao, 2016; Moeller et al., 2008).

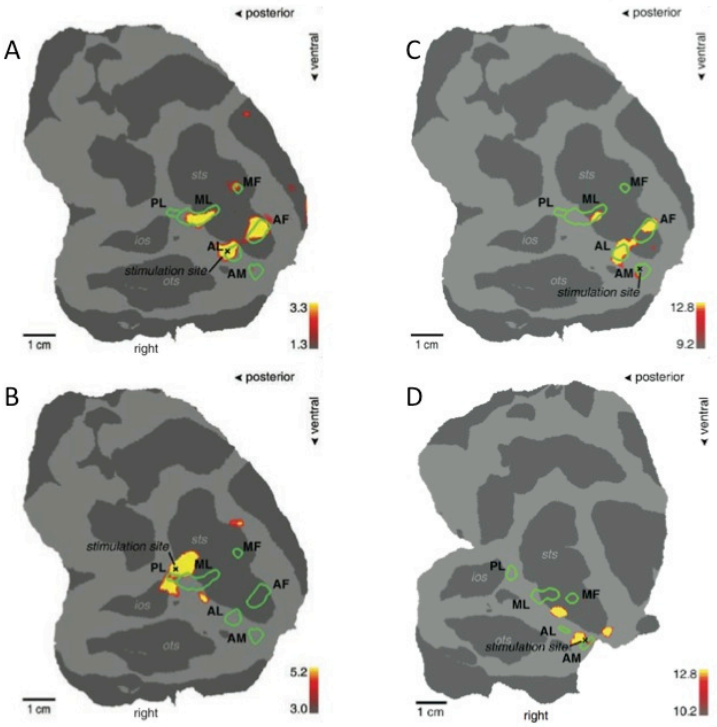

Figure 1.6 Activity elicited by microstimulation

(A) stimulation in the AL selectively elicited activity in ML MF, AF, and to a lesser extent AM. (B) stimulation outside the ML results in patches of activity that exclude face patches. (C) Stimulation in AM elicited activity in ML, MF, AL, and AF. (D) Stimulation immediately adjacent to AM elicited activity in patches that exclude face patches face patches. Adapted from (Moeller et al., 2008)

1.6.1.3 Development

The inferior temporal cortex of the macaque has been shown to have a stable topography of selectivity for novel object shapes, and this topography persists after months of extensive training with the shapes (Op de Beeck, Deutsch, Vanduffel, Kanwisher, & DiCarlo, 2008). Training experiments on juvenile macaques who learned several symbol sets in different orders demonstrated that regions of cortex to each of trained symbol sets emerged. Moreover, these regions had the same spatial distribution across individuals (Srihasam et al., 2014) regardless of training order. Tests regarding stimulus sets attributes revealed that the spatial distribution of these regions was associated with stimulus curvature (and to a lesser extent, eccentricity) rather than category, spatial frequency, or expertise. In humans, the selectivity of the visual word form area (VWFA) for familiar graphemes (Baker et al., 2007) demonstrates that some degree of functional specialization also occurs within the human ventral temporal cortex.

Behaviorally, there seems to be evidence for both an intrinsic system for face processing as well as the significant functional refinement of this system through experience (Sugita, 2008). Infant Japanese macaques (Macaca Fuscata) reared with no exposure to faces showed preferential looking to both human and macaque faces, and to novel faces over repeatedly presented faces. After the initial experiments, the macaques were either exposed to human or macaque faces for three months. Subsequently, their behavior shifted such that they no longer showed discriminative capacity for the still unexposed (other than the initial experimental session) species faces. These behavioral patterns suggest a genetic predisposition to foveate face-like stimuli, which likely then refines selectivity within face patches through Hebbian mechanisms.

1.6.1.4 Functional Roles

In a fMRI study in macaques (Liu et al., 2013), the posterior face patches showed face selectivity, as well as similar spatial patterns of responses for exemplars of particular categories (such as faces or objects), but differing patterns for stimuli which came from different categories. Anterior face areas also showed face selectivity, but did not show similar responses to stimuli within non-preferred categories. Additionally, replicable within-category-selectivity for faces (e.g., one face reliably elicits a higher response than another in independent data) was only observed in the anterior face patch.

Interestingly, Section 5.4.1 below describes similar results from an fMRI analysis on human subjects that I conducted around the same time as the previously mentioned study. Specifically, the results show that the response patterns within the FFA are similar for stimuli within several categories of stimuli, despite only having a high univariate response to faces. More anterior face areas, including the AFP, still have selective responses to faces, but no longer display similar patterns of activity across the cortical surface for examples within other categories.

Another fMRI study in humans evaluated recognition-related activity to normal, upside-down, and contrast-reversed faces in three faces areas: the occipital face area (OFA), FFA, and AFP (Nasr & Tootell, 2012). In a control condition, subjects viewed the same stimuli while performing an unrelated dot detection task. While the two posterior regions responded more strongly to faces than non-face stimuli regardless of task, the AFP showed little response when subjects were directing attention to an orthogonal task and only had increased activity for faces when subjects performed a face recall task. The magnitude of task modulation in the AFP was also found to be related to the subject's behavioral performance, which suggests that subject's recall accuracy may be in part mediated by the activity of the anterior face patch.

Results from an early optical intrinsic signal imaging (OISI) suggests that one of the more anterior lateral face patches contains topographically arranged neurons selectively tuned to face orientation (G. Wang, Tanaka, & Tanifuji, 1996). In a later electrophysiological study on macaques who trained to associate abstract patterns

with particular individuals (shown in a range of views), neurons in AM were shown to respond selectively to particular individuals in a view-invariant manner, suggesting a high-level role in face perception, however, a partially overlapping set of neurons also responded to the associated abstract pattern for that individual, suggesting a role in semantic association with face identities (Eifuku, Nakata, Sugimori, Ono, & Tamura, 2010).

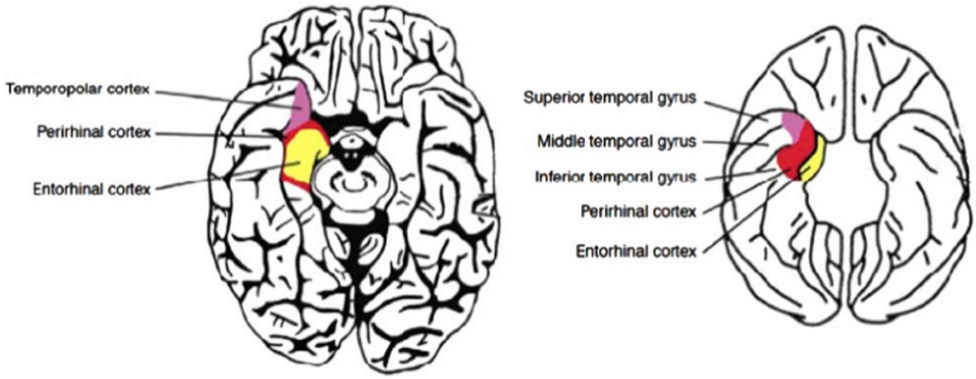

Figure 1.7 Anatomy of the medial portion of the anterior temporal lobe in humans and macaques

The AFP is found in the collateral sulcus in perirhinal cortex. Descriptions of AM also suggest that it is in (or directly adjacent to) perirhinal cortex. Adapted from (J. A. Collins & Olson, 2014).

These results suggest the human AFP and macaque AM possess a functional role at the intersection of high-level vision and semantic association. This role is consistent with their anatomical location at the anterior extent of the ventral visual pathway and situated within the perirhinal cortex (see Figure 1.7), as well as previous theoretical descriptions of the role of the inferior temporal lobe in recognition (DiCarlo & Cox, 2007; DiCarlo et al., 2012).

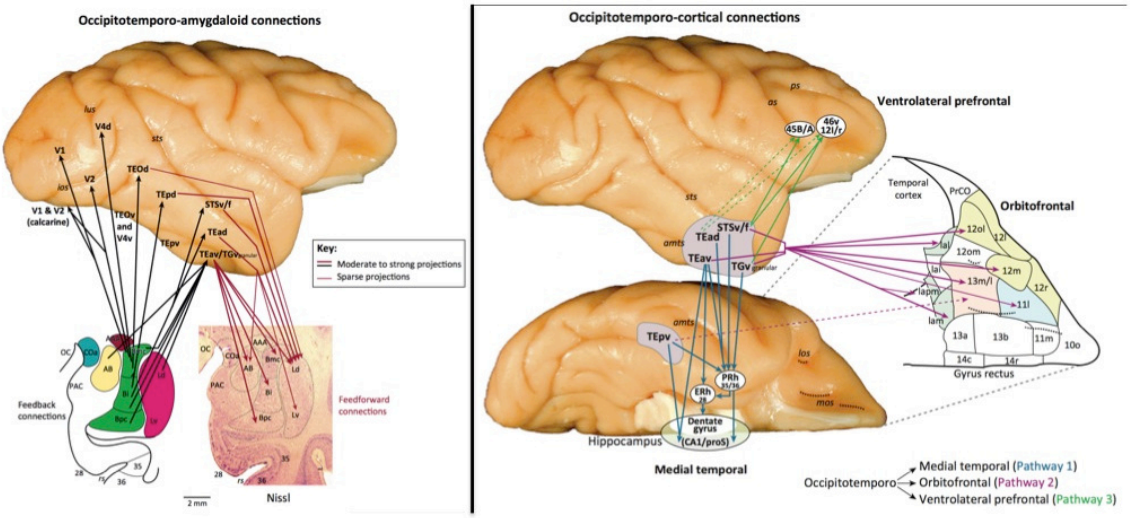

Figure 1.8. Two primary output pathways from the ventral visual cortex

Adapted from(Kravitz, Saleem, Baker, Ungerleider, & Mishkin, 2013)

A recent detailed review of the macaque ventral visual pathway (Kravitz et al., 2013) describes the connectivity of the regions involved in face processing (Figure 1.9). The level of detail is primarily schematic, with regions ranging from established cortical areas to gross anatomical regions. It also includes a partial cytoarchitectonic parcellation scheme (which includes TEad PRh, as mentioned above). The level of detail never approaches precision of the microstimulation research of Friewald and colleges, which seems to more closely correspond to the activity 'spots' observed with optical intrinsic signal imaging (OISI) (Tanifuji, Sato, Uchida, Yamane, & Tsunoda, 2010). However, two particularly interesting patterns of connectivity in this review are worth highlighting. First, there are connections between PRh and the amygdala, lateral frontal cortex, and orbitofrontal cortex. All three of these structures contain face-selective regions which have previously been noted in both the human and macaque literature. Second PRh is connected to the hippocampus, which is a crucial structure for recognition and memory formation (see Figure 1.8).

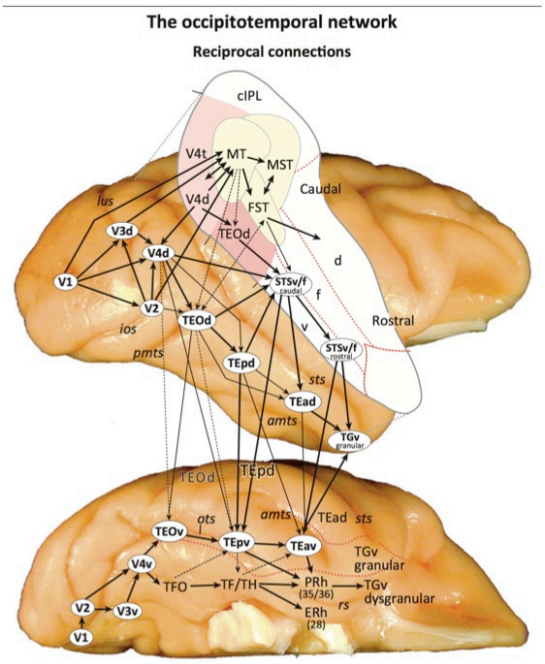

Figure 1.9. Ventral pathway connections
Adapted from (Kravitz et al., 2013)

1.6.2 Other category-selective regions

In addition to the face-selective regions, several other functional regions within the VTC have been identified. As the following chapters primarily focuses on face areas, the evidence regarding the status of these areas will be more succinctly summarized here for expository purposes.

1.6.2.1 Motion

The first discovered and most well studied functionally-defined area of the primate visual system is area MT (also sometimes referred to as V5). Due to its distinct connectivity as well as functional, anatomical, and histological properties, research into area MT played an historical role in the understanding of cortical function and establishing cross-species homologies (Born & Bradley, 2005). Neurons in this area are arranged in a columnar organization of direction-selective responses (Dubner & Zeki, 1971). These columns are arranged in larger scale gradients of disparity tuning (DeAngelis & Newsome, 1999). The primary inputs to area MT are themselves direction selective V1 neurons (Movshon & Newsome, 1996), which tend to be disparity selective (Prince, Pointon, Cumming, & Parker, 2000). One of the noteworthy computational advantages of bringing these signals together in MT is the ability to efficiently establish an inhibitory surround (Bradley & Andersen,

1998), allowing for the detection of objects moving relative to the background, even during eye or whole-body movement. Another advantage is addressing the aperture problem (whereby the speed and direction of motion are confounded within small receptive fields) by the segmentation of flow fields to allow for the computation of pattern motion (Adelson & Movshon, 1982).

1.6.2.2 Bodies

The first evidence for a body-selective region of in the ventral visual pathway was the discovery of the Extra-striate Body Area (EBA) (Downing, Jiang, Shuman, & Kanwisher, 2001). The EBA is adjacent to the occipital face area in the lateral aspect of the occipitotemporal cortex. Subsequently, a region that responded selectively to body parts was discovered lateral to the fusiform-face area of individual subjects and was termed the Fusiform Body Area (FBA) (Peelen & Downing, 2005). Interestingly, this same analysis performed on group averaged data did not show a distinction between face and body areas, but rather a broader scale animate/inanimate distinction. However, even in individual subjects, there always seemed to be an overlap between face- and body-selective areas. Given the nature of fMRI data, such an overlap may or may not be indicative of interleaving of the underlying neural populations; due to the vascular sources of the BOLD signal, the measured changes in BOLD activity can reflect a complex change in neural activity in space and over time (Kriegeskorte, Cusack, & Bandettini, 2010). Another study addressed whether the FFA and FBA were two distinct areas or one area with a gradual change in selectivity over the cortical surface. Data was collected from a group of subjects with different fMRI resolutions. The number of voxels showing preferential responses to both faces and bodies decreased as the voxel size decreased in a manner consistent with a distinct border between the two regions (Schwarzlose, Baker, & Kanwisher, 2005).

More recently, a study of body-selective responses on the lateral surface of the temporal lobe suggested that the EBA might be a series of functionally related but distinct areas (Weiner & Grill-Spector, 2011), much as previously been observed for posterior-fusiform face area and mid-fusiform face area. As a result of their analysis, the researchers proposed a subdivision of the EBA into three separate regions, and that these regions largely encircled the motion-selective area MT.

1.6.2.3 Objects

After the initial discovery of relatively simple tuning properties in the early visual areas of cats (Hubel & Wiesel, 1959), neurons were identified in the inferotemporal cortex of macaques that responded line drawing of complex objects, including faces and hands (Desimone et al., 1984). Subsequently, a region was discovered in the lateral occipitotemporal cortex, typically referred to as the Lateral Occipital Complex (LOC), which responded selectively to objects relative to scrambled objects or textures (Malach et al., 1995). This complex was later subdivided into the tentative Lateral Occipital (LO) and posterior Fusiform (pFs) regions, with the latter

displaying more translation-tolerant responses (Grill-Spector et al., 1999). Experiments with ambiguous stimuli suggest that these object-selective areas are responsive to the perceptual organization of stimuli rather than their local feature properties (Hasson, Hendler, Ben Bashat, & Malach, 2001).

1.6.2.4 Scenes

Following on electrophysiological findings of place and navigation-related information in parahippocampal cortex (Moser, Kropff, & Moser, 2008), a region was found in the posterior portion of the medial temporal lobe, termed the Parahippocampal Place Area (PPA). The PPA is selective for the spatial layout of scenes relative to objects or textures (Epstein & Kanwisher, 1998). The representations in this area seem to be egocentric, as scene geometry-preserving changes in viewpoint result in nearly as much release from adaptation as the presentation of novel scenes (Epstein, Graham, & Downing, 2003).

A second scene-selective region was discovered along the medial wall of the occipitotemporal cortex posterior to the splenium of the corpus callosum. Named for its anatomical location, the retrosplenial cortex (RSC) differs in responses from the PPA in that it seems particularly sensitive to global orientation information and tasks that relate the scene to the larger spatial context (Epstein, 2008).

A third region in or around the transverse occipital sulcus (TOS) was often seen but initially not widely remarked upon when contrasting the neural response to scenes versus objects (Grill-Spector, 2003). This area was initially referred to by its anatomical location as the TOS, but subsequent studies referred to the area as the occipital place area (OPA) since it has a functional rather than anatomical definition, is demonstrably and selectively involved in scene perception (Dilks, Julian, Paunov, & Kanwisher, 2013), and was not located in the transverse occipital sulcus in all subjects (Nasr et al., 2011). Relative to the PPA and RSC, the OPA seems to be more involved in the processing of presence of spatial boundaries rather than their specific relations and to scene contents, such as individual items of furniture (Kamps, Julian, Kubilius, Kanwisher, & Dilks, 2016).

Mounting evidence suggests that the 'area' known as PPA is a complex of adjacent functionally related regions. They are part of a 'cluster' of quasi-retinotopically organized regions sharing a foveal representation, but having distinct maps of space (Arcaro, McMains, Singer, & Kastner, 2009). Moreover, the anterior and posterior aspects of the PPA differ in patterns of corticocortical connectivity (Baldassano, Beck, & Fei-Fei, 2013) and functional selectivity (Arcaro et al., 2009), and possibly also cytoarchitecture (Weiner et al., 2017).

1.6.2.5 Color

Color processing has been an intensively studied for early visual processing, but only comparatively recently have the color responsive regions of the high-level visual cortex been identified (Tootell, Nelissen, Vanduffel, & Orban, 2004). Earlier electrophysiological (S. Zeki, 1980) and neuropsychological (Meadows, 1974) findings

lead to the seemingly mistaken view of area V4 as a 'color center.' However, later lesion research of area V4 did not result in achromatopsia (Heywood, Gadotti, & Cowey, 1992) and imaging research revealed that the color responsive regions of V4 are clusters of columns which are sparsely distributed throughout the area (reminiscent of the thin strips of V2) (Roe et al., 2012; Tanigawa, Lu, & Roe, 2010), while more wide-spread color selective regions are found further along the ventral pathway (Tootell et al., 2004).

A more recent MION-enhanced fMRI study in macaques identified a series of color-selective 'globs' starting slightly anterior to V4 and extending throughout the inferotemporal cortex (R. Lafer-Sousa & Conway, 2013). Interestingly, there seemed to be a corresponding color-selective area for adjacent or very nearly adjacent (inferior and slightly posterior) to each of the face areas. In human subjects, color regions were found medial to all of the face regions except the anterior face patch. In both species, the more posterior color regions seem to code color independently of shape (Lafer-Sousa, Conway, & Kanwisher, 2016).

1.7 Considerations for fMRI Research of the VTC

While a substantial amount of work has been done to elucidate the nature of the ventral temporal cortex in macaques and humans, there are still several interesting questions that remain. The technology best suited to answer questions about patterns of activity within each region as well as the interaction between regions is currently fMRI. It also provides a bridge between human studies and macaque microstimulation, electrophysiological recording, and optical intrinsic signal imaging - particularly as methods for non-invasive imaging of awake monkeys have been developed (Srihasam, Sullivan, Savage, & Livingstone, 2010). However, there are several challenges for fMRI studies of the medial and anterior ventral temporal cortex.

For studying progressively high-level visual cortex, stimulus and task seem to be increasingly important. Several studies have found retinotopic organization (or at least biases) can be found well into the parietal and temporal cortices using either particular tasks (e.g., memory-guided saccades) or complex stimuli (e.g., retinotopic wedge and ring mapping, but using a rapidly changing collage of faces, scenes, and words instead of luminance flicker). Nasr & Tootell's study was able to identify the AFP in some subjects using stimulus contrasts but found much larger effects in that region for a task manipulation that involved face recognition. The planning of studies involving high-level areas should pay particular attention to the appropriateness of the stimuli and the task.

An alternative reason that split-half beta-weight correlations in this part of the temporal lobe may be low is the magnetic susceptibility artifact due to the proximity to the external auditory meatus. Several proposals have been made for compensating with this artifact. One approach that may be financially infeasible for many institutions is moving to higher field strength. Another possible approach is the use of Spin-Echo (SE) sequences instead of the more commonly used Gradient-Echo (GE) sequences (Op de Beeck, Dicarlo, et al., 2008). However, to achieve the necessary resolution to for examining functional organization in the anterior temporal

lobes with SE sequences, field strength stronger than 3 Tesla may be still be required. One approach that several groups have adopted is the use of readout sequences that sample the fMRI spatial frequency data in a pattern that spirals inward, then outward. A straightforward approach that only requires the changing of a few parameters in a standard BOLD sequence is to acquire coronal (instead of the more common axial) slices to make up each of the fMRI volumes (Axelrod & Yovel, 2015). To my knowledge, there has been no published systematic comparison of the quality of these alternatives.

An additional consideration with fMRI is that voxels sample from tens to hundreds of thousands of neurons. While some pattern classification and adaptation methods may allow access to information that is organized at a scale smaller than the voxel size, attempts to study functional organization will require voxel sizes above the Nyquist limit of the pattern of information in the local neural network. Again, the most straightforward, but perhaps least accessible means of doing this is using a higher MR field strength. Nonetheless, whatever the voxel size, it is important to be aware of how information at the neural level would be sampled to the voxel level (Issa, Papanastassiou, & DiCarlo, 2013). This is one likely factor contributing to the inability to detect information with fMRI multi-voxel pattern analysis that has been detected with electrophysiological recording (Dubois, de Berker, & Tsao, 2015).

1.8 SUMMARY

The visual systems of the human and macaque are some of the most well understood neural systems studied to date. A wide range of methodologies have been developed to study aspects of the structure and function of neural systems, and these methods largely suggest complimentary answers regarding the organization of early visual cortex. However, there currently a range of hypotheses about the organization of higher-level visual regions within the VTC. While it is possible that only one of these pictures is correct, it seems likely that the cortical organization in the VTC displays aspects of each of these proposals. For example, there might be large-scale biases for particular stimulus features that span all or most of the VTC which contain a series of distinct functional regions, each of which at some scale representing information in a distributed fashion.

Regardless, the near ubiquity of cortical areas in regions of the cortex that are well understood, along with the substantial body of research regarding the existence of category-selective regions, suggests the ventral temporal cortex may be tiled with a series of cortical areas with distinct functions, architectures, patterns of connectivity, and topographic organization.

ToC

Chapter 2 : Neural Plasticity in the Visual System: A case study of subject M.M.

This chapter will consider how category-selective regions arise and are modified as a result of experience, as well as provide a context for the research described in the following chapter. Specifically, this chapter addresses various forms of neural plasticity with the goal of demonstrating how the unique history of subject M.M. provides the opportunity to address novel research questions regarding the formation of category-selective regions in the ventral temporal cortex.

2.1 Mike May: A case study

Subject M.M. has a unique history of sensory deprivation and recovery that allows for the posing of novel questions regarding the nature of neuronal reorganization. M.M. was normally sighted until three and a half years old when the explosion that took his sight resulted in severe corneal scarring in one eye and the complete loss of the other. After recovering from the injury, he was able to detect the presence or absence of bright light but had no form vision, a condition which would persist for the next forty years. In 2000, M.M. received an experimental sight restoration surgery which restored monocular vision. His behavioral and neural responses to a range of visual tasks were studied shortly after this surgery (Fine et al., 2003).

The following chapter presents research that evaluates the extent of experience dependent plasticity in M.M.'s ventral visual pathway after more than ten years of restored vision. This chapter will address the issues of plasticity surrounding this research, as well as discussing what this research suggests about the organization of the ventral temporal cortex. From a developmental perspective, M.M. lost sight before the full development of the visual system and had ample time to reorganize to adapt to his loss of sight. When his visual capacities were studied shortly after sight restoration, he seemed to have relatively intact abilities to process things like color and motion, though performed poorly on high-level visual tasks, suggesting that portions of his ventral temporal and possibly lateral temporal cortices had indeed undergone some form of reorganization. However, it was unclear if these regions of the adult cortex would retain sufficient plasticity to revert to circuitry capable of supporting high-level visual function after extensive visual experience.

2.2 The Roles of Plasticity

Neural plasticity is the modification of the functional characteristics of a neuron and thus its role in the neural circuits in which it is embedded. The primary mechanism by which this occurs is the adjustment of synaptic efficacy (Citri & Malenka, 2008), which occurs through both presynaptic (Byrne & Kandel, 1996) and postsynaptic (Granger & Nicoll, 2014) modifications. Distinct fields have studied aspects of plasticity that differ

in the biological timing and context in which such modifications in neural function occur. The following sections will discuss three of these areas of the plasticity literature: developmental plasticity, adult neural plasticity, and neural reorganization. In particular, each of these sections will discuss plasticity literature relevant to M.M.

2.2.1 Developmental Plasticity

Unlike most sight recovery patients who have congenital visual deficits or who become blind late in life through progressive visual disorders, M.M. had normal visual development until his sudden blinding at three and a half years of age. While the time course of human visual development has not been thoroughly documented, it has been shown to be a progressive process that extends to early adolescence with contributions from both genetics and experience.

2.2.1.1 The role of genetics

The influence of genetics is evident in the structure and function of the adult brain (Christova & Georgopoulos, 2018). Chemical gradients during the early embryonic development of the nervous system provide spatial molecular cues that in turn govern subsequent stages of increasingly specialized gene expression (Yoon, Vissers, Ming, & Song, 2018). These chemical gradients are also part of the mechanisms that guide long-range axonal projections which form the foundation of the white matter (Flanagan, 2006; McLaughlin & O'Leary, 2005; O'Leary & McLaughlin, 2005). Within the visual system, region-to-region axonal projections are guided along molecular gradients (Huberman, Feller, & Chapman, 2008). The general retinotopic organization of early visual processing is also primarily driven by coordinated molecular gradients in the retina, lateral geniculate nucleus, superior colliculus, and early visual cortex (Cang & Feldheim, 2013).

Some aspects of high-level visual function may also develop under relatively specific genetic guidance. For example, the heritability of the face-processing disorder prosopagnosia (Lee, Duchaine, Wilson, & Nakayama, 2010) suggests that specific gene expression pathways are necessary to establish normal function of the network of face-selective regions, such that disruptions can profoundly and selectively diminish a particular visual capacity. More surprisingly, genetic similarity also accounts for a substantial amount of individual differences in face recognition ability (Shakeshaft & Plomin, 2015; Wilmer et al., 2010). Findings such as these are suggestive of genetic influences on the region-to-region connectivity throughout the ventral visual pathway, and moreover that these innate constraints not only contribute to the spatial distribution 'category-selective' regions but also individual differences in visual capacities (Mahon & Caramazza, 2011).

2.2.1.2 The role of experience

There is far from enough genetic information to encode the specific wiring diagram of the human brain. However, rather than a biological limitation, this may instead be an adaptation to aspects of the environment are too novel, complex, or rapidly changing for genetic adaptation to track.

In addition to the genetically-driven ontogenetic processes, typical development also requires endogenous as well as experience-driven retinal activity (Movshon & Van Sluyters, 1981). While the initial retinotopic organization of the early visual cortex occurs under genetic control, it is further refined prenatally by 'experience' due to retinal waves (Ackman & Crair, 2014; Huberman et al., 2008). Additionally, many of the tuning properties of V1 neurons depend on early visual experience (Hubel & Wiesel, 1959, 1998; Raviola & Wiesel, 1978; Wiesel & Hubel, 1963, 1965).

Importantly, these effects of experience on development primarily occur during particular developmental windows. Originally known as *critical periods* (Hensch, 2005), these windows are increasingly conceived of as *periods of sensitivity to deprivation* (Lewis & Maurer, 2005). More recent research has shown that these periods of sensitivity are also found for higher-level cognitive and social processes (Hartshorne, Tenenbaum, & Pinker, 2018; Kaler & Freeman, 1994).

Substantial research has elucidated the cellular and genetic mechanisms that are involved in the onset and maintenance of the windows of plasticity (Hooks & Chen, 2007). The developmental timing of periods of sensitivity vary from species to species, but the ordinal pattern of particular developmental stages is largely evolutionarily conserved (Finlay & Darlington, 1995; Workman, Charvet, Clancy, Darlington, & Finlay, 2013). This systematic relationship facilitates inferences on human development based on experiments in model organisms (Clancy, Finlay, Darlington, & Anand, 2007).

2.2.1.3 Arealization

The peri-natal and post-natal distribution of windows of susceptibility to deprivation suggest that visual experience is required for the development of almost all mid- and high-level visual capacities. Although the development of high-level visual capacities has been less extensively investigated, several studies have evaluated the role of visual experience for conventional indicators of high-level face processing as well as the influence on the development of cortical 'face-selective' regions (McKone, Crookes, Jeffery, & Dilks, 2012).

Experience seems to play an important role in the development of some high-level visual processes. One study addressed this by assessing face processing in macaques reared without exposure to faces (Sugita, 2008). Very young monkeys showed a preference for looking at images either human or monkey faces over objects, suggesting an innate predisposition for viewing behavior. After the deprivation period of up to two years,

monkeys were either exposed to human or conspecific faces for one month and tested again. This time preferential looking only occurred for the species whose faces they had experienced. Moreover, after the deprivation period, they displayed face processing deficits toward whatever species' faces which they had not been exposed.

More recently, another lab extended these results with a separate group of macaques reared without exposure to faces (Arcaro, Schade, Vincent, Ponce, & Livingstone, 2017). Immediately after the deprivation period, they found no preferential looking toward faces. However, in contrast to the previous study, their stimuli were not isolated faces, but naturalistic images of humans or conspecifics. Rather than looking at faces, their subjects preferentially looked at hands or other body parts indicative of posture. Additionally, they used fMRI to assess the development of known category-selective regions in face deprived and control individuals. Monkeys reared without exposure to faces develop regions selective for bodies and scenes which looked indistinguishable from controls, however, they showed little or no evidence of face-selective regions.

Other research from the same lab suggests that the formation category-selective areas results from the interplay of ethologically-relevant looking behavior and an innate set of spatially distributed biases for particular visual properties (Srihasam et al., 2014). Rather than depriving research subjects of typical patterns of visual stimulation, they provided juvenile macaques with artificial stimulus sets. These stimuli were made 'relevant' by associating each symbol with a particular reward (number of drops of juice) and having pairs of stimuli presented in their home cages on a touchscreen. Each macaque was trained on each of three symbol sets in a different order. Not only did they develop 'category-selective' domains for these novel stimulus sets, the formed in the same cortical locations across individuals regardless of training order. Follow-up studies suggested that the location where these domains emerged was associated with gradients for curvature and to a lesser extent eccentricity (but not spatial frequency). These results suggest that experience-dependent plasticity coupled with visual experience (which is in part due to ethological relevance) drive the formation of category-selective regions, and that their cortical locations are due to a preexisting proto-organization in IT (which may itself be at least partially experience-dependent). However, an important caveat is that, to date, this experiment has only been carried out on juveniles, so it remains to be seen whether these effects hold for adults.

2.2.2 Adult Neural Plasticity / Perceptual Learning

After an initial three and a half years of sight, M.M. was blind for the next 43 years. Developmental plasticity would have shaped the changes which occurred in M.M.'s visual system for several years following the accident. While large-scale morphological changes slow in adulthood and many of the dramatic changes in tuning properties that can be observed earlier in development no longer occur, neural plasticity continues to various extents for different regions in the adult brain.

Experience-dependent plasticity is a pervasive phenomenon within nervous systems of many species in which the efficacy of communication at the synapses of two or more neurons is modified as a function of neural responses to external stimuli. These changes operate at a range of spatial and temporal scales.

Perceptual learning is the behavioral manifestation of the adaptation of an organism's nervous system to (in many cases repeated) presentation of a sensory stimulus. These changes are often measured in the changes in detection threshold, difference thresholds, or general increases in accuracy.

While perceptual learning studies often target relatively basic phenomena such as detection or difference thresholds, the techniques are applicable to a wide range of phenomena and provide a method for assessing the variety and extent of plasticity that a given system can undergo. Perceptual learning forms the foundations of many complex cognitive capacities (Goldstone, 2000); a clear example is learning the graphemic and phonemic components of language. As such, perceptual learning is well suited for researching the processes might occur on a particular type of sensory information for a high-level task.

Perceptual learning is also involved in the development of categorical perception – the ability perceptually group behaviorally related stimuli such that within category variation is deemphasized and between category distinctions are facilitated. Learning phonemes or graphemes would be an example, as would perceiving the difference between a car and truck. As the known functionally defined areas in the ventral temporal cortex are putatively 'category-selective', this form of perceptual learning might be particularly relevant in the establishment in children or the reestablishment of such regions in sight recovery patients.

In the visual system, there are dramatic difference between both the rate and amount of perceptual learning for different tasks. Interestingly, this seems to be related to the depth of neural processing. Tasks involving precortical or early visual areas require extensive training to achieve even modest gains, while tasks primarily involving high-level areas within the VTC can display dramatic improvement after a minimal amount of training (Beyeler, Rokem, Boynton, & Fine, 2017). This phenomenon is consistent increasingly later windows of developmental plasticity for increasingly higher-level regions of the visual system. Specifically, there seems to be a gradient of increasing plasticity that follows a posterior to anterior gradient along the ventral temporal pathway, which might also be interpreted as increasing plasticity for increasing levels along the visual processing hierarchy (Fine & Jacobs, 2002). It is also consistent with the observation that training on a task with diverse sets of stimuli increase the amount of generalization (Ahissar & Hochstein, 1997).

Regarding M.M., the implication of these lines of research is that the particular areas of the visual system involved in the behavioral tasks which he was largely unable to do when studied shortly after recovering sight are the most likely to retain plasticity in adulthood. While he performed similar to controls on a range of tasks involving color, motion, and basic shapes, he had difficulty with tasks involving faces, complex objects, and

recognition of objects across different views. The ventral temporal cortex is involved in all of these tasks, and the plasticity literature suggests that these the VTC has a comparatively greater capacity for experience-dependent learning.

2.2.3 Neural Reorganization

This poor performance that M.M. displayed for mid- to high-level visual tasks suggested that portions of his ventral temporal and possibly lateral temporal cortices have undergone some form of reorganization. The research reported in : A Lack of Functional Reorganization After More than a Decade of Recovered Sight addresses the extent to which there was sufficient plasticity within the VTC further reorganize to take advantage of his recovered sight.

The interaction between evolutionary and developmental demands of the nervous system requires it to serve multiple complex functions while also being robust or at least tolerant to perturbations (Anderson & Finlay, 2014). In some cases where sufficiently dramatic changes to the input to the nervous system occur, the cortex can reorganize neural circuits to effectively processes the novel stimulus information.

Loss of cortical sensory input resulting from damage to pre-transduction mechanisms, sensory receptor loss, or deafferentation often leads to some form of reorganization. Early research involved the surgical severing of peripheral afferents (Merzenich et al., 1983). A common theme among these results, as well as studies which instead use increased sensory stimulation of a specific portion of the sensory surface (Jenkins, Merzenich, Ochs, Allard, & Guic-Robles, 1990), was that reorganization occurs based on innervation from nearby regions. Potential mechanisms for this type of local rewiring include homeostatic mechanisms that equilibrate neural activity through synaptic reweighting or changes in intrinsic excitability (Nitsche et al., 2007).

Larger-scale changes of sensory input, such as the loss of an entire sensory modality, may result in phenomena which are unlikely to be accounted for by these local mechanisms. However, the most dramatic changes do not frequently occur in adults, and thus likely reflect the role of mechanisms of developmental plasticity (Wittenberg, 2010). Research in juvenile barn owls found that during a particular developmental window, displacing visual input with prism goggles or altering auditory input through auditory canal inserts resulted in rotated maps in the superior colliculus such that there is cross-laminar correspondence between the auditory and visual receptive fields (Knudsen, 1985).

Phenomenologically similar patterns have been observed in human recipients of cochlear implants. The devices provide direct electrical input to the spiral nucleus in the cochlea of individuals who are deaf for peripheral, often non-neural reasons (Tisch, 2017). While, most adult patients can still make use of the signals from modern implants well enough for conversation within hours to months of training (Shannon, 2012), their ability segregate sounds never approaches normal levels. However, the earlier in life an individual receives the implant,

the better their ability to utilize the information relayed by the device (McKinney, 2017), which is consistent with the greater capacity for plasticity seen in developmental studies.

The patterns of visual deficits M.M. displayed shortly after his sight restoration surgery suggested that his ventral temporal cortex had undergone substantial reorganization, and most of this like occurred during his childhood development. For experience-dependent plasticity to be capable of restoring high-level visual capacities to M.M. would require substantial reorganization. While the literature on reorganization document many cases of adult experience-dependent plasticity, these tended to be relatively minor changes to tuning or modest amounts of cortical recruitment. Large-scale reorganization has mostly only been observed in juvenile subjects. These findings would suggest a more pessimistic view on the possibility that M.M. would have recovered his high-level visual capacities. However, one mitigating consideration is that the majority of research on reorganization has focused on primary sensory or motor areas, which have less residual plasticity under cases of normal development than the ventral temporal cortex.

2.3 Dynamic Localizers: a tool uniquely suited to studying M.M.

In humans, face processing is qualitatively adult-like at the earliest age where it has been investigated, with most behavioral capacities having been observed by age four or earlier (McKone et al., 2012). These findings suggest that by the time M.M. lost his sight, the many of the basic structural aspects of his ventral visual pathway which underlie these tasks would have formed. His performance on psychophysical tasks post-surgery suggested that he was still within the period of sensitivity to deprivation for these areas when the accident occurred and that these regions had reorganized to subserve other functions. Specifically, his loss of face processing abilities would be consistent with findings that face processing continues to develop into adolescence when quantitatively adult-like performance or behavioral tasks is reached (Mondloch, Le Grand, & Maurer, 2003). However, it was unclear if the adult ventral temporal cortex would retain sufficient plasticity to revert to circuitry capable of supporting high-level visual functions as a result of extensive visual experience.

The dynamic localizer, a method for functionally identifying known category-selective regions, is a tool that is uniquely suited to study high-level visual regions in M.M. Before coming to the University of Washington, I worked in Kanwisher Lab at MIT, where I developed and validated a dynamic localizer for a series of studies of autistic and normally developing children. The stimuli were first described in another line of research regarding the automated identification of functionally defined regions (Julian, Fedorenko, Webster, & Kanwisher, 2012). Unlike previous methods for identifying functional areas in the ventral visual pathway, this localizer used freely-viewed colorful, full-screen videos. The conventional localizers at the time required subjects to fixate throughout the scan, something which is challenging for M.M., and the stimuli consisted of relatively small (about four degrees of visual angle, too small for M.M.s relatively low visual acuity) greyscale images. Moreover, static the stimuli for static localizers were frequently equated for luminance, contrast, or other low-

level visual properties. I ran a series of (unpublished) studies that established that not only did localizing the functional areas not require these controls, but the dynamic localizers also provided better functional signal to noise. The dynamic localizer thus avoided some of the stimulus and tasks characteristics that would have complicated the interpretation of M.M.'s results, while also providing earlier areas of his visual system with the features on which we know he performs comparably to normally sighted subjects, specifically, color and motion.

ToC

Chapter 3 : A Lack of Functional Reorganization After More than a Decade of Recovered Sight

Elizabeth Huber, Jason M. Webster, Alyssa A. Brewer, Donald I. A. MacLeod, Brian A. Wandell, Geoffry M. Boynton, Alex R. Wade, and Ione Fine. Psychological Science 1–9 © The Author(s) 2015. DOI:10.1177/0956797614563957

In 2000, monocular vision was restored to M. M., who had been blind between the ages of 3 and 46 years. Tests carried out over 2 years following the surgery revealed impairments of 3-D form, object, and face processing and an absence of object- and face-selective blood-oxygen-level-dependent responses in ventral visual cortex. In the present research, we reexamined M. M. to test for experience-dependent recovery of visual function. Behaviorally, M. M. remains impaired in 3-D form, object, and face processing. Accordingly, we found little to no evidence of the category-selective organization within ventral visual cortex typically associated with face, body, scene, or object processing. We did observe remarkably normal object selectivity within lateral occipital cortex, consistent with M. M.'s previously reported shape-discrimination performance. Together, these findings provide little evidence for recovery of high-level visual function after more than a decade of visual experience in adulthood.

3.1 Introduction

M. M. was 3.5 years old when a chemical explosion destroyed his left eye and caused severe corneal damage in his right. As described previously (Fine et al., 2003), M. M. had some perception of light but no experience of contrast or form over a period of 43 years. He reported no visual memories or imagery, despite one unsuccessful corneal replacement attempt in childhood. In 2000, M. M. received a corneal transplant and stem cell therapy, which restored vision in his remaining eye. In tests carried out over the first 2 years after surgery, M. M. showed severe amblyopia (an acuity limit of ~1.2 cycles per degree, corresponding to Snellen acuity of ~20/500) and substantial deficits in high-level visual processing (Fine et al., 2003).

Most cases of early visual deprivation are due to congenital cataracts that are diagnosed and removed within the first year of life. Thus, these cases differ substantially from that of M. M., who was blinded in early childhood and remained blind for much of his adult life. Indeed, M. M.'s period of deprivation and the period found in more traditional examples of bilateral cataracts are practically nonoverlapping. Infants treated for congenital cataracts early in life regain useful visual function, though deficits in a variety of low-level (Maurer, Mondloch, & Lewis, 2007), mid-level (Ellemberg et al., 2005; Lewis et al., 2002), and high-level (Le Grand, Mondloch, Maurer, & Brent, 2004; Robbins, Nishimura, Mondloch, Lewis, & Maurer, 2010) capacities remain.

The period of visually driven normal development differs from both the sensitive period for damage and the sensitive period for recovery, and these developmental windows differ substantially across various types of visual processing (Lewis & Maurer, 2005) and depend upon a complex balance between inhibitory and excitatory circuits that are themselves affected by deprivation (Bavelier, Levi, Li, Dan, & Hensch, 2010). At present, some uncertainty exists in the literature as to whether people whose sight is restored in adulthood can regain useful vision and over what timescale such improvement might occur. Previous studies and case reports (Cheselden, 1727; Fine et al., 2003; Gregory & Wallace, 1963; Šikl et al., 2013; Sinha & Held, 2012; Valvo, 1971) suggest that adults who have recovered their sight tend to find the visual world confusing and difficult to interpret even many months after surgery, although certain visual abilities seem to improve after surgery (Kalia et al., 2014; Ostrovsky, Meyers, Ganesh, Mathur, & Sinha, 2009), and some spared high-level visual function has been reported in one case of sight recovery in early adolescence (Ostrovsky, Andalman, & Sinha, 2006).

When tested shortly after surgery, M. M. had normal perception of color and motion, and only modest deficits in perception of simple form (Fine et al., 2003), consistent with the comparatively early sensitive periods proposed for these capacities. In contrast, M. M. showed severe deficits in many aspects of complex form, object, and face processing, accompanied by a lack of category-selective responses for faces or objects within ventral visual cortex, as measured using functional MRI (fMRI). Although these capacities are qualitatively present at 3 to 4 years of age, when M. M. lost vision, certain aspects of object and face processing continue to develop well into early childhood (Lewis & Maurer, 2005; McKone, Crookes, Jeffery, & Dilks, 2012; Nishimura, Scherf, & Behrmann, 2009), and the degree of plasticity within these areas after early childhood has not yet been established in humans. Thus, it remains possible that M. M. could have recovered these capacities with sufficient visual experience. In the work reported here, we used behavioral measures and fMRI to assess whether M. M.'s processing of complex form, objects, and faces has changed after more than 10 years of restored sight.

3.2 Method

3.2.1 Subjects

M. M. and 2 age- and gender-matched control subjects participated in both the behavioral and fMRI portions of the experiment. Two additional control subjects were excluded from the analysis because they fell asleep during the fMRI portion of the experiment. All procedures, including recruitment and testing, followed the guidelines of the University of Washington Human Subjects

Division and were approved by the institutional review board. All subjects provided informed consent.

3.2.2 PROCEDURE FOR BEHAVIORAL EXPERIMENTS

MM's spatial CSF was measured on a CRT display, which was calibrated using a PR-650 spectroradiometer (Photo Research, CA) and linearized using custom software written in Matlab. The monitor had a peak luminance of 152 cd/m^2 and a black level of 0.14 cd/m^2, and the screen subtended 28-by-22 degrees of visual angle at a viewing distance of 64 cm. Vertical gratings occupying the central 20 degrees of the display were sinusoidal modulations around an average gray level, presented within a Gaussian aperture.

MM's spatial CSF was measured using a 2-interval forced-choice procedure. Trials were initiated by button press and consisted of two 500 ms test intervals separated by a 500 ms ISI. To help orient MM to the trial structure, a brief tone was played to signal the onset of each test interval. After the second interval, he was given unlimited time to respond by button press with the number corresponding to the interval containing the grating. Grating contrast decreased after three correct responses and increased after each incorrect response. Feedback was given in the form of a brief, low tone for incorrect responses. Five logarithmically spaced spatial frequencies were tested, ranging from 1/4 to 2 cpd. As expected, MM was unable to detect gratings at 1.4 cycles per degree and above, even at full contrast. As such, fewer trials were completed at these frequencies.

Because M. M. had studied the original object and face stimuli and received feedback after the original experiments (Fine et al., 2003), different databases were used in the experiments described here to obtain novel but analogous stimuli. Object identification and emotion classification were tested using gray-scale images adapted from a standard stimulus set courtesy of Michael J. Tarr, Center for the Neural Basis of Cognition and Department of Psychology, Carnegie Mellon University (http://www.tarrlab.org/). Gender classification was tested using stimuli adapted from the Stirling face set (http://pics.stir.ac.uk/2D_face_sets.htm). To ensure that M. M. was familiar with the objects in our stimuli, we selected com- mon household items to which he was regularly exposed. We chose novel face stimuli in which the number of non-configural cues, such as eyebrow shape and hair length, was minimized; M. M. had previously reported using such cues to discriminate male from female faces.

All stimuli were presented on a large flat-screen monitor, which subtended 56 × 42 degrees of visual angle at a viewing distance of 35 cm. Stimulus images subtended roughly 12° and were presented in gray scale on plain, achromatic backgrounds. As in our original experiments (Fine et al., 2003), M. M. viewed unblurred stimuli, whereas control subjects viewed stimuli that were convolved with a Gaussian filter centered at 1 cycle per degree to match M. M.'s psychophysically determined acuity (see Figure 3.1). M. M.'s acuity has remained stable since the initial tests conducted shortly after he recovered his sight (Fine et al., 2003; Levin, Dumoulin, Winawer, Dougherty, & Wandell, 2010). We chose the number of trials to run per task prior to the start of data collection to allow presentation of several exemplars from each category while minimizing fatigue in M. M., for whom the tasks were challenging.

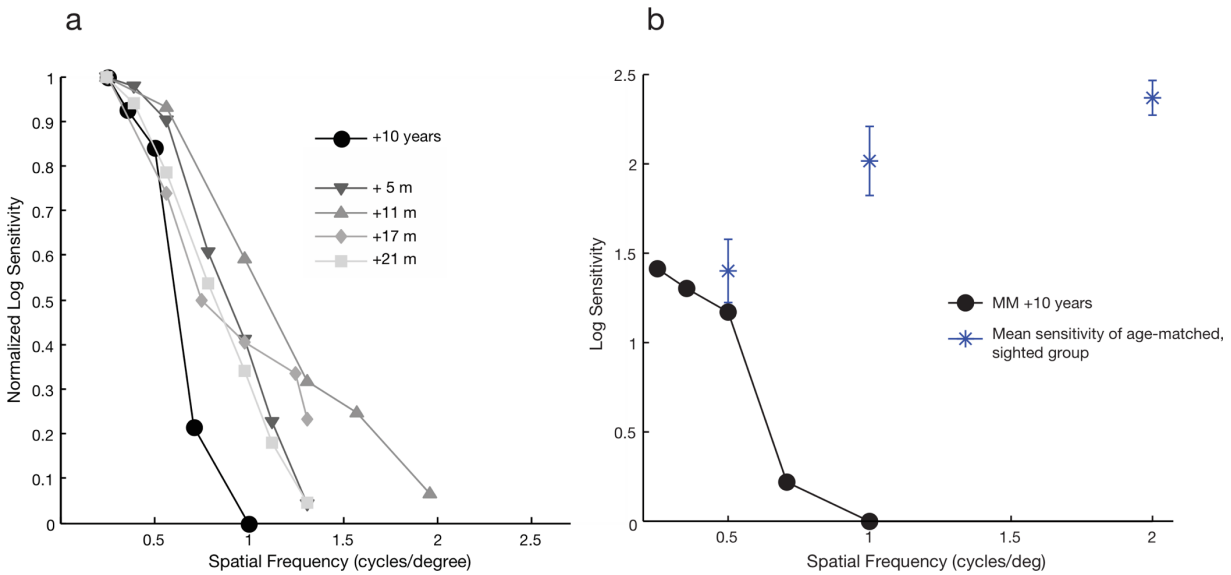

Figure 3.1. Contrast sensitivity functions for M. M. over time and compared to control subjects

Contrast sensitivity in MM 11 months to 10 years post-surgery (a): Large black symbols represent MM's normalized sensitivity as a function of spatial frequency measured psychophysically using a two-alternative forced-choice over 10 years after surgery. Smaller gray symbols represent MM's normalized sensitivity measured psychophysically using a method of adjustment 5-21 months after surgery, data re-plotted from (Fine et al., 2003). It is not clear whether the loss in apparent sensitivity is due to changes in MM's optics, changes in equipment (e.g. a brighter monitor) or the changes in psychophysical procedure from adjustment to forced choice. The small deterioration in his measured CSF did not result in a discernible quality difference in the blurred photographs presented to control subjects. *CSF in MM compared with an age-matched sighted group (b):* Large black symbols represent MM's sensitivity (un-normalized), alongside average sensitivity values measured in a group of normally sighted subjects in their 50s, re-plotted from (Owsley, Sekuler, & Siemsen, 1983). Error bars reflect standard deviation.

To assess perception of complex 3-D form, we presented subjects with line drawings of cubes that were intact, had a single line missing, or were rearranged to disrupt the 3-D structure while preserving local junctions. Subjects completed 32 trials in total. On each trial, a stimulus was presented for 4 s, followed by an unlimited response interval. Subjects were asked to report via key press whether each image depicted a cube or a jumbled shape.

To further test perception of simple shape and 3-D form, we adapted a set of stimuli containing images of 3-D forms photographed from various viewpoints spanning a 360° rotation (Scharff, Palmer, & Moore, 2013). To create a version of the task that did not require interpolation in depth, we modified a subset of the stimuli by tracing their outer contours and then filling them with a uniform gray (see Figure 3.2 for example stimulus images). Subjects matched 3-D images across rotations in depth and 2-D images across rotations in the x-y plane. There were 60 trials in each condition. Stimuli remained on- screen until subjects pressed one of two keys to report whether two images, shown simultaneously on the left and right halves of the display, contained rotated versions of the same object or different objects. All subjects completed the 2-D version of the task first.

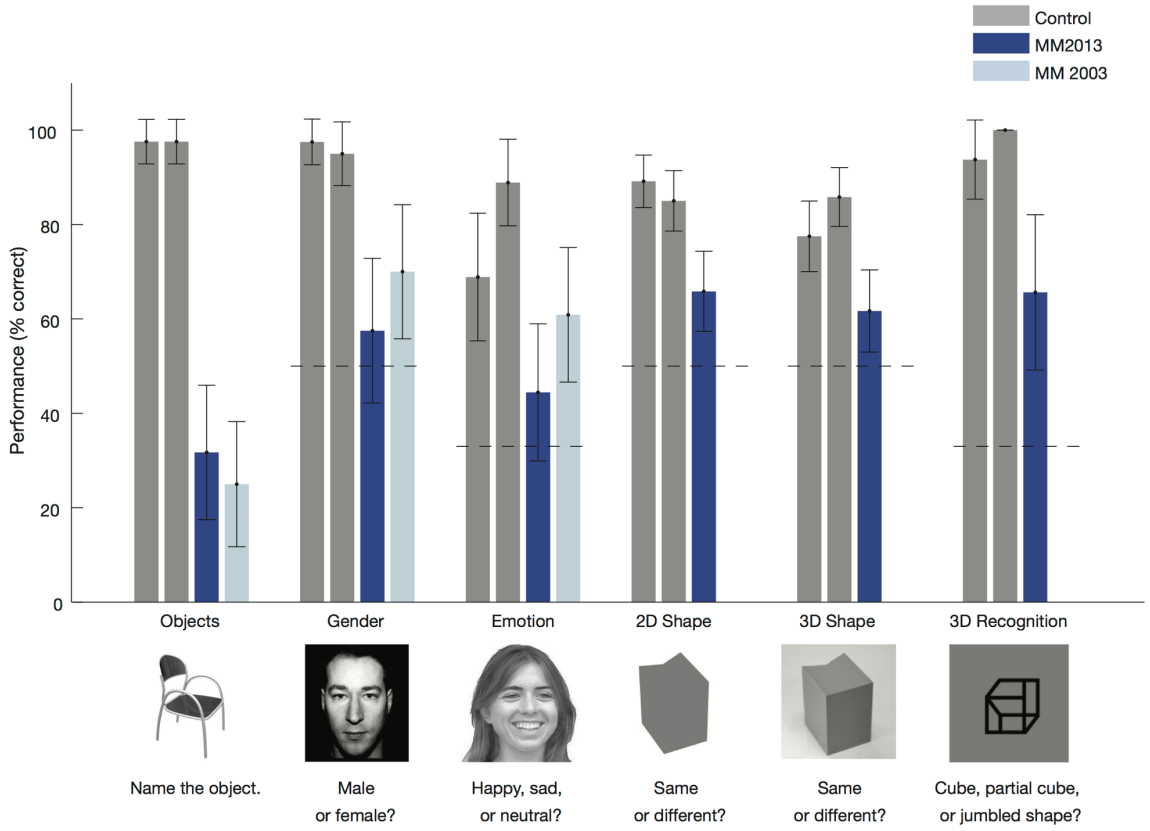

Figure 3.2. Mean percentage of correct responses as a function of stimulus category.

An example unblurred stimulus image is shown for each category; however, in this experiment, all stimuli shown to control subjects were blurred to match M. M.'s visual-acuity losses. Where applicable, chance performance is indicated with a dashed line. Error bars represent 95% confidence intervals.

For the object-identification task, subjects were asked to verbally identify each of 41 unique items, advancing to the next trial by pressing a key when they were unsure of an object's identity. Gender (male, female) and emotion (happy, neutral, sad) classification were tested via two- and three-alternative forced-choice paradigms, respectively. The gender-classification task consisted of 40 trials (20 faces of each gender) and the emotion-classification task consisted of 45 trials (15 individuals dis- playing each emotional expression). As with the shape stimuli, face and object stimuli were presented individually for 4 s at the center of the display, and subjects had unlimited time to respond by pressing a key.

3.2.3 Procedure for fMRI experiment

Category-selective regions in the ventral visual pathway have been well characterized in subjects who have normal sight (Kanwisher & Dilks, 2013). To ensure that any absence of this organization in M. M. could not be attributed to his reduced acuity, we showed control subjects blurred as well as unblurred versions of the stimuli.

Subjects viewed stimuli presented on a screen at the end of the scanner bore via a mirror attached to the head coil. Cortical category-selective blood-oxygen-level-dependent (BOLD) responses were estimated using freely viewed, colorful, full-screen 3-s video clips presented using a block design that alternated between faces, bodies, scenes, objects, and scrambled objects (Julian, Fedorenko, Webster, & Kanwisher, 2012). Face, body, and object videos were recorded against a black background. Scene stimuli consisted mostly of rural locations and included buildings, yards, and forested roads. To create scrambled versions of the object stimuli, we segmented each object clip into a 15 × 15 grid, and spatial locations were shuffled in a pseudorandom order. Example frames are shown in Figure 3.3.

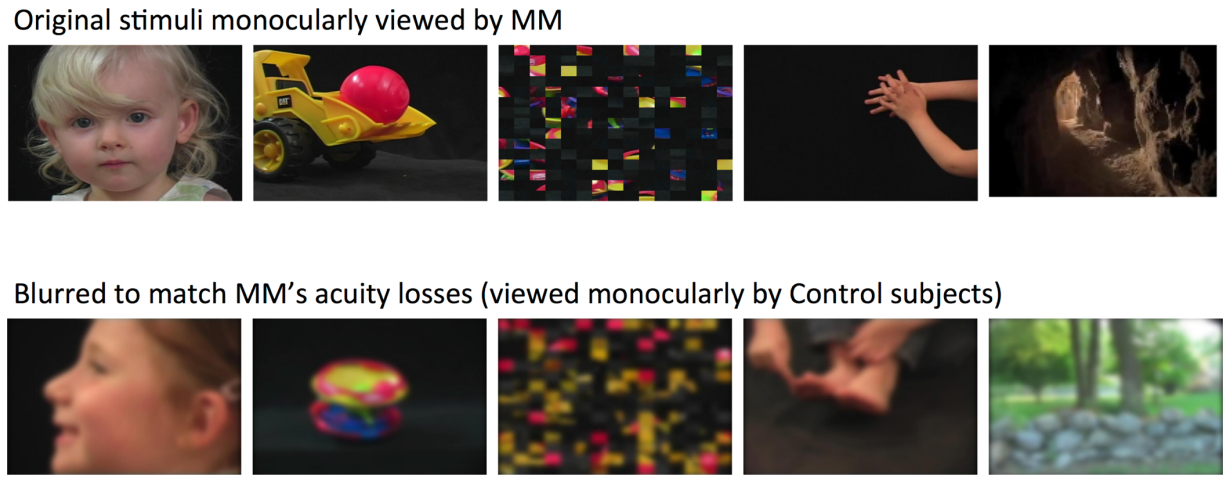

Figure 3.3. Example frames from the video clips used to examine category specific BOLD activity.

Each block lasted 18 s and consisted of six clips. Uniformly colored screens were used as a baseline and were presented at the beginning, middle, and end of each run. The blocks of movie clips in each run were presented in a palindromic order (e.g., one order used was cFSOBGcGBOSFc, where F = faces, B = bodies, S = scenes, O = objects, G = grid-scrambled objects, and c = uniformly colored screens). Each subject completed eight 234-s runs. Control subjects first completed four runs with an eye patch over the left eye. In these runs, the stimuli were blurred with a Gaussian filter to match M. M.'s psychophysically determined acuity. In the following four runs, control subjects binocularly viewed unblurred stimuli, which allowed us to directly assess the effects of blurring and monocular viewing on category-selective organization. M. M. always viewed unblurred stimuli with his remaining (right) eye.

Scanning was performed using a 3-T Allegra scanner with a 32-channel head coil at the Diagnostic Imaging Sciences Center at the University of Washington. High-resolution T1-weighted magnetization-prepared rapid-acquisition gradient-echo images were collected in 128 sagittal slices (repetition time, or TR = 7.6 ms, echo time, or TE = 3.5 ms, voxel size = 1 mm isotropic). BOLD images were acquired with a gradient-echo echo-planar

image sequence (TR = 1,500 ms, TE = 25 ms, flip angle = 75°, field of view = 220 × 220, voxel size = 3 mm isotropic). The acquisition window was positioned off axial to include the temporal and occipital lobes.

Structural MRI data were analyzed with FreeSurfer (Version 5.2; https://surfer.nmr.mgh.harvard.edu/) to construct cortical surface models for each subject. FsFast (Version 5.2; https://surfer.nmr.mgh.harvard.edu/fswiki/FsFast) was used to process fMRI data. Preprocessing involved motion correction using the 3dvolreg algorithm in the Analysis of Functional and Neural Images (AFNI) software suite (Cox & Jesmanowicz, 1999) and the FMRIB Software Library Brain Extraction Tool (Smith, 2002). Each functional run was then registered to that subject's cortical surface model using boundary-based registration (Greve & Fischl, 2009). A general linear model was used to estimate the cortical response to each experimental condition. Statistical contrasts were computed for faces and objects, objects and scrambled objects, bodies and objects, and scenes and objects. Contrast maps were assessed at a threshold of $|p| < .0001$, uncorrected, prior to further analyses, as in numerous previous studies of the ventral visual stream (Downing, Jiang, Shuman, & Kanwisher, 2001; Epstein & Kanwisher, 1998; Kanwisher & Dilks, 2013; Kanwisher, McDermott, & Chun, 1997; Malach et al., 1995). Data were not smoothed or normalized to a template.

3.3 Results

3.3.1 Behavioral experiments

M. M. discriminated images of cubes from incomplete and scrambled versions with accuracy greater than chance level, but his performance was significantly below that of control subjects, which suggests that M. M. remains impaired in 3-D form perception. Similarly, M. M.'s performance on a simple 2-D rotation task was higher than expected from chance alone, but significantly worse than control subjects' performance. When required to match 3-D forms at varying rotations in depth, M.M.'s performance was indistinguishable from chance and significantly below that of control subjects. M.M. correctly named several household objects, though significantly fewer than did control subjects, for whom the task was trivial. For both the gender- and emotion-classification tasks, M. M.'s performance was significantly worse than that of control subjects and not distinguishable from chance. Finally, M. M. showed no significant improvement in performance between 2003 and 2013 for any of the tasks. See Table 3.1 and Figure 3.2 for a summary of these results.

Table 3.1. M. M.'s Performance in the Six Behavioral Tasks Compared with Chance, Control Subjects' Performance, and M. M.'s Prior Performance

Comparison	Object recognition	Face classification: gender	Face classification: emotion	2-D shape constancy	3-D shape constancy	3-D shape recognition
M. M. vs. chance	—	.075 [–.14, .29]	.11 [–.085, .31]	.16* [.035, .28]	.12 [–.0081, .24]	.33** [.095, .56]
M. M. vs. control subjects	–.66** [–.81, –.51]	–.43** [–.58, –.27]	–.34** [–.53, –.16]	–.21** [–.32, –.11]	–.20** [–.31, –.088]	–.31** [–.49, –.14]
M. M. 2013 vs. M. M. 2003	.067 [–.15, .28]	–.13 [–.35, .099]	–.16 [–.41, .082]	—	—	—

Note: The table presents the difference in the proportion of correct responses and the corresponding 95% confidence intervals.
*p < .05. **p < .01.

3.3.2 fMRI EXPERIMENTS

Control subjects' responses to monocularly viewed, blurred stimuli and binocularly viewed, unblurred stimuli were qualitatively similar (data for the latter are not reported).

Face and object selectivity. Consistent with previous research (for a review, see Kanwisher & Dilks, 2013), our results showed that control subjects had robust category- selective responses for faces and objects within lateral occipital and ventral temporal cortex. Figure 3.4a and Figure 3.4b show data from the right hemisphere of 1 control subject (four runs with blurred, monocularly viewed stimuli). Data from the other hemisphere are in Supplementary Figure 3.1. Data from another control subject are in Supplementary Figure 3.5. As expected, a contrast between faces and objects (Figure 3.4a) isolated face-selective regions in the lateral occipital cortex (LOC), superior temporal sulcus, and fusiform gyrus in both control subjects. Similarly, a contrast between objects and scrambled objects revealed a typical pattern of object-selective regions (Figure 3.4b).

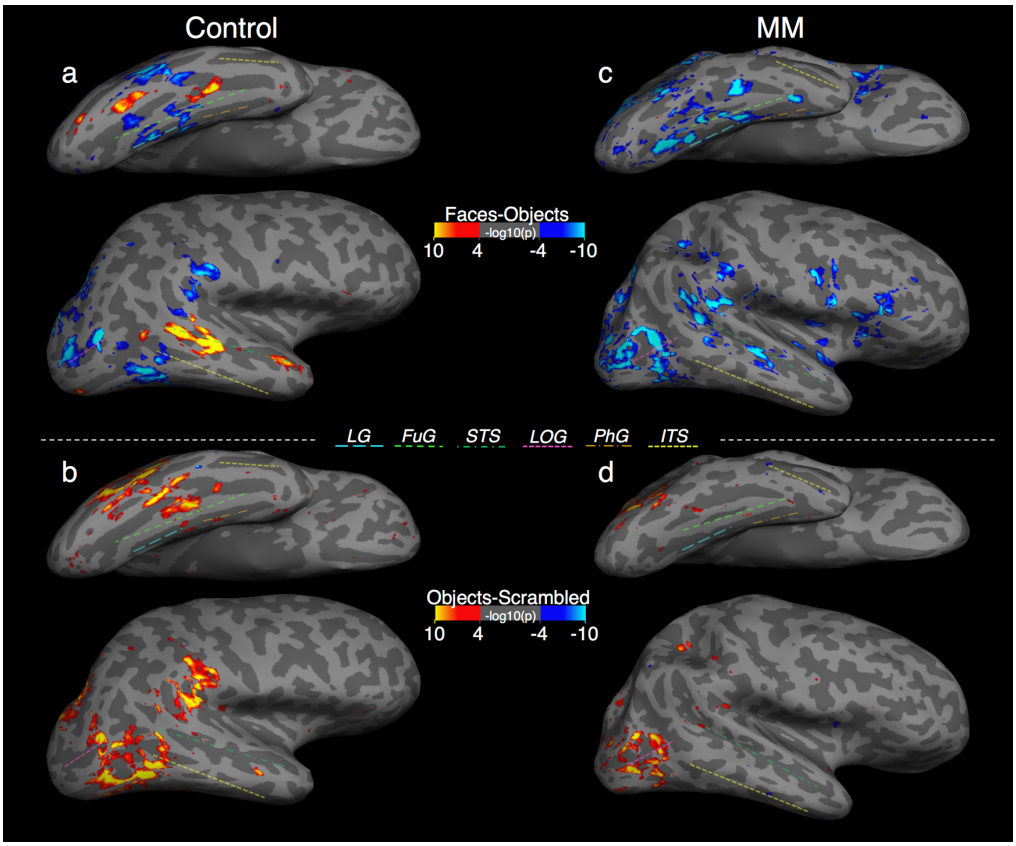

Figure 3.4. Face and object localizers for control subjects and M. M.

Ventral and lateral views of inflated right hemispheres showing results of the contrasts between faces and objects (a, c) and between objects and scrambled objects (b, d). Results are shown separately for 1 control subject (left column) and for M. M. (right column). Data were averaged across four scans (in which stimuli were blurred and monocularly viewed) for the control subject and eight scans for M. M. Results are displayed at a threshold of $|p| < .0001$. (See Supplementary Figure 3.1 for left-hemisphere activations in response to the same contrasts.)

In contrast, M. M. showed no evidence of face selectivity, even after more than a decade of recovered sight (Figure 3.4c). While some regions in ventral temporal cortex responded more to objects than to faces, these regions did not show a selective response to objects in a contrast between objects and scrambled objects (Figure 3.4d), which suggests that M. M. also lacks typical high-level object- selective cortical responses. With a very lenient threshold, there was some evidence for a highly attenuated object-selective response in the ventral temporal cortex, though this potential activity was not clearly differentiable from noise (see Supplementary Figure 3.3).

M. M. did show object-selective activity in the contrast of objects versus scrambled objects on the lateral surface in a location consistent with the object-selective region LOC. Given that M. M. has no difficulty discriminating different 2D shapes (Fine et al., 2003), this finding is compatible with those of previous studies suggesting that LOC encodes shapes without being involved with matching those shapes to stored object representations (Grill-

Spector et al., 1999; Kanwisher & Dilks, 2013; Kourtzi & Kanwisher, 2001; Malach et al., 1995), though we caution that our finding of relatively intact responses in LOC should not be taken as evidence for fully functional shape encoding.

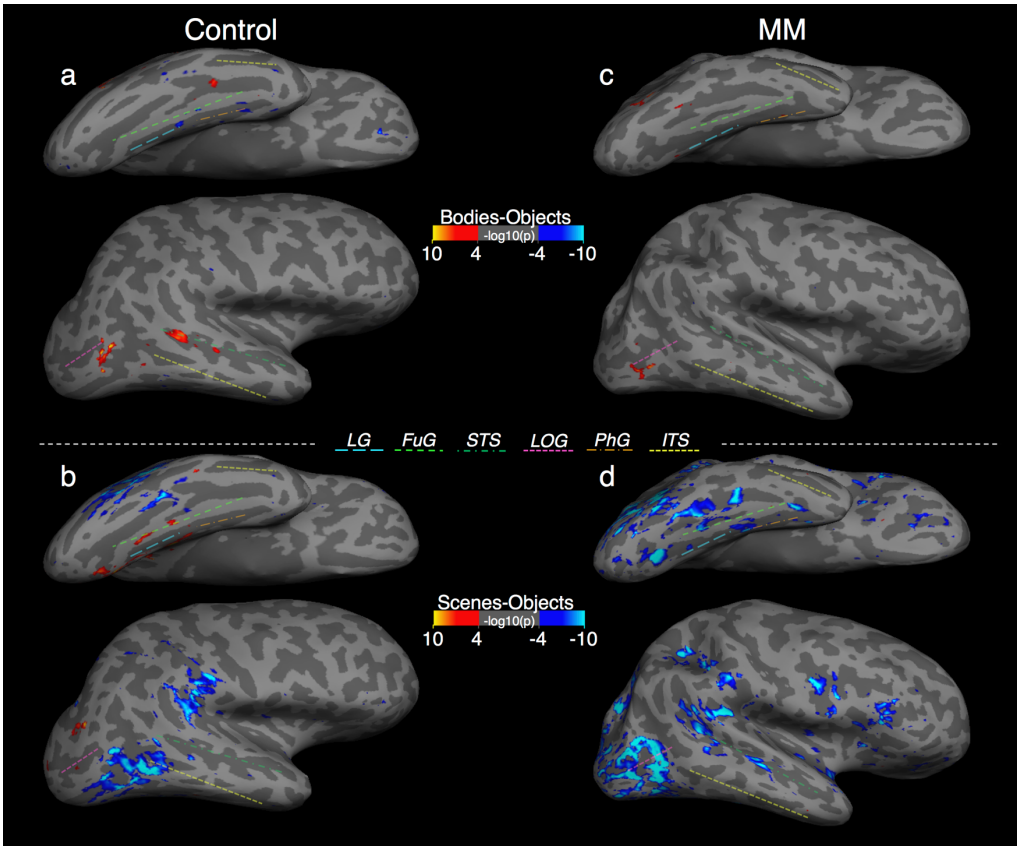

Figure 3.5. Body and scene localizers for 1 control subject and M. M.

Ventral and lateral views of inflated right hemispheres showing results of the contrasts between bodies and objects (a, c) and between scenes and objects (b, d). Results are shown separately for 1 control subject (left column) and for M. M. (right column). Data were averaged across four scans (in which stimuli were blurred and monocularly viewed) for the control subject and eight scans for M. M. Results are displayed at a threshold of $|p| < .0001$. (See Supplementary Figure 3.2 for left-hemisphere activations in response to the same contrasts.)

Scene selectivity. The contrast of scenes versus objects did not yield the expected results in our control subjects. Monocular viewing of blurred stimuli produced attenuated responses in the right parahippocampal cortex of 1 subject (Figure 3.5b), although this subject had a robust response in the left hemisphere (see Supplementary Figure 3.2). In a second control subject, we found very little scene-selective response for the blurred stimuli (see Supplementary Figure 3.6b and Supplementary Figure 3.6d). Both of these subjects showed typical responses to unblurred stimuli. It is possible that the lack of scene- selective response, particularly in the parahippocampal place area, results from a high-spatial-frequency bias in this region (Rajimehr, Devaney, Bilenko, Young, & Tootell, 2011). M. M. showed no scene-selective responses in either the lateral occipital or ventral temporal

cortex (Figure 3.5d) in either hemisphere (see also Supplementary Figure 3.2). At a lower threshold, we observed a small region consistent with the parahippocampal place area that responded slightly more to scenes than to objects, though this potential activity was not clearly differentiable from noise (see Supplementary Figure 3.4b and Supplementary Figure 3.4d).

Body selectivity. In control subjects, body-selective responses were evident in the lateral occipital and ventral temporal cortex (Figure 3.5a) in both hemispheres (see Supplementary Figure 3.2a; for the body-selective responses in the other control subject, see Supplementary Figure 3.6a and Supplementary Figure 3.6c). While we saw little evidence of the typical ventral temporal responses to bodies at a conventional threshold in M. M., we did observe body-selective responses in a region consistent with the extrastriate body area within the right hemisphere (Supplementary Figure 3.4c). There were no corresponding body-selective responses in the left hemisphere (see Supplementary Figure 3.2c). With a very lenient threshold, we did observe a region in a location consistent with the fusiform body area responding more strongly to bodies than to objects (see Supplementary Figure 3.4a and Supplementary Figure 3.4c), though these responses were again not clearly differentiable from noise.

3.4 Discussion

Visual function continues to develop throughout childhood and into early adolescence, with performance on tasks such as object recognition and face processing reaching adult-like levels between the ages of 5 to 8 and 4 to 6 years, respectively, while remaining sensitive to deprivation for several years afterward (McKone et al., 2012; Nishimura et al., 2009). Subject M. M.'s vision developed normally up to 3.5 years of age, after which he experienced an extended period of visual deprivation until his sight was restored well after adolescence. Thus, his case provides a unique opportunity to assess both the limits of plasticity in later adulthood and the influence of early vision on recovery from long-term blindness.

Tests carried out with M. M. shortly after surgery suggested that he had normal perception of color and motion, and only modest deficits in perception of simple form. M. M. shows essentially normal cortical responses to visual-motion stimuli (Fine et al., 2003), consistent with his behavioral sensitivity to motion cues, though these responses seem to coexist with auditory-motion responses not present in sighted individuals (Saenz, Lewis, Huth, Fine, & Koch, 2008). Consistent with M. M.'s ability to interpret simple 2-D forms, described first by Fine et al. (2003) and examined further here, our present results show relatively normal responses in the cortical region known as LOC, which has been implicated in the processing of object shape (Grill-Spector et al., 1999). One possibility is that spared perception of color, motion, and shape reflects hard wiring of these faculties; indeed, evidence suggests that this may be the case with basic color processing (Mancuso et al., 2009). Alternatively, preservation of these faculties may indicate that their periods of sensitivity to deprivation end prior to 3.5 years of age.

Several recent studies have suggested that cross-modal responses resulting from early blindness may follow an organization that is analogous to that of at least some high-level visual areas in normally sighted individuals. For instance, cortical regions typically associated with visual object processing have been implicated in object-size estimation in the congenitally blind (Mahon, Anzellotti, Schwarzbach, Zampini, & Caramazza, 2009), and these regions contain information about similarities in object shape in both sighted and blind participants (Peelen, He, Han, Caramazza, & Bi, 2014). Activity has also been reported in the visual word form area during Braille reading (Buchel, Price, & Friston, 1998; Reich, Szwed, Cohen, & Amedi, 2011), and the emergence of body-selective regions in congenitally blind subjects has been reported as a result of training with soundscapes representing bodies (Striem-Amit & Amedi, 2014). Similarly, activation of common regions during visual and haptic recognition of facial expressions in sighted and blind subjects (Kitada et al., 2013) suggests that haptic experience may be sufficient for development of these regions in the absence of visual input.

Although M. M. had normal sight until 3.5 years of age, the literature suggests that this is well within the period when some forms of cross-modal plasticity occur (e.g., Burton et al., 2002; Gougoux et al., 2009; Sadato, Okada, Honda, & Yonekura, 2002), and he shows robust cross-modal responses to auditory-motion stimuli (Saenz et al., 2008). However, we do not know the extent of cortical cross-modal responses in M. M. beyond these auditory-motion responses in cortical visual motion areas. Further, it is unclear whether any existing cross-modal responses would facilitate or interfere with restored visual function. As described previously, M. M. has essentially normal perception of visual motion, and his cortical responses to both visual and auditory motion are robust. In contrast, despite several years of early visual experience and more than a decade of recovered sight, M. M. remains profoundly impaired at interpreting visual facial expressions, which suggests that his haptic experience with faces and voice perception (Gougoux et al., 2009) did not lead to the preservation of neural architecture relevant for visual face recognition. Similarly, although we did observe relatively normal selectivity for bodies and objects within LOC, we found little to no evidence of high-level visual responses in ventral temporal cortex selective for face, body, scene, or object stimuli in M. M.

Shortly after recovering his sight, M. M. showed severe behavioral deficits in high-level visual tasks, and our follow-up tests revealed these to be long-standing impairments. When asked what challenges to vision remained in his daily life, M. M. replied, "I have learned what works with vision and what doesn't, so I really don't challenge my vision much anymore." M. M. now uses a combination of vision and other modalities for specific tasks. "This means where motion or color might be clues, I use my vision. Where details might be required, like reading print or recognizing who someone is, I use tactile and auditory techniques."

In conclusion, M. M. continues to show severe behavioral impairments in 3-D form, object, and face processing with no evidence of improvement of recognition performance even after more than a decade of recovered vision. These behavioral impairments are associated with highly attenuated category-selective activity in ventral visual

cortex, which suggests that adult high-level vision is based on a visual architecture that is still sensitive to deprivation at the age of 3 years and that has only limited plasticity in adulthood.

3.5 Supplementary Figures

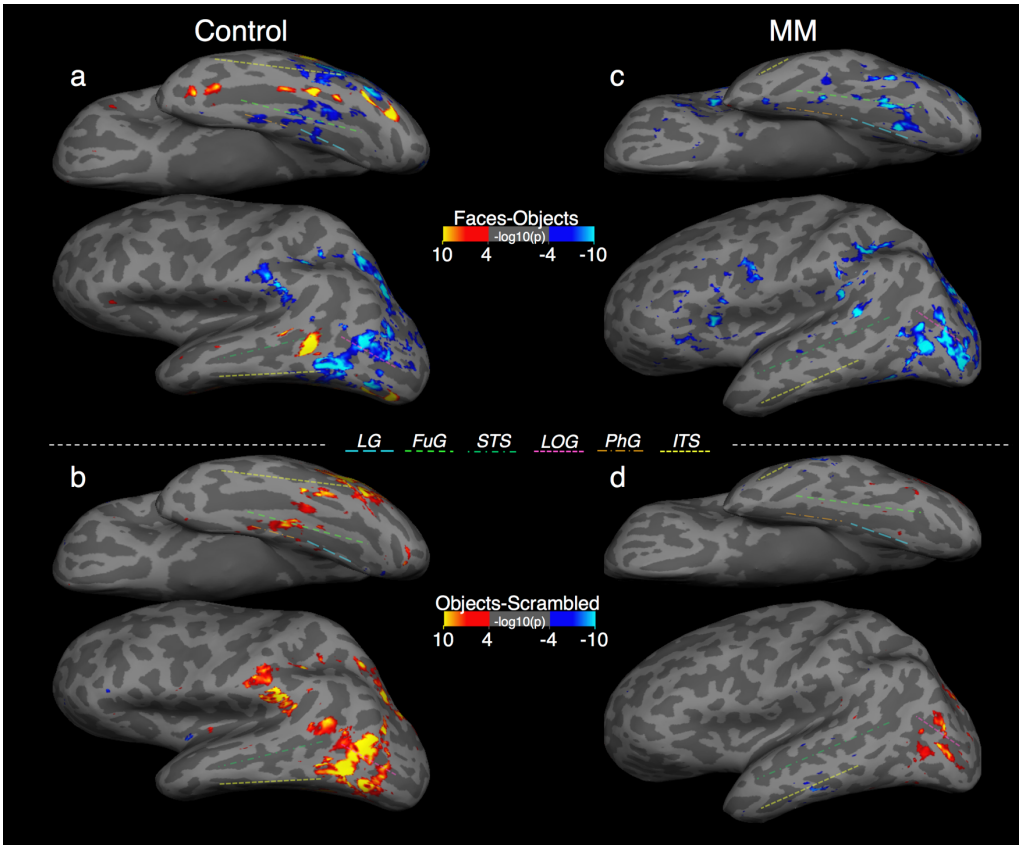

Supplementary Figure 3.1. Face and object localizers for the left hemispheres of 1 control subject and M. M.

Left hemisphere responses, thresholded at |p|<0.0001. *Faces vs. Objects (a, c)*: The control subject showed a typical pattern of regions giving greater responses to faces than objects in both the lateral occipital and ventral temporal cortex. In contrast, MM lacked category specific responses to the face stimuli. *Objects vs. Scrambled Objects (b, d):* The control subject showed a typical pattern of regions responding more to objects than scrambled objects in the lateral occipital and ventral temporal cortex. MM almost completely lacked category specific responses to object stimuli on the ventral surface, though he showed near normal object selective responses in the lateral occipital cortex. FuG: Fusiform gyrus; LG: Lingual gyrus; PhG: Parahippocampal gyrus; STS: Superior temporal sulcus; LOG: Lateral occipital gyrus; ITS: Inferior temporal sulcus.

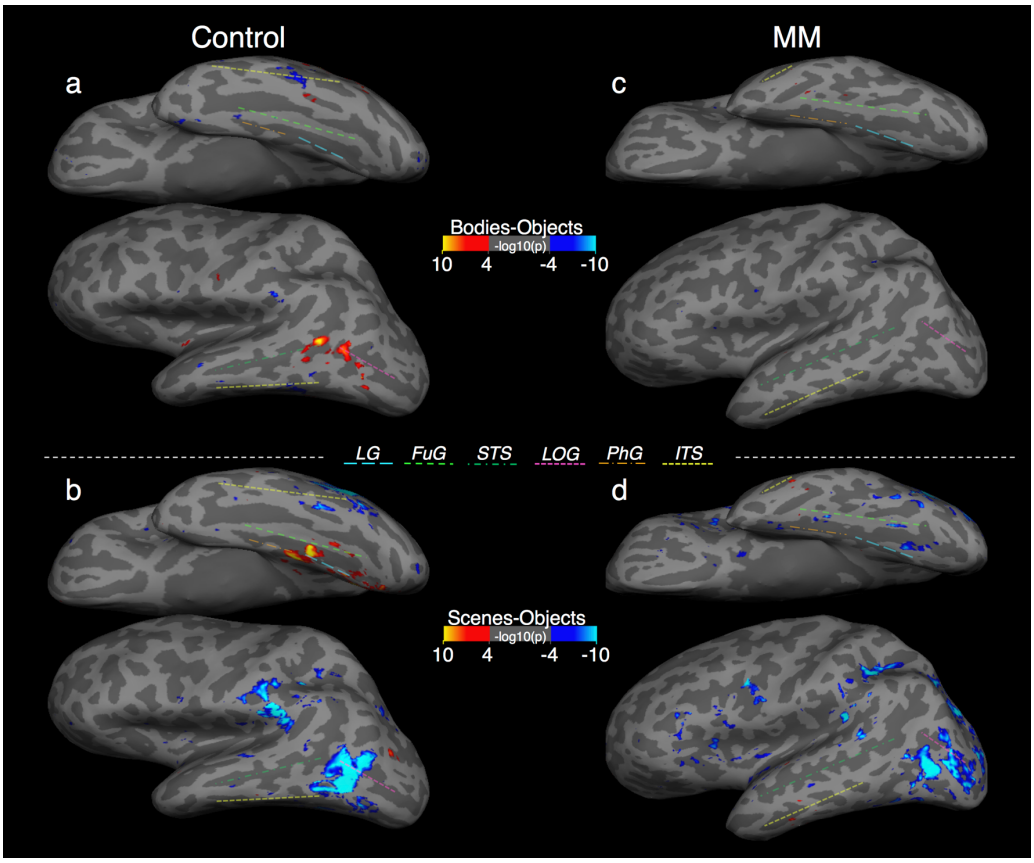

Supplementary Figure 3.2. Body and scene localizers for the left hemispheres of 1 control subject and M. M.

Left hemisphere responses, thresholded at |p|<0.0001. Bodies *vs. Objects (a, c)*: The control subject showed a typical pattern of regions giving greater responses to bodies than objects in both the lateral occipital and ventral temporal cortex. In contrast, MM lacked category specific responses to the body stimuli. *Scenes vs. Objects (b, d):* The control subject showed a typical pattern of regions responding more to scenes than objects in the lateral occipital and ventral temporal cortex. MM almost completely lacked category specific responses to scene stimuli on the lateral occipital or the ventral temporal cortex. FuG: Fusiform gyrus; LG: Lingual gyrus; PhG: Parahippocampal gyrus; STS: Superior temporal sulcus; LOG: Lateral occipital gyrus; ITS: Inferior temporal sulcus.

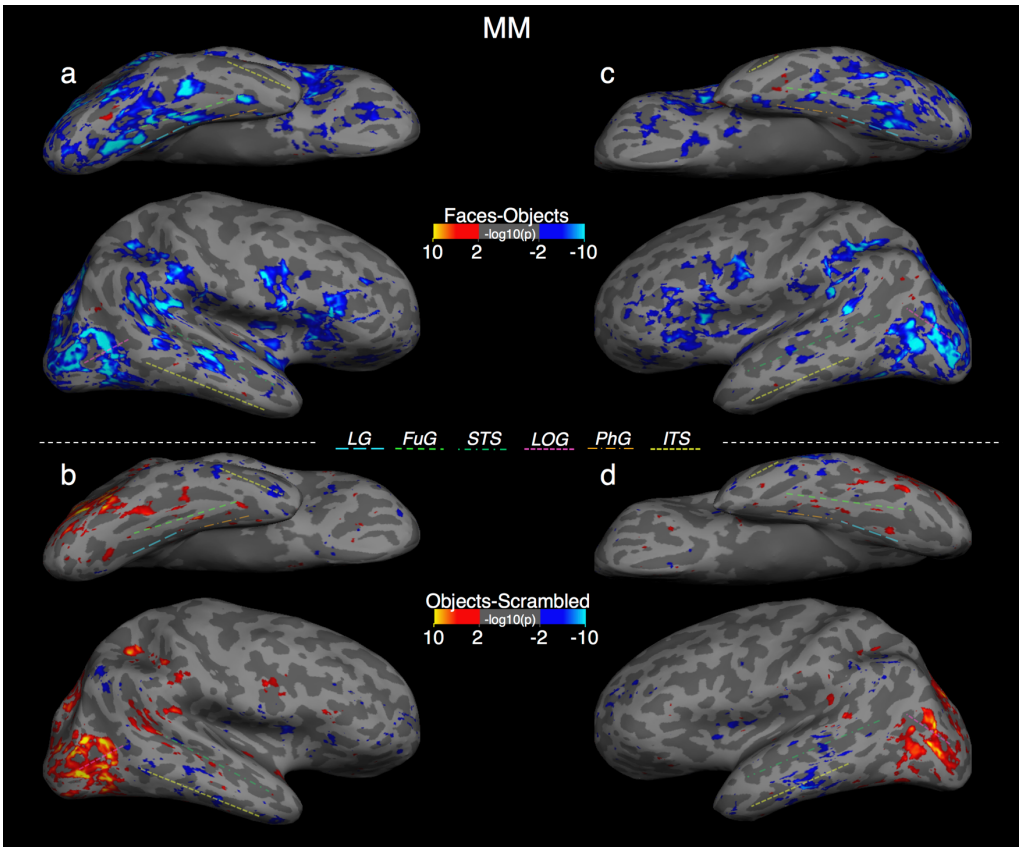

Supplementary Figure 3.3. Face and object localizers for M. M. with a lowered threshold

Right *(a)* and left *(c)* hemisphere responses to faces versus objects, thresholded at |p|<0.01. Even at a very lenient threshold, MM shows none of the typical category specific responses to the face stimuli. Right *(b)* and left *(d)* hemisphere responses to objects versus scrambled objects, thresholded at |p|<0.01. With a lowered threshold, there is some evidence for a highly attenuated object selective response in the ventral temporal cortex. FuG: Fusiform gyrus; LG: Lingual gyrus; PhG: Parahippocampal gyrus; STS: Superior temporal sulcus; LOG: Lateral occipital gyrus; ITS: Inferior temporal sulcus.

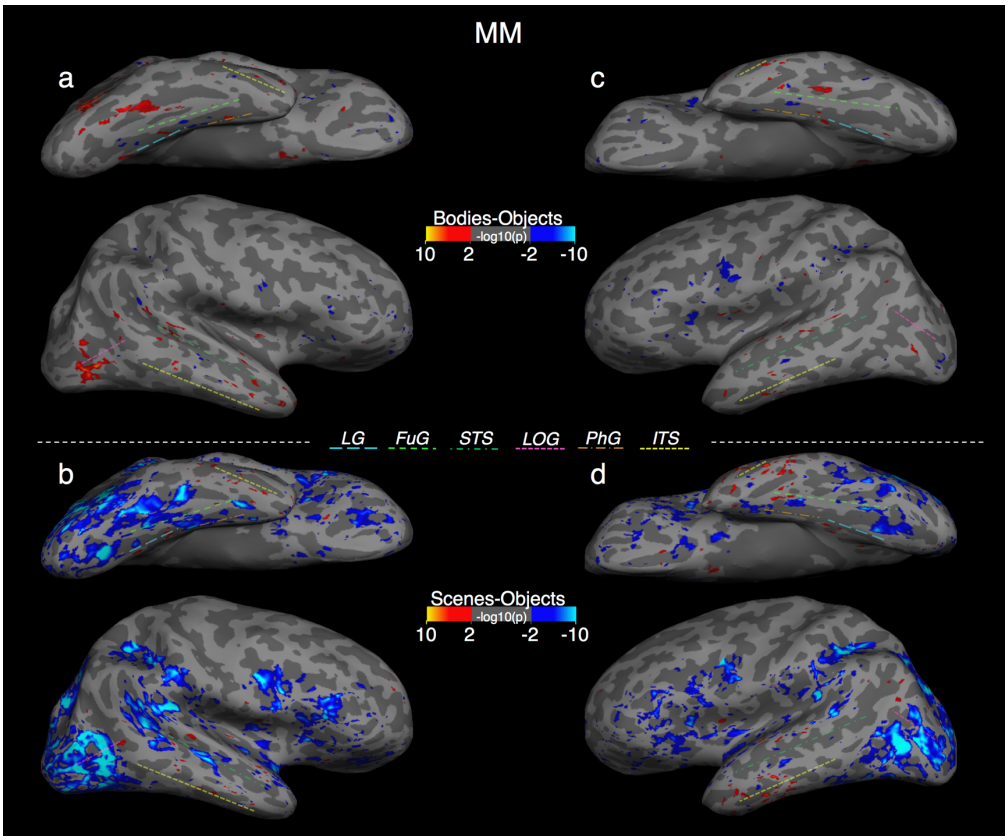

Supplementary Figure 3.4. Body and scene localizers for M. M. with a lowered threshold

Right *(a)* and left *(c)* hemisphere responses to bodies versus objects, thresholded at |p|<0.01. With a very lenient threshold, MM shows some evidence of category specific responses to the body stimuli in a region consistent with the Fusiform Body Area (FBA). Right *(b)* and left *(d)* hemisphere responses to scenes versus objects, thresholded at |p|<0.01. At a lowered threshold, there is an extremely attenuated scene selective response in the region consistent with the Parahippocampal Place Area (PPA). FuG: Fusiform gyrus; LG: Lingual gyrus; PhG: Parahippocampal gyrus; STS: Superior temporal sulcus; LOG: Lateral occipital gyrus; ITS: Inferior temporal sulcus.

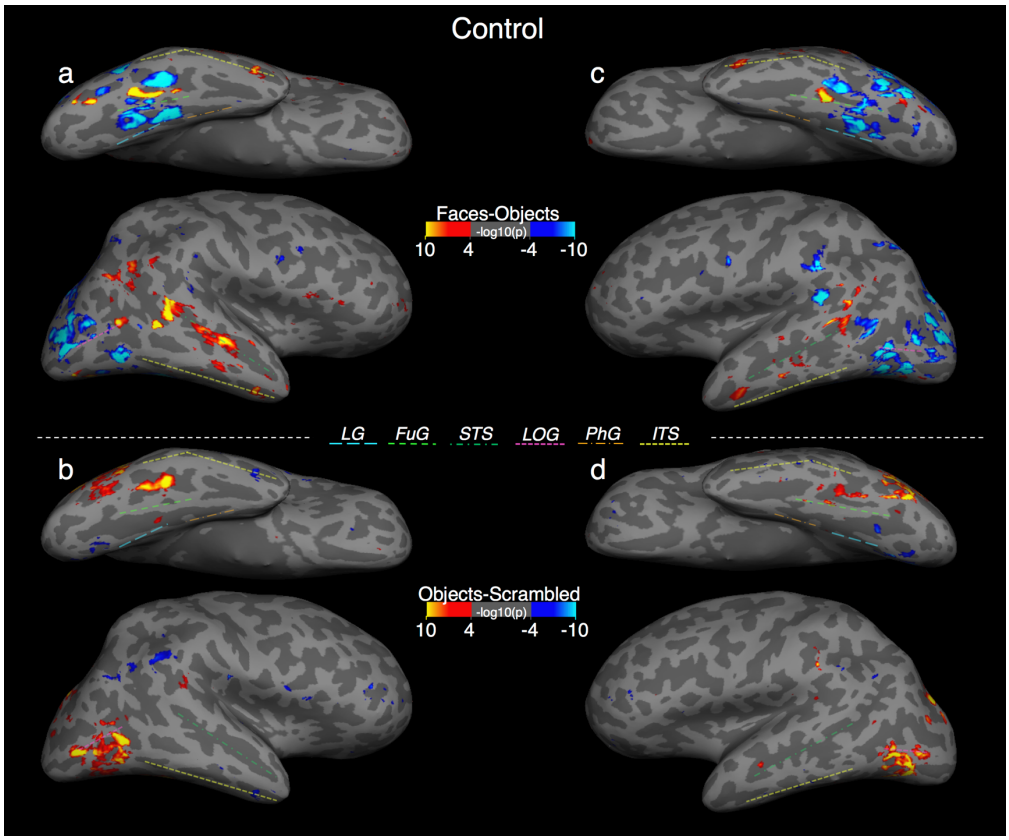

Supplementary Figure 3.5. Face and object localizers for a second control subject

Right hemisphere *(a,c)* and left hemisphere *(b,d)* responses, thresholded at |p|<0.0001. *Faces vs. Objects (a, c)*: The second control subject showed a typical pattern of regions with greater responses to faces than objects in both the lateral occipital and ventral temporal cortex. *Objects vs. Scrambled Objects (b, d):* The second control subject showed a typical pattern of object selective regions in the lateral occipital and ventral temporal cortex. FuG: Fusiform gyrus; LG: Lingual gyrus; PhG: Parahippocampal gyrus; STS: Superior temporal sulcus; LOG: Lateral occipital gyrus; ITS: Inferior temporal sulcus.

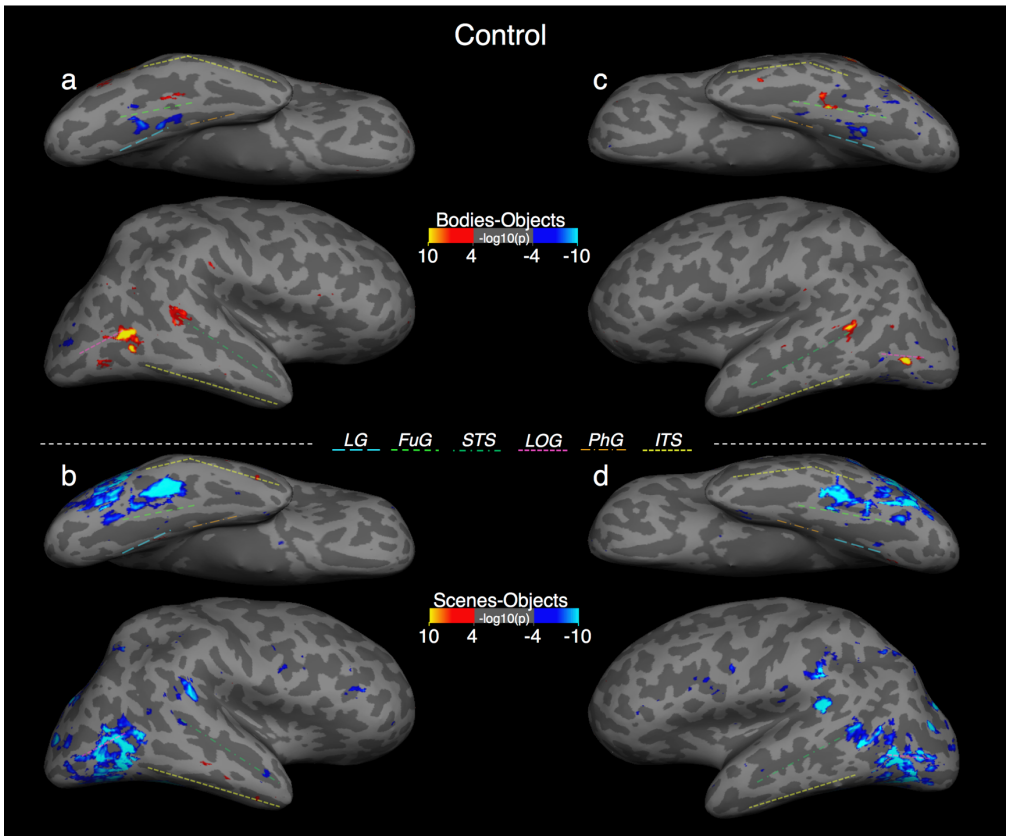

Supplementary Figure 3.6. Body and scene objects localizers for a second control subject

Right*(a,b)* and left *(c,d)* hemisphere responses, thresholded at |p|<0.0001. *Bodies vs. Objects (a, c)*: The second control subject showed a typical pattern of regions giving greater responses to faces than objects in both the lateral occipital and ventral temporal cortex. *Scenes vs. Objects (b, d):* The second control subject showed atypically little scene selective regions in the lateral occipital and ventral temporal cortex. FuG: Fusiform gyrus; LG: Lingual gyrus; PhG: Parahippocampal gyrus; STS: Superior temporal sulcus; LOG: Lateral occipital gyrus; ITS: Inferior temporal sulcus.

ToC

Chapter 4 : Parcellation Methods and Application to the Ventral Temporal Cortex

While evaluating the functional organization of the ventral temporal cortex in M. M., it became apparent that not only were there a lack methodological tools for understanding such a unique functional organization, but there were also large swaths of the ventral visual pathway in normally sighted subjects for which the functional organization remains unknown. The research reviewed in 1.6 Evidence for functional areas in the VTC suggested that functional areas may tessellate the ventral temporal cortex. However, there seems to be a lack of systematic approaches that could directly address whether there the VTC contains functionally coherent regions outside of the known category-selective regions. The next chapter introduces a novel, data-driven method for investigating whether the VTC consists of a series of functionally coherent regions. While the method has no information regarding the spatial distribution of these responses, applying it to the VTC results in a series of fully-filled contiguous patches on the cortical surface. In other words, the method results in a functional parcellation of the ventral temporal cortex. This chapter addresses the other approaches to parcellation, and in particular what these approaches might reveal about the organization of the ventral temporal cortex.

Parcellation of the cerebral cortex is a challenging problem for which there is currently no consensus exists regarding appropriate methods, criteria for replicability, criteria for establishing validity, appropriate null models, or even the appropriateness of parcellating cortex into a single set of discrete regions. Parcellation methods exist for many aspects of brain organization, though it is unclear how well these parcellations correspond or how differences between parcellation based on different aspects of brain organization (such as histology and connectivity patterns) should be interpreted where they provide differing results.

This review will address parcellation approaches based on anatomical structure, structural connectivity, myeloarchitecture, cytoarchitecture, receptor architecture, resting-state correlations, functional responses, and topographic organization. As the latter three methods are based on neural responses and are thus more directly relevant to the work in the following chapter, these will be considered in greater detail.

4.1 Gross Anatomical Parcellations

There are two general approaches to anatomical parcellation. The goal of the first approach is to parcellate the cortical surface into descriptive labels for gross anatomical features while the goal of the second approach is to label cortical areas based on systematic correspondences to anatomical features such as cortical folding patterns.

Currently, the most well-validated automated anatomical parcellations are implemented in the FreeSurfer package (http://surfer.nmr.mgh.harvard.edu/). The Desikan-Killiany atlas parcellates the cortical surface into

34 regions based on gyral nomenclature (Desikan et al., 2006). While this approach provides an efficient way to create unambiguous labels with relatively high reliability, the anatomical regions are substantially larger than the orientation information typically given in a neuroimaging article when describing a cortical location.

A more detailed an automated parcellation method was introduced into FreeSurfer in 2005 to assign each location on the cortical surface to a particular sulcus or gyrus (Fischl et al., 2004). A more sophisticated version of this method was introduced in 2009 and described the following year (Destrieux, Fischl, Dale, & Halgren, 2010). This atlas provided a parcellation into 74 regions which correspond to particular sulci and gyri based (as well as regions such as the occipital and temporal poles) on a previously established nomenclature (Duvernoy, 1991). The accuracy of this method rivals the interrater reliability of manual labeling by neuroanatomists. These gross anatomical labels provide an efficient, standardized method for referring to discrete cortical regions, though regions in most cases are purely based on gross anatomy and do not correspond to the established cortical areas.

However, that is not to suggest that cortical folding patterns are unrelated to cortical areas. The FreeSurfer package also provides discrete and probabilistic regions of interest which correspond to cytoarchitectonic regions and well-established cortical areas. FreeSurfer also includes functions which predict a subset of the more reliable cytoarchitectonic areas initially described by Korbinian Brodmann (Brodmann, 1909) based on the patterns of cortical folding of individual brains (Fischl et al., 2008). Subsequently, a method was introduced into the FreeSurfer package that would predict the boundaries of primary visual cortex based on folding patterns that was comparable to the interrater reliability for the boundary based on myeloarchitecture as well as functional definitions using retinotopic mapping (Hinds et al., 2009).

4.2 Cytoarchitectural Parcellations

The laminar profiles of neuron shape and density are relatively distinct across many cortical areas. Through various methods of histological staining of cortical slices, these characteristics have been widely studied by neuroanatomists since the turn of the last century, and cortical cytoarchitectonic maps developed by Korbinian Brodmann are still in use today. While Brodmann's map is the most widely known, there have been several attempts to develop cytoarchitectonic parcellations of the cortex (see Figure 4.1).

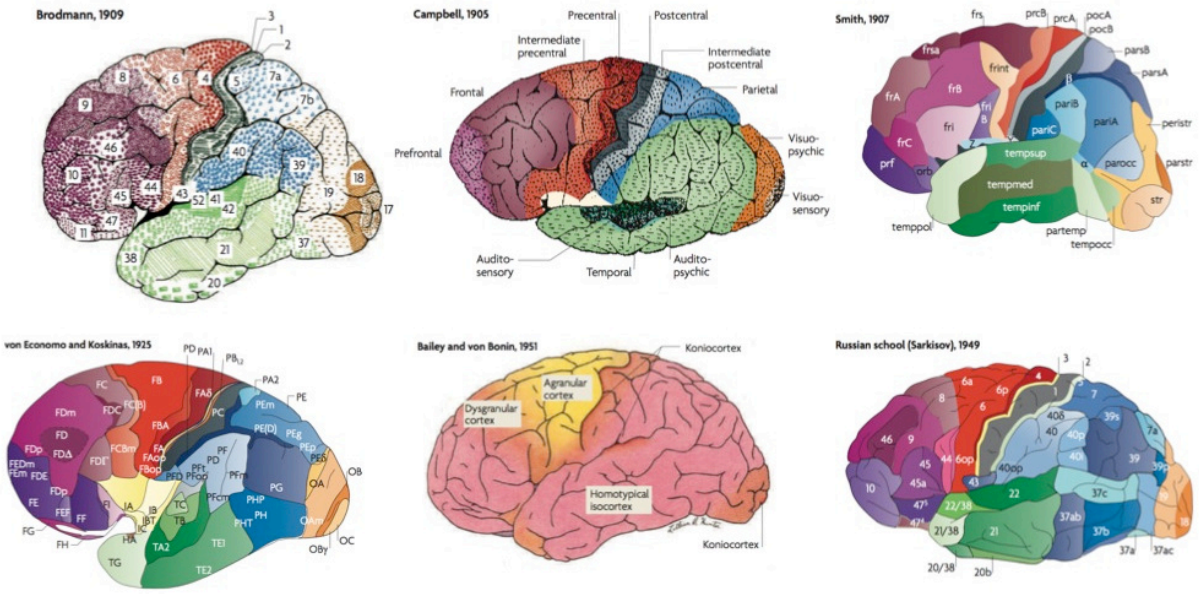

Figure 4.1. Cytoarchitectonic parcellations

Multiple groups have attempted to parcellate the brain on the basis of cytoarchitecture. Colors of areas have been modified to correspond to the Brodmann map. Adapted from (Zilles & Amunts, 2010)

While most parcellations agree on particular distinctions, particularly near primary sensory and motor areas, there is also widespread disagreement for particular regions and borders. Unfortunately, it is difficult to know whether the differences in parcellation between research groups were due to differences in methodology, differences in the donor brains, or differences in the renderings (e.g., borders from within sulci were often drawn on gyri).

Modern anatomical techniques (Amunts et al., 2013; Ding et al., 2016) allow the brain to be sectioned and computationally studied in unprecedented detail. In particular, the development of observer-independent quantitative cytoarchitecture mapping (Schleicher et al., 2009) has provided the ability to do unbiased analysis of both within and between subject patterns of cortical microstructure. Recently, a series of studies have begun the process of developing a parcellation of the ventral temporal cortex based on laminar patterns of cell size and density. (Caspers et al., 2014; Caspers et al., 2013; Lorenz et al., 2017; Weiner et al., 2014; Weiner & Zilles, 2015). An important application of this technology to vision science was the delineation of two previously undescribed areas on the posterior portion of the fusiform gyrus (Caspers et al., 2014). These cytoarchitectonic domains predictably align to the mid-fusiform sulcus (Weiner et al., 2014; Weiner & Zilles, 2015).

The previously mentioned research explicitly focused on the ventral temporal cortex, which is rare in most parcellation research. This focus provides substantially more detail for comparing parcellations of the visual system and relating them to known category-selective regions. These parcellation results support the existence

of four cytoarchitectonic domains in the posterior ventral temporal cortex, FG1, FG2, FG3, and FG4. Data from individual subjects suggests a boundary along the mid-fusiform sulcus (Weiner et al., 2014), which separates two pairs of increasingly anterior cytoarchitectonic domains (Lorenz et al., 2017). However, their posterior to anterior borders do not seem likely to correspond to known functional or structural subdivisions of the cortex. Interestingly though, when the cytoarchitectonic profiles of the VTC parcels and surrounding regions are hierarchically clustered, there are greater similarities between the two posterior areas and between the two anterior areas than across the mid-fusiform sulcus that separates both pairs, and has figured so prominently in the comparison of other modalities (Grill-Spector & Weiner, 2014).

Functional data has not yet been collected for any subjects whose cytoarchitectonic data later became available. As a result, the spatial extent and anatomical locations of known category-selective regions can only be qualitative compared with these cytoarchitectonic domains. It seems likely that each of the functionally-defined regions will be contained within a single cytoarchitectonic region. However, each of the cytoarchitectonic regions is considerably larger than any functionally defined regions. Thus, cytoarchitectonic domains likely contain more than one functional area (Lorenz et al., 2017; Weiner et al., 2017).

4.3 Myeloarchitectural Parcellations

The correspondence between differences myelination patterns within cortical layers and particular functional properties has a long history for the identification of particular brain areas. In the visual system, both area MT (Bridge, Clare, & Krug, 2014) and area V1 (Hinds et al., 2009; Trampel, Bazin, Pine, & Weiskopf, 2017) are known to have particularly noticeable myeloarchitectonic differences from neighboring areas. The heavy myelination of layer 4 in the primary visual cortex is so distinct that it has been widely referred to as striate cortex. The first myelin parcellations were at least 100 years ago. However, it has only been comparatively recently that full brain parcellations based on cortical myelin have been possible for living subjects.

The amount of myelin effects both T1-weighted and T2-weighted images, though in different directions. Taking the ratio of T1w to T2w images compensates for bias in MR image intensity, increases the myelin signal's contrast to noise ratio, and results in a reasonable proxy for cortical white matter concentration. Previous neuroanatomical results suggest that most cortical areas have a spatially consistent pattern of laminar myelination and that this pattern tends to differ between neighboring areas. As these findings would predict, the gradient of the T1w/T2w maps largely agree with the boundaries coregistered atlases of cortical areas (Glasser & Van Essen, 2011).

A full parcellation is never shown in this paper, which concludes with caveats and a future direction of combining this technique with other data from the Human Connectome Project to create a multimodal parcellation. While myeloarchitecture may not fully disambiguate all cortical areas, it is possible that the regions

in which the approach performs poorly may be those which exhibit greater individual variability in size and position.

The majority of the results in this paper come from data that has been spatially smoothed, normalized to a template, averaged across subjects, and averaged across hemispheres. All of these methodological choices have been shown to produce poor results in regions such as the pars triangularis (Fedorenko, Duncan, & Kanwisher, 2012) and fusiform gyrus (Weiner & Grill-Spector, 2013). Results are only shown for the posterior portion of the ventral temporal cortex. No obvious subdivisions correspond to known VTC functional areas, though there is evidence for a higher myelin content medial to the mid-fusiform sulcus and a general decrease in myelin proceeding posterior to anterior along the fusiform gyrus.

4.4 Receptor Architecture Parcellations

The cerebral cortex is a layered structure mostly consisting of the six-layered isocortex. Across layers, different cell types express different receptor types. As these receptors are involved in different functional roles, regions which differ in function are also likely to differ in the laminar distribution of receptor types. The distribution of each receptor can be observed in serial cryostat sections using specific radiolabeled receptor ligands through a process known as quantitative receptor autoradiography (Geary & Wooten, 1989).

When compared with neuroanatomical methods such as cytoarchitecture or myeloarchitectural parcellation, receptor autoradiography seems to identify the same boundaries. Often such a boundary can be seen for all measured receptor types. However, in other cases, only a subset of receptors types in certain layers will differ across area borders. Most interestingly, there are clear boundaries revealed by receptor architectonics that are not apparent in either cyto- or myeloarchitecture (Zilles, Palomero-Gallagher, & Schleicher, 2004). These findings, along with the close link between brain function and receptor architecture, argue that receptor architectonics are a more meaningful type of parcellation than other neuroanatomical methods (Zilles & Amunts, 2009).

A subsequent study performed quantitative *in vitro* receptor autoradiography in two cytoarchitectonic regions of the ventral temporal cortex. However, despite examining several receptor types, the researchers were unable to find a subdivision of the cytoarchitectonic areas that would likely correspond to known category-selective regions. However, their results did support the division between FG1 and FG2 (Caspers et al., 2015). To date, there are no published parcellations of the VTC based on receptor architecture.

4.5 Connectivity-Based Parcellations

Another observation that has led to parcellation methods is that long-range white matter connections tend to originate from and terminate in distinct regions. The organized axon bundles that constitute the long-range corticocortical projections are relatively stereotyped across individuals, particularly for those associated with primary sensory and motor areas (Yendiki et al., 2011). While there seems to be greater variability in the projections to association areas of cortex, recent research has demonstrated that the cortical locations of the idiosyncratic 'category-selective' regions of the ventral visual pathway can be predicted based on white matter pathways (Osher et al., 2015; Saygin et al., 2012). This association suggests that individual differences in fiber pathways correspond to individual differences in cortical position functional areas. Thus, parcellation based on connectivity may be particularly likely to correspond to those based on response characteristics.

The basic approach shared by most connectivity-based parcellation method is to establish a 'connectivity fingerprint' for each parcel, such that all locations in the parcel have white matter fibers pathways. A recent analysis demonstrated that a neighborhood-based similarity metric results in automated DTI fiber segmentation that more closely matches tracts as defined by neuroanatomists (Siless, Chang, Fischl, & Yendiki, 2018), though this method has yet to be widely adopted. The simplest of these approaches greedily merges locations based on similarity in average connectivity to create a hierarchy which is then cut at a certain depth to create the clusters, while other approaches explicitly take into account the adjacency relationships and search for discontinuities in the similarity of projections (Eickhoff, Thirion, Varoquaux, & Bzdok, 2015). Others combine these two approaches by finding an optimal clustering with the constraint that parcels be contiguous (Baldassano, Beck, & Fei-Fei, 2015).

4.6 Resting-State Parcellations

In the mid-1990's, it was observed that low-frequency BOLD oscillations (<~.1 Hz) were correlated (see Figure 4.2) across functionally related though spatially distant regions of cortex (Biswal, Yetkin, Haughton, & Hyde, 1995). This approach came to be known as functional connectivity MRI (fcMRI), or, in studies where the participant is not presented with stimuli or given an explicit task, resting-state fcMRI (rs-fcMRI) (Raichle, 2009). While it took some time for this methodology to catch on in the neuroscientific community, the recent rate of publication for resting-state articles has been increasing exponentially. Independent Components Analysis (ICA) of fs-fcMRI became a popular basis for studying this phenomenon, and a subset of the ICA components was found to be replicable across subjects (Damoiseaux et al., 2006).

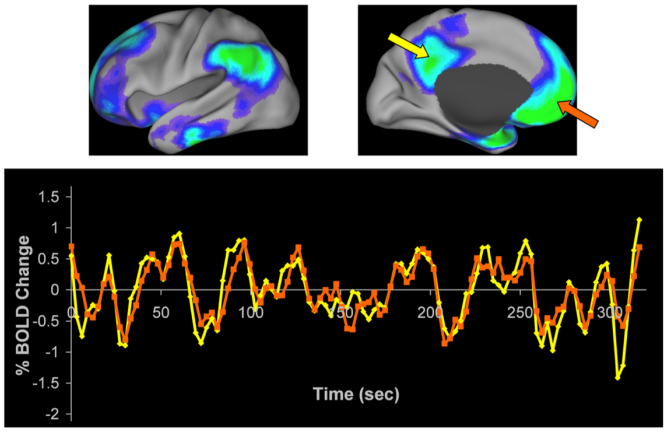

Figure 4.2. the basis of resting state fcMRI

Top: regions correlated with the location indicated by the yellow arrow with regions in green most highly correlated. Bottom: time courses from the locations indicated by the yellow and orange arrows. Adapted from (Raichle, 2009)

Here, the evidence that rs-fcMRI can provide information about cortical functional organization will be discussed. Several potential criticisms of this approach will be addressed. Finally, recommendations will be given for evaluating whether particular rs-fcMRI analysis results reflect neuronal functional organization. Subsequently, a number of other studies would link differences in resting state networks with a range of disorders (Baggio, Segura, & Junque, 2015; Filippi, Agosta, Spinelli, & Rocca, 2013; Hafkemeijer, van der Grond, & Rombouts, 2012; Karbasforoushan & Woodward, 2012; Li et al., 2015; Luo et al., 2015; Marchetti, Koster, Sonuga-Barke, & De Raedt, 2012; Poston & Eidelberg, 2012; Schmidt et al., 2014; Sorg, Gottler, & Zimmer, 2015; Sutherland, McHugh, Pariyadath, & Stein, 2012; Tracy & Doucet, 2015).

4.6.1 Some Caveats Regarding the Interpretations of rs-fMRI

As resting-state analyses derive from BOLD data, they constitute an inherently indirect measure of associations in neural activity (Buckner, Krienen, & Yeo, 2013). While some of the evidence reviewed above suggests that certain aspects of resting-state networks reflect functional connectivity in neural networks, there remains the possibility that some of the structure that is seen in fcMRI is a result of the vasculature or other confounding factors.

The signal-to-noise ratio for fMRI is relatively low, and there are multiple sources of variability in the signal unrelated to the neural activity of interest. In conventional task-based fMRI studies, this can be partially compensated for in ways that are not available with fcMRI methods. For example, nearly all task-based studies leverage some form of averaging across trials or presentations, and model-based approaches allow for relating the signal to the temporal onset of events. Since there are no external indications of the identity or onset of particular neural processes, in fcMRI this cannot be achieved.

Several groups have noted that signal correlations change over time, not only across sessions but within sessions. While particular processing methods may be able to achieve stable results under these conditions, it suggests that unlike patterns of anatomical connectivity or stable patterns of functional organization, fcMRI is more dynamic than typically portrayed. While some of these fluctuations may be cognitively meaningful, and thus neutrally based (Madhyastha, Askren, Boord, & Grabowski, 2015), there may also be aspects of the data that fluctuate due to sources of variability like scanner or physiological noise. Specifically, it has been noted that these networks change as a function of physical, cognitive, and biological states such as having eyes open verses closed [bianciardi 2009], being awake verses asleep [Horovitz 2009], resting verses recalling [Shirer 2011], and whether or not one has had a coffee [Wong 2010]. While nature of the states that elicit the differences suggests that they are in fact signals of neural origin, they are more reflective of the dynamic functional state rather than indicators of the structure of the brain's functional organization.

As with other investigations of functional organization, individual differences in anatomy have to be respected in order to achieve unambiguous results (Weiner & Grill-Spector, 2013). While much of the work on resting-state has involved admirably large numbers of subjects, group-level analysis and the associated methods likely degrade the information in the data beyond interpretability. A related point comes from a recent intensive study on a single subject (hundreds of hours of scan time) which found that within-subject patterns of variability among networks was opposite to that from group rs-fMRI (Laumann et al., 2015). This both highlights the dynamic nature of these networks, particularly for relatively short scans, and emphasizes the importance of how anatomical variability when not properly coregistered can degrade information at the group level that is stable at the subject level. Since the anatomical locations of functional areas likely have idiosyncratic location between individuals, the results of group analysis should be evaluated with extreme caution. The results reflect a combination of how well regions delineated by rs-fMRI correspond to cortical anatomy and the particular algorithms used to map between subjects and the group space. Given the relationships that have been demonstrated between other measures of cortical organization and cortical folding patters, any reasonable attempt at evaluating group data should use minimally surface-based registration methods.

One remaining concern is that part of the fcMRI signals is due to systemic low-frequency oscillations in blood flow. One study investigated this by using near-infrared spectroscopy measured in the finger to produce a 'seed' and found that they could resting-state networks that strongly resemble those of primary areas (Tong et al., 2013).

They further showed that with different lags, the NIRS signal was connected with several components from and ICA analysis of the simultaneously acquired BOLD data. While these authors do suggest methods for addressing this particular issue, it suggests that particular attention should be paid to the preprocessing in fcRMI research.

Finally, the results from a very different approach to examining brain function have suggested that intrinsic fluctuations in the BOLD signal may be obscuring information about the underlying neural representations and inflating the difference in the response of comparable brain regions between subjects. Representational Similarity Analysis (RSA) is an approach that examines the similarity in responses within a region of interest to large sets of stimuli in order to determine the extent to which an area considers particular pairs of stimuli as different. This method allows for comparing regions across subjects without concerns about the alignment of anatomy (as long as corresponding regions have been appropriately selected). Typically, this analysis is done with a single dataset, however, a recent study showed that when the correlations are made between independent splits of the data, the similarity between regions within a subject decreased (e.g. the similarity between V1 and LO). Perhaps more importantly, the similarity between the same region in different subjects increased (L. Henriksson, Khalighi-Razavi, Kay, & Kriegeskorte, 2015). This finding suggests that there are aspects of the spontaneous low-frequency oscillations that not only are unlikely to be indicative of underlying neural activity but may create patterns of apparent functional connectivity which are not neutrally based.

4.6.2 Parcellation Results

Much of the literature on parcellation is currently being produced for resting-state data. A diversity of clustering approaches are being explored, including edge-detection methods (Cohen et al., 2008), spatially-constrained hierarchical clustering (Blumensath et al., 2013), spatially-constrained spectral clustering (Craddock, James, Holtzheimer, Hu, & Mayberg, 2012), and resting-state-functional-connectivity (RSFC)-snowballing (Wig et al., 2014). The goal of these parcellations has generally been to provide seed regions for connectomics or nodes for functional connectivity analysis.

Some methods for parcellating individual subjects show impressively high dice coefficients, however, upon closer inspection, these methods are often doing something other than detecting parcel structure. For example, one study reporting individual parcellation with dice coefficients near .8 was merely mapping 18 'networks' onto individual subjects with iterative refinement (D. Wang et al., 2015). The networks they used came from a previous study (Yeo et al., 2011) where the parcellation came from smoothed, highly down-sampled resting-state data averaged over hundreds of subjects. Parcellation into a higher number of regions (758) produces similar metrics of correlational structure and sparseness (Dornas & Braun, 2018). Both Wang et al and Yeo et al use parcellations that group all much of the occipital and temporal lobe into one or a small number of parcels, and when they do so, these often subdivide known cortical areas, such as breaking early visual cortex into

increasingly peripheral eccentricity bands. These borders are both orthogonal to the actual area boundaries and a segmenting along a continuum rather than at some kind of functional border. As a result, while this approach tells us something about brain organization, its mapping onto functional regions is not satisfactory.

Few if any fcMRI compare their parcellations to well-characterized functionally-defined areas within the VTC, such as face or scene areas. Most articles do not even show the ventral surface of the brain. The approach described in the following chapter was designed to emphasize the stimulus-driven component of the BOLD response by using a naturalistic, stimulus-driven paradigm and estimating responses using a GLM that accounted for the hemodynamic response, repeated stimulus presentations, and nuisance repressors. It is an interesting question how well resting-state parcellations within the VTC will correspond with parcellations based on functional preferences given that resting-state analyses evaluate very low frequency (< .08 Hz) BOLD fluctuations (Power, Schlaggar, & Petersen, 2014) which likely contain components not driven by task-related neuronal responses (Tong et al., 2015).

4.7 Functional Parcellation

The neurons of the currently identified cortical areas have distinct functional properties, and it is plausible that all other aspects of cortical organization serve to bring about these functional roles. Until comparatively recently, the closest thing to a functional parcellation of the ventral temporal cortex was a collection of the known category-selective regions, identified with the localizer method. These regions collectively constituted a minority of the ventral temporal cortex. The coverage was limited to those areas which had been discovered by hypothesis-driven research, stimuli needed to be carefully designed for the relevant condition contrasts, and the contrasts were carried out averaging over stimuli within each category.

One line of fMRI research has attempted to identify functional regions by clustering locations (in their case voxels) based on beta-weight estimates to individual stimuli (Lashkari, Sridharan, & Golland, 2010; Lashkari, Sridharan, Vul, et al., 2010; Lashkari et al., 2012; Lashkari, Vul, Kanwisher, & Golland, 2008; Vul, Lashkari, Hsieh, Golland, & Kanwisher, 2012). However, their research to date has been restricted to categorical stimuli. It is unclear how well their approach will generalize to the diverse naturalistic stimuli that are likely needed to understand the representational content of uncharacterized regions of VTC.

Their algorithm characterizes voxel responses as hyper-dimensional clusters in a response space (Lashkari et al., 2008; Vul et al., 2012); assuming that voxels can be described either as mixtures of (independently and identically distributed) activation profiles for pre-specified categories, or as a circular Gaussian around a 'canonical selectivity profile'. Generalization to more diverse representational topologies would significantly add to the complexity of their algorithm, which is already quite complex.

A critical limitation of these assumptions is that the algorithm cannot individuate regions which do not differ in their univariate responses. For example, their approach characterizes the three ventral face areas (see Figure 5.7) as a single 'face system' (e.g. Lashkari et al., 2008; Vul et al., 2012). While their approach reveals that these areas are functionally related, it is not sensitive to the important functional differences between these regions (see section 5.4.1 below).

Importantly, and in contrast to most other work on parcellation, they do compare their results to category-selective regions identified using the localizer method (Lashkari et al., 2008), which is currently one of the only methods available for establishing the validity of a parcellation for the ventral temporal cortex. A substantial contribution of this work is the demonstration that the known category-selective regions are identified by all versions of their algorithms, which supports the notion that these are genuine functionally distinct regions and not only a result of the particular stimuli selected and statistical contrasts that have been used in functional localizers.

4.8 Topographic Parcellation

Topographic organization is as promising a candidate as any for being a fundamental principle of cortical organization, and is evolutionarily widespread, with origins going at least as far back as the common ancestor of vertebrates (Krubitzer & Kaas, 2005). With the possible exception of olfactory cortex (Chuck Stevens, presentation at ISB 2013), topographic organization has been identified for all primary sensory and motor areas, as well as for many non-primary areas.

The clearest example of topographic organization in the visual system is retinotopy, the arrangement of cortical circuits such that information from neighboring regions of the retina (and hence, of the visual field) are processed in neighboring regions of the cortex (Engel, Glover, & Wandell, 1997; Engel et al., 1994). While retinotopic organization is often thought of as a paradigmatic property of early visual areas, retinotopic maps can be found throughout around a dozen early- and mid-level regions of the dorsal and ventral pathways (Wandell, Brewer, & Dougherty, 2005). Furthermore, these maps may be organized into several map clusters, each sharing a foveal region and eccentricity organization (Wandell et al., 2007). As a result, retinotopic mapping is commonly used in individual subjects for the purpose of obtaining a partial parcellation occipital and parietal regions.

While it is unclear if topographic organization is also a universal attribute for higher-level regions of cortex, there is evidence that at least some high-level regions contain topographic organization (Linda Henriksson, Mur, & Kriegeskorte), though they may not be as complete and orderly as those seen in primary areas (Patel, Kaplan, & Snyder, 2014). Electrophysiological recording in the macaque temporal lobe has provided conflicting results with regard to the spatial arrangement of tuning properties. Several authors have suggested that neighboring cells in inferotemporal cortex are tuned to disparate properties (Issa et al., 2013; Tanaka, 2003). Other results

suggest an organization on the scale of several millimeters (Kreiman et al., 2006), as is seen with color and orientation tuning in V4 (Tanigawa et al., 2010). However, in at least the case of one of the face patches, electrophysiological recording guided by fMRI localization showed that more than 95% of cells within the face patch were face-selective (Tsao, Freiwald, Tootell, & Livingstone, 2006), though it remains possible that the precise feature selectivity within the category of faces may be heterogeneous and spatially discontiguous. Indeed, it has been suggested that many higher-level visual areas may contain multiple feature maps organized in a seemingly randomly interspersed fashion, with each set of features occurring in a tiling manner throughout a larger scale topographic organization (Jain, Millin, & Mel, 2015) similar to orientation tuning in the rodent early primary visual cortex (Ohki, Chung, Ch'ng, Kara, & Reid, 2005). Further evidence comes from superior temporal lobe in the auditory-visual association cortices where there is local intermixing of populations that have biases toward one or the other modality or both on the scale of millimeters (Dahl, Logothetis, & Kayser, 2009).

To my knowledge, there have been no parcellation methods that have explicitly sought to identify functional regions by detecting topographical organizations in the ventral temporal cortex. Part of the difficulty in such an approach is that the properties that may be topographically organized in these regions are unknown, and conventional approaches to revealing topographic organization have relied on the systematic modulation of the mapped property and an analysis that leverages knowledge about when each aspect of the property was present in the stimulus.

4.9 SUMMARY

There are multiple aspects of the brain that display systematic organization. Systems neuroscience research found that several of these aspects often undergo relatively sharp transitions in register. The regions bound by these borders have come to be known as cortical areas. These areas and their spatial arrangements are often evolutionarily conserved. Knowledge of these areas has been crucial insights that have guided a vast number of experimental designs.

However, the goal of parcellation is not always to identify cortical areas. While multiple modalities often agree on a particular border, not all borders are present in all modalities. For example, cytoarchitectonic domains in the ventral temporal cortex seem to encompass several areas as suggested by functional and connectivity based borders. Also within modalities, not all measures will suggest borders at the same locations. For instance, the laminar pattern of certain receptors might span several cortical areas, while only a small number of receptors in particular layers display changes in expression across a given border.

An additional complication in finding cortical areas is that they are often not homogenous for all aspects of organization. For example, while the cytoarchitecture and myeloarchitecture of the primary visual cortex are fairly uniform, the large-scale topographic organization changes systematically across the area such that activity

of distant neurons within the region are likely to be uncorrelated. While the retinotopic response properties change in a smooth manner across the area, the topographic organization for orientation selectivity exists on a much smaller spatial scale and instead forms a motif and it is absence of this motif that would signify the border with neighboring areas. The greater the spatial scales at which the brain displays hierarchical organization, the more parcellation into a discrete set of areas may have multiple meaningful solutions (Eickhoff, Constable, & Yeo, 2017).

Although primary sensory and motor areas are shared across all typically developing individuals, this universality is often assumed to apply to the entirety of cortex. However, it remains possible that the higher level associative areas of the cortex may become arealized in more idiosyncratic ways.

For any method of assessing cortical organization, a set of results, even if highly reliable, must be evaluated for consistency with other methods. For example, it has been proposed that to qualify as a cortical area, a region of cortex should be identified by cytoarchitecture and myeloarchitecture, inter-regional structural connectivity, internal response properties, and a coherent topographical representation (David C Van Essen, 2004), though even more stringent criteria may be appropriate.

The following chapter will address how to identify functionally coherent regions in the ventral temporal cortex.

ToC

Chapter 5 : Grouping by Response Similarity: A Data-Driven Method for Exploring Cortical Functional Organization

Jason Webster and Ione Fine

Increasing evidence suggests that representations across much of ventral cortex cannot be characterized in terms of univariate stimulus responses. As a result, identifying the representational subunits of ventral temporal cortex has proved extremely difficult. Here, we describe a novel method for identifying cortical regions with coherent functional responses based on 'grouping by response similarity' (GRS). The algorithm does not require the experimenter to code the relationship among stimuli, makes no assumption about the spatial distribution of responses, and does not require the resulting functional clusters to be spatially contiguous on the cortical surface. With fMRI responses in the ventral temporal cortex, GRS finds regions corresponding to previously identified category-selective regions (e.g. face, body, and scene areas) using both categorical stimuli and unconstrained naturalistic video clips. Outside known category-selective areas, GRS subdivides ventral temporal cortex into multiple regions that form discrete patches on the cortical surface that differ in their functional response profiles. Across much of ventral cortex these regions show consistent and coherent stimulus selectivity across repeats of the same stimuli, showing that that they are primarily driven by stimulus-driven BOLD responses, rather than non-neural components. Thus, grouping by response similarity provides a powerful tool for studying cortical organization in regions of cortex where neither functional roles nor regional boundaries are clearly known.

5.1. Introduction

Accumulating evidence suggests that cortex is tiled by a complex mosaic of areas (Felleman & Van Essen, 1991; Krubitzer, 2009; David C Van Essen, 2004) that differ in gene-expression (Hawrylycz et al., 2012), neurotransmitter receptor distribution (Zilles & Amunts, 2009), cytoarchitecture (Schleicher et al., 2009), connectivity (Johansen-Berg et al., 2004), and intrinsic activity (Power et al., 2014). These areas have distinct functional roles (Huberman et al., 2008; O'Leary, Chou, & Sahara, 2007), so identifying their boundaries and response properties is crucial for understanding cortical function. Nonetheless the functional organization of a substantial portion of parietal (Patel et al., 2014), frontal (Silver & Kastner, 2009), and temporal (Buckner & Yeo, 2014; Malach et al., 2002; Wandell et al., 2007) cortex remains unclear.

Ventral temporal cortex (VTC) contains several discrete functional areas with category-selective responses to faces, objects, bodies, graphemes, and scenes (for reviews see Grill-Spector & Weiner, 2014; Kanwisher & Dilks,

2013). However, category-selective regions constitute a minority of VTC. Though there is evidence for a certain amount of super-areal organization (Konkle & Oliva, 2012; Malach et al., 2002), the representational organization of the remainder of VTC remains fairly opaque.

It is presumed that non-category-selective ventral cortex is not "a single monolithic computational mess in which output features are randomly intermixed across the cortical surface" (Yamins & DiCarlo, 2016b). Many now believe that VTC may contain distributed representations (Haxby et al., 2001; Ifat Levy, Hasson, & Malach, 2004; Patel et al., 2014), perhaps analogous to those of hierarchical convolutional neural networks (Yamins & DiCarlo, 2016b), in which individual neurons do not represent specific features or objects; instead the collective response of many millions of neurons are jointly optimized to solve perceptual goals. However, because 'task-related regions' cannot necessarily be identified on the basis of stimulus selectivity, novel methods are required to identify them.

Here, we introduce a method, Grouping by Response Similarity (GRS), that is designed to find cortical regions with coherent response profiles. Inspired by gene expression algorithms, GRS re-orders a vertex (or voxel) correlation matrix such that similarly responding vertex pairs are close to each other in the matrix. GRS does not require coding of stimulus categories or features, and can discover regions with a wide range of topological organizations, including those that are spatially distributed (i.e. do not form a patch on the cortical surface) or whose functional selectivity varies smoothly across cortex (e.g. nearby locations respond similarly throughout the region, but distant locations within the region may be uncorrelated, as found in primary visual or auditory cortex).

Using GRS, we were able to reliably identify known VTC category-selective areas (e.g. face and scene areas) using both categorical localizer stimuli and unconstrained naturalistic stimuli**.** Outside of these areas, GRS reliably identifies novel functionally coherent regions that form unitary patches on the cortical surface across much of ventral cortex, with boundaries that are reasonably consistent across different stimulus sets. These regions contain replicable, coherent, and distinct functional response profiles, though the stimuli that elicit similar patterns do not seem to share any obvious stimulus or semantic information. Thus, we demonstrate that much of VTC is comprised of discrete functional units whose functional selectivities are not describable with 'word models'. Identifying these regions is likely to be critical first step for furthering understanding of how VTC represents the visual world.

5.2. Materials and Methods

5.2.1. Participants

Three human participants (two female) from the Seattle area were recruited for the experiment. All participants were free of ophthalmic, neurologic, and general health problems. Participants provided written informed consent in accordance with the Institutional Review Board at the University of Washington.

5.2.2. Stimuli

Each subject participated in three MR scanning sessions, each consisting of a different stimulus set. Overall scan time was roughly equal across all three stimulus sets. Stimuli were presented on a screen at the end of the magnet that was viewed through a mirror attached to the head coil. Stimuli were presented full screen (approximately 28x20.5° of visual angle). Each subject completed eight 270 second runs in each scanning session.

Stimulus Set 1 consisted of 3s movie clips containing only faces, bodies, scenes, objects, scrambled objects (Julian et al., 2012), or uniformly colored screens (examples in **Error! Reference source not found.**A). There were 12 unique clips for each category (with each clip containing only the stimulus category of interest) for a total of 72 unique clips. Stimuli were presented in a pseudorandom order while subjects freely and passively viewed the video clips.

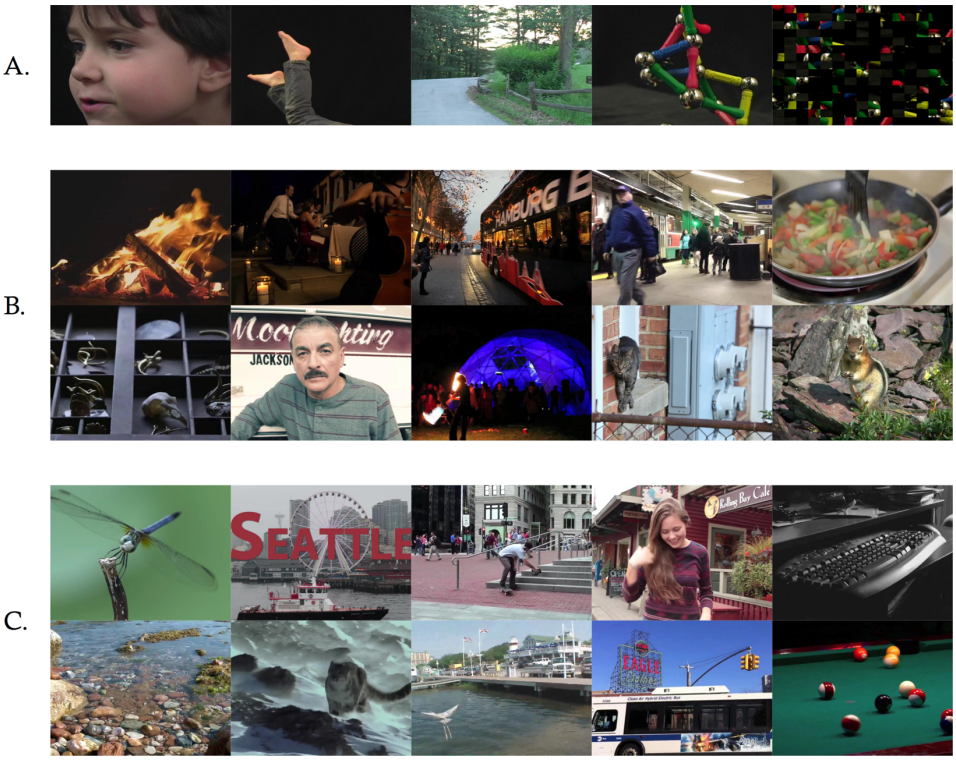

Figure 5.1. Stimuli

Stimuli. (A) Example frames from the video clips of faces, bodies, scenes, objects, and scrambled objects used in Stimulus Set 1 (full stimulus set in Supplementary Figure 5.1). (B, C) Example frames from the naturalistic video clips used in Stimulus Sets 2 and 3 respectively (full stimulus set in Supplementary Figure 5.2 and Supplementary Figure 5.3).

Stimulus Sets 2 and 3 each consisted of a different selection of 60 3s naturalistic video clips from Vimeo (https://vimeo.com), and 12 uniformly colored screens (frames from example stimuli are shown in Figure 5.1B and Figure 5.1C, see Supplementary Figure 5.2 and Supplementary Figure 5.3 for full stimulus sets), for a total of 72 unique stimuli in each set. The main criteria used in selecting clips was that each clip consisted of colorful, full-screen, high-resolution video, did not include a change of scene or camera angle, and that the 60 naturalistic clips of each set varied widely in content. Video clips were presented in a pseudorandom order that varied across each run. Subjects freely viewed the clips while performing a one-back task in which subjects pressed a button when the same clip was shown twice in a row. This occurred on average once (at pseudo-random intervals) during each 270s run. Subjects completed eight runs in separate scanning sessions for each stimulus set. In total, each stimulus was presented 10 times.

5.2.3. Data acquisition

All fMRI data were acquired on a 3 Tesla Philips Scanner with a 32-channel head coil at the Diagnostic Imaging Sciences Center at the University of Washington. T1-and T2-weighted images were collected in 128 sagittal slices with 1mm isotropic voxels. Blood-oxygen level dependent (BOLD) images were acquired with a gradient-

echo EPI sequence (TR=1500ms, TE=25ms, FOV=240x240x78mm matrix=80x80, slices=26) with a 3mm isotropic voxel resolution. The acquisition window was positioned off-axial to include the temporal and occipital lobes.

5.2.4. Data analysis

5.2.4.1. Preprocessing

MRI data were preprocessed with Freesurfer / FSFAST (https://surfer.nmr.mgh.harvard.edu) (Dale, Fischl, & Sereno, 1999; Fischl, Sereno, & Dale, 1999). Grey-white and pial surfaces were estimated from T1 and T2 weighted images. BOLD data from each functional run were motion corrected to the central time-point. Each run was then separately aligned to the grey-white surface using boundary-based registration (Greve & Fischl, 2009). No additional smoothing or normalization to anatomical templates was applied. For computational efficiency, all analyses were restricted to a large region that provided coverage of the entire ventral temporal cortex, based on FreeSurfer's anatomical labels (Figure 5.2A).

5.2.4.2. Category-specific statistical contrasts

Using Stimulus Set 1, we identified known category-selective areas using a standard localizer approach. A General Linear Model (GLM) was fit across all runs and the resulting beta-weights for each category were used to create statistical parametric maps contrasting responses to Faces vs. Objects, Bodies vs. Objects, and Scenes vs. Objects (thresholded at $p <= 10^{-4}$, uncorrected).

5.2.4.3. GRS analysis

All subsequent analyses were carried out using custom Matlab (https://www.mathworks.com) code. For the GRS analysis, for each stimulus set (1-3), we began by using a GLM to estimate the beta-weights for each movie clip. For each stimulus set, this produced a vector of 72 beta-weights for every vertex within VTC.

The unsorted vertex similarity matrix (unsorted VSM, Figure 5.2B) is defined as the Pearson's correlation between the beta-weight vectors for every pair of vertices, with the rows and columns of the matrix determined by the ordinal rank of the FreeSurfer vertex numbers.

Next, a permutation vector obtained from optimal leaf ordering for hierarchical clustering was used to reorder the unsorted VSM in order to maximize the summed similarity of neighboring vertices in the matrix, thereby maximizing the values along the subdiagonal. As schematized in Figure 5.2C, agglomerative hierarchical clustering was carried out on the beta-weight vectors to produce a binary tree that successively linked vertices on the basis of the similarity of their beta-weights, using correlation distance (1-r) as the distance measure. We then used Fast Optimal Leaf Ordering (Bar-Joseph, Gifford, & Jaakkola, 2001) to find the permutation vector

that maximized the summed similarity of adjacent leaves. This permutation vector was used to simultaneously permute the rows and columns of the unsorted VSM to produce the GRS matrix (Figure 5.2D).

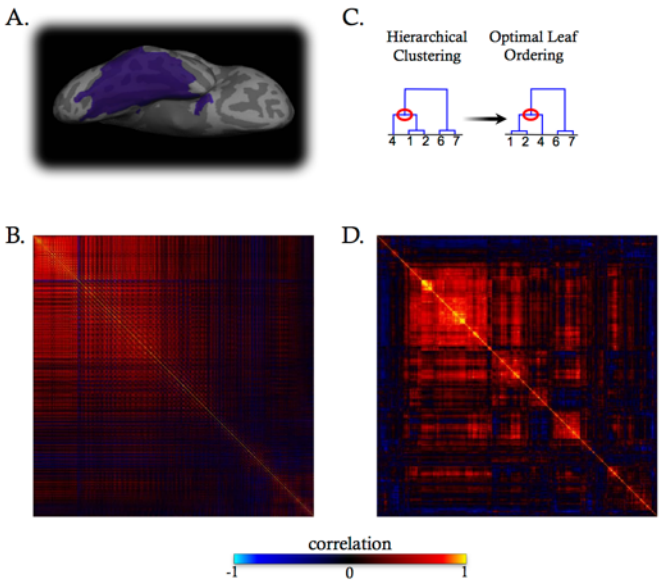

Figure 5.2. Schematic of Grouping by Response Similarity.

(A) Beta-weight vectors were estimated for each stimulus within ventral temporal cortex (purple). (B) The unsorted vertex similarity matrix is calculated as 1 - r (the Pearson correlation distance) between beta-weight vectors for each pair of vertices. The row and column order of the unsorted vertex similarity matrix are determined by the ordinal rank of the FreeSurfer vertex numbers. (C) The dendrogram of the agglomeratively-clustered beta-weights was reordered using Fast Optimal Leaf Ordering to maximize the summed similarity of adjacent leaves. (D) The unsorted vertex similarity matrix was then sorted based on the resulting permutation vector to obtain the GRS matrix.

5.2.4.4. Downsampling

While Fast Optimal Leaf Ordering requires dramatically less computational time than a full search of the permutation space (less than $O(n^4)$ rather than $O(n!)$), processing times can still be on the order of tens of hours for datasets of the size described here. To further reduce processing time, downsampling was performed prior to Fast Optimal Leaf Ordering. Beta-weight vectors for vertices correlated at 0.98 or above were averaged, and Fast Optimal Leaf Ordering for Hierarchical Clustering (OLO) was performed on the reduced data set. Data were then upsampled, with the ordering of the upsampled values determined by running OLO on each group of downsampled beta-weight vectors. The generalized Szymkiewicz-Simpson Coefficient (SSCg, see below) between OLO results for original and downsampled matrices were 0.745, 95% CI: 0.732-0.762 across our 18 datasets (3 subjects x 2 hemispheres x 3 datasets).

The permutation vector obtained from optimal leaf ordering reorganizes the similarity matrix to have maximal values along the subdiagonal of the VSM. Importantly, both hierarchical clustering and optimal leaf ordering were based entirely upon correlative similarity between the beta-weights; reordering of the vertices does not use information about either the content of the stimuli or the spatial location of the vertices. Moreover, because the algorithm focuses on maximizing correlation values along the subdiagonal it is capable of identifying clusters with a wide range of cortical topologies, such as those with a smooth progression of selectivity across the cortical surface (see Results, The nature of clusters).

5.2.4.5. Automated cluster selection

After permutation based on OLO, distinct clusters can be seen in the reordered matrix (Figure 5.2D). A cluster can be thought of as a collection of voxels with pair-wise mutually similar response profiles, represented by high correlations along the subdiagonal. We identified these separate clusters using an algorithmic approach, though other methods of cluster selection, including manual selection, produced similar results. The algorithm used here identified clusters in a two-stage process: (1) identifying potential cluster boundaries and then (2) recursively merging clusters. The left panel of Figure 5.3 shows a simulated example of a small GRS matrix, and the right panel shows a region from a real GRS dataset (S1, right hemisphere).

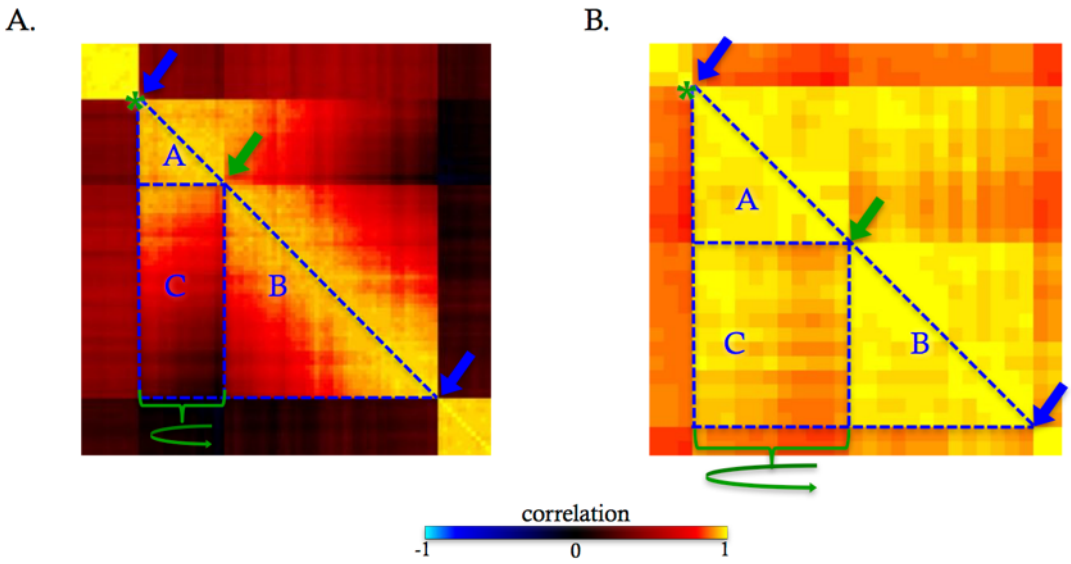

Figure 5.3. Selecting and merging clusters.

A small subsection of simulated (A) and real (B) GRS correlation are shown. The simulated matrix contains 86 vertices, and the subsection of a real GRS matrix contains 30 vertices (out of ~10,000 VTC vertices). Potential boundaries identified by a sliding window are shown with blue and green arrows in each panel. The green arrows are spurious boundaries: if the region outlined in C were flipped A, B and C would form a single cluster. To deal with this known limitation of optimal leaf ordering we carried out a merging step, as described in the main text. If the correlation values within rectangular results in region C were consistent with A-C belonging to a single cluster then A-C were merged. Parameters used in potential boundary detection and merging stages were selected by a parameter analysis (see Supplementary Figure 5.4).

5.2.4.6. Identifying potential cluster borders

Potential cluster borders were identified by finding values on the subdiagonal that were significantly lower than nearby subdiagonal values (Figure 5.3, blue and green arrows). This was done using an adaptive threshold, based on a sliding window. Based on a parameter analysis (see below) we chose a sliding window of size w=253. After removing outliers using the Tukey method (Tukey, 1977) subdiagonal correlation values were Fisher-transformed and fit with a gamma distribution. Potential boundaries were identified as locations where the Fisher-transformed correlation value at the center of the sliding window fell below the value corresponding to an estimated left-tailed probability of α=0.01 (i.e. the subdiagonal correlation value was significantly lower than its neighbors).

5.2.4.7. Recursively merging clusters

One limitation of OLO is that maximizing the correlation values along the entire subdiagonal can result in spurious boundaries. In the examples shown in Figure 5.3, regions A, B, and C belong to a single cluster; if region C were flipped along the vertical axis, it would seamlessly merge with A and B. These spurious boundaries

result from the GRS algorithm maximizing pairwise correlations across the entire subdiagonal: minimizing the drop in correlation value at the upper boundary shown by the green * causes a reversal of the ordering within the column of vertices containing A and C. This limitation in the optimal leaf ordering algorithm required an additional step in which we recursively merged clusters by examining whether the correlation values within the full region of C (not just the subdiagonal) were consistent with A-C belonging to a single cluster.

To determine if two clusters should be merged we calculated the distribution of Fisher-transformed correlation values of the subdiagonal for both clusters in question (e.g. clusters A and B in Figure 5.3). Once again, this distribution was fit with a gamma function to find the Fisher-transformed correlation value, $\rho_{\alpha 2}$, corresponding to an estimated left-tailed probability of α_2=0.01.

We then calculated the number of vertex pairs (values in the matrix) within regions A and B that had correlation values above this correlation value, $\rho_{\alpha 2}$. We divided this by the number of vertices in A and B to get the expected number of vertex pairs above threshold in a given column $E_{rAB>\rho_{\alpha.}}$.

If A, B, and C were part of a single cluster, then we would expect (when properly sorted) that the high correlation values in C would fill a triangular corner, with two sides of length E_{rAB}. As a result, the expected number of vertex pairs above threshold was calculated as an arithmetic progression

$$E_{\mathrm{rC}} = \frac{E_{\mathrm{rAB}}}{2}(E_{\mathrm{rAB}} + 1)$$

(Or, in a formulation that explicitly describes the arithmetic progression, $E_{\mathrm{rC}} = \sum_{m=1}^{E_{\mathrm{rAB}}} m$.) When the number of vertices in either A or B was less than E_{rAB}we applied an appropriate correction. We merged A-C into a single cluster if the number of vertices above threshold in C was greater or equal to E_{rC}.

5.2.4.8. Parameter analyses

Parcellation stability was estimated during parameter analysis using a generalization of the Szymkiewicz-Simpson coefficient (SSCg). The original Szymkiewicz-Simpson coefficient uses the following equation to calculate the overlap between two binary matrices, X and Y.

Table 5.1. Categories for agreement of vertex pair assignment

		Dataset Y	
Dataset X		a vertex pairs where X=1 & Y=1	b vertex pairs where X=1 & Y=0
		c vertex pairs where X=0 & Y=1	d vertex pairs where X=0, Y=0

$$Overlap\ O(X,Y) = \frac{a}{\min(a+b, a+c)}$$

Our extension simply calculated the weighted (by the number of vertices) average of O(X, Y) across all possible parcel pairs. The advantage of using this metric was that it does not penalize the strict subset relationships, and differs from the metric used to calculate final parcellation consistency.

The parameters for the window size (w) and the two alpha values (α_1 and α_2) were selected by a parameter analysis that explored how parcellation consistency (across stimulus sets) and the number of parcels varied as a function of w, α_1, and α_2. The following range of values was examined: w=3-1001, α_1 = 0.001-0.2, α_2 = 0.001-0.2. Parcellations were robust across a wide range of parameter values (see Supplementary Figure 5.4). We chose a final set of parameter values that reliably produced a reasonable number of clusters with a high mean parcellation consistency, w=253, α_1 = 0.01, α_2 = 0.01.

5.2.4.9. Assessing consistency of parcellations and null models

Consistent with previous research (Honnorat et al., 2015; D. Wang et al., 2015), parcellation consistency was assessed with the Dice coefficient, which measures binary similarity between two regions X and Y, as shown in Table 5.1, and is computed as:

$$Dice\ Coefficent(X,Y) = \frac{2a}{2a+b+c}$$

5.2.4.10. Null models

GRS results were compared to two null models.

Region growing null model. For each dataset, we pseudorandomly distributed n nodes across the cortical surface, where n was the number of parcels obtained for a corresponding real dataset. Null model parcels were then 'grown' using an iterative approach where, for each node in turn, the nearest unassigned vertex was assigned to that node, until every vertex had been assigned (Zalesky et al., 2010). This model provides the estimated Dice

value that might be expected due to chance on that cortical surface, given the number of pseudorandom contiguous parcels obtained for a given dataset.

Local BOLD correlations null model. This model was designed to examine whether our parcels might be the result of non-neural spatial correlations in the BOLD signal or artifacts related to representing the data on a non-uniform surface mesh. For each dataset, we reassigned beta weights by pseudorandomly permuting the data across both stimuli and vertices. We then reintroduced spatial structure by convolution with a 2D Gaussian with a FWHM of 3.9 mm, designed to match the scale of hemodynamic blurring observed with a gradient echo pulse sequence at 3T (Parkes et al., 2005). This model should have relatively high replicability, though should be driven purely by locally smoothed data and regions with higher vertex density more likely to form a parcel due to smoothing being applied as a function of cortical distance.

Comparisons between null models and the real data were carried out using a bootstrap approach where each dataset (3 subjects, 2 hemispheres, and 3 stimulus sets) were repeatedly and randomly selected to generate 1008 null models in total.

5.2.4.11. Comparing RDMs across parcels

Once parcels had been identified, we calculated the representational dissimilarity matrix (RDM) as the correlation distance (1-*r*) between the response patterns elicited by each pair of stimuli, across all the vertices within each individual parcel (Kriegeskorte et al., 2008). This produces a matrix of 72 rows and columns, where each value in the matrix represents similarity in spatial response profiles across vertices elicited by a pair of stimuli. We then calculated the correlation between the lower triangular portion of each pair of RDMs.

We compared these results to the values obtained in two simulations to determine whether the results suggest that the parcels contained distinct representational content and internal spatial structure.

The first simulation evaluated the expected correlation across parcel RDMs if different parcels had identical representational content, such that differences in the RDMs were simply due to vertex sampling and noise in beta-weight estimates. All parcels within the analysis were combined into a single parcel. For each pair of parcels, across 1000 iterations, the appropriate number of vertices was sampled from the combined ROI, and zero-mean normally-distributed noise was added to the beta weight values. Correlations between the lower triangular portions of each pair of stimulated RDMs were used to create 95% confidence intervals. The noise level for these simulations was chosen conservatively, to exceed that observed in the real data and therefore underestimate the expected similarity between RDMs. We selected a noise level that resulted in lower split-half reliability in beta weights and lower vertex-wise within parcel correlations than were observed in the real data.

The second simulation evaluated the expected correlation across parcel RDMs if individual parcels contained no spatial structure. For each pair of parcels, across 1000 iterations, we shuffled the beta weight vectors across location, thereby scrambling spatial structure, but leaving other statistical dependencies (such as average beta weight responses) intact. Correlations between the lower triangular portions of each pair of stimulated RDMs were used to create 95% confidence intervals.

5.3 RESULTS: RELIABILITY AND VALIDITY

5.3.1 BETA-WEIGHTS ARE CONSISTENT ACROSS ODD AND EVEN RUNS OF THE DATA.

Beta-weight correlations between odd and even runs of the data for all three stimulus sets are shown in Figure 5.4. Within posterior VTC we find strong correlations between the beta-weights across split halves of the data. Thus, stimulus beta-weight estimates were reliable and were not strongly affected by non-stimulus driven variations in the BOLD response over time (e.g. fluctuations in the vasculature). This consistency in stimulus preference is important because it suggests that, at least for posterior regions, functional rather than vascular responses were the primary determinant of parcellations.

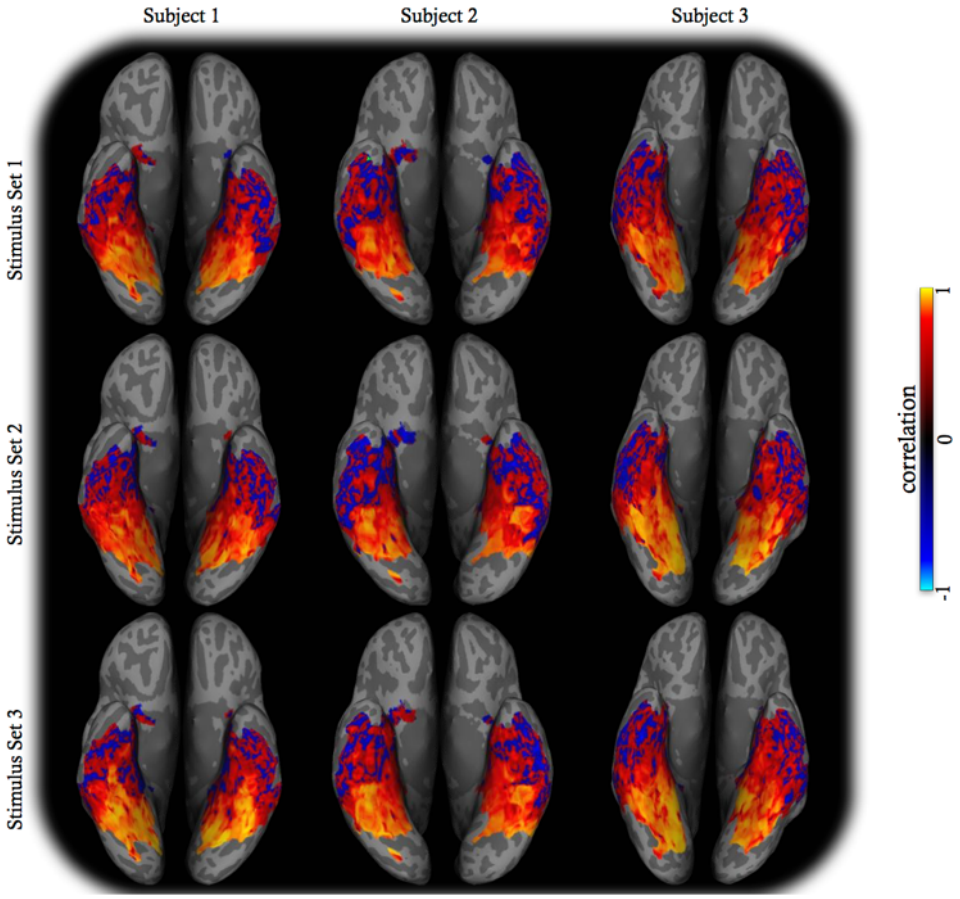

Figure 5.4. Beta-weight correlations across even and odd runs for all three stimulus sets for each subject.

5.3.2 GRS FINDS CONTIGUOUS CORTICAL REGIONS

Figure 5.5 shows parcellations of the cortical surface using the naturalistic stimuli of stimulus sets 2 (top) and 3 (bottom) for all three subjects. Although the GRS algorithm is not provided with information about the spatial location of functional data, identified clusters almost always formed discrete and fully-filled patches on the cortical surface. These discrete patches are very different from those that are generally produced by functional parcellations that do not impose spatial constraints, such as ICA of resting state fMRI or variants of K-means clustering, see Discussion.

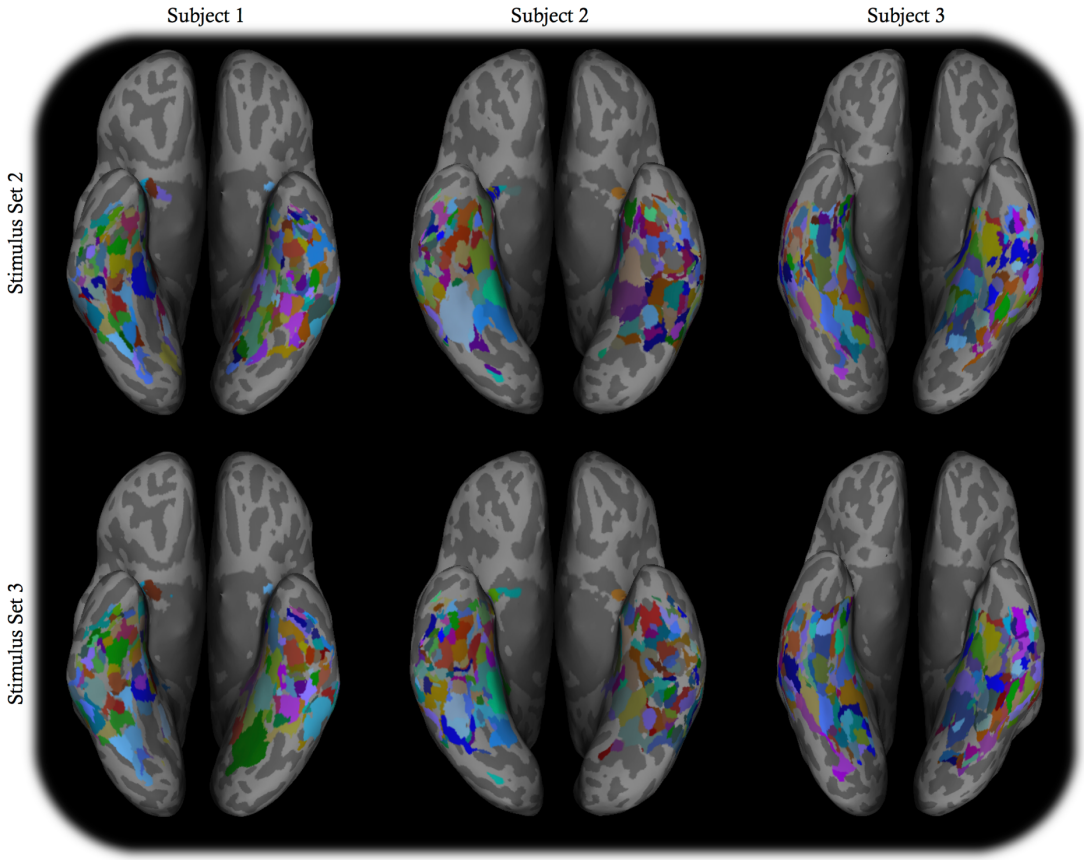

Figure 5.5. Parcellations identified by GRS form discrete and fully-filled patches on the cortical surface. Parcellations are shown for Stimulus Sets 2 (top) and 3 (bottom) for all three subjects.

5.3.3 Comparison of GRS Parcellations to Null Models

In

Figure 5.6A the outlines of the parcellations of Figure 5.5 are replotted, with parcellation based on Stimulus Set 2 in red, parcellation based on Stimulus Set 3 in blue, and shared boundaries in magenta. Many boundaries are shared, and many non-shared boundaries are either due to slight displacements of the boundary across the two stimulus sets or are due to the stimulus sets differently subdividing a larger cluster.

Our null region growing analysis on the cortical surface had a moderate replicability (Dice M=0.3940, 95%, CI=0.3910 - 0.3939) that was not significantly different than that found with a region growing algorithm on a uniform grid (Dice M=0.3936, 95%CI=0.3917 -0.3948).

The local BOLD correlations null model had higher replicability than predicted by region growing on a uniform grid (Dice M=0.4174, 95%CI=0.4027 - 0.4278). This is because beta-weights were permuted across vertices as

well as condition, and smoothing was carried out as a function of distance across the cortical surface. As a result, vertex-wise similarity was higher in regions of the cortical surface where vertex density was high.

Using the GRS algorithm, parcellation reliability (Dice *M=0.4426, CI95=0.4089 - 0.4773)* was significantly higher than predicted by region growing on a uniform grid (p=0.0017, 95%CI=0.0208-0.0763) and the region growing model (p=0.0018, 95%CI=0.0213-0.0768) but was *not* significantly higher than for the local BOLD correlations null model (p=0.0841, CI=-0.0037-0.0540), see also Table 5.2.

Critically, the boundaries generated using GRS differed significantly from those predicted by the local BOLD correlations null model. Boundary overlap was actually *lower* than what one would expect by chance (Dice M = 0.3054, 95%CI = 0.2980 - 0.3091) and was significantly lower than replicability across sessions with the GRS algorithm ($p=2.4980x10^{-9}$. 95%CI=0.1141-inf), Figure 5.6B. Thus, our boundaries were not determined by non-neural spatial correlations due to non-uniform vertex spacing and the point-spread function of the BOLD signal.

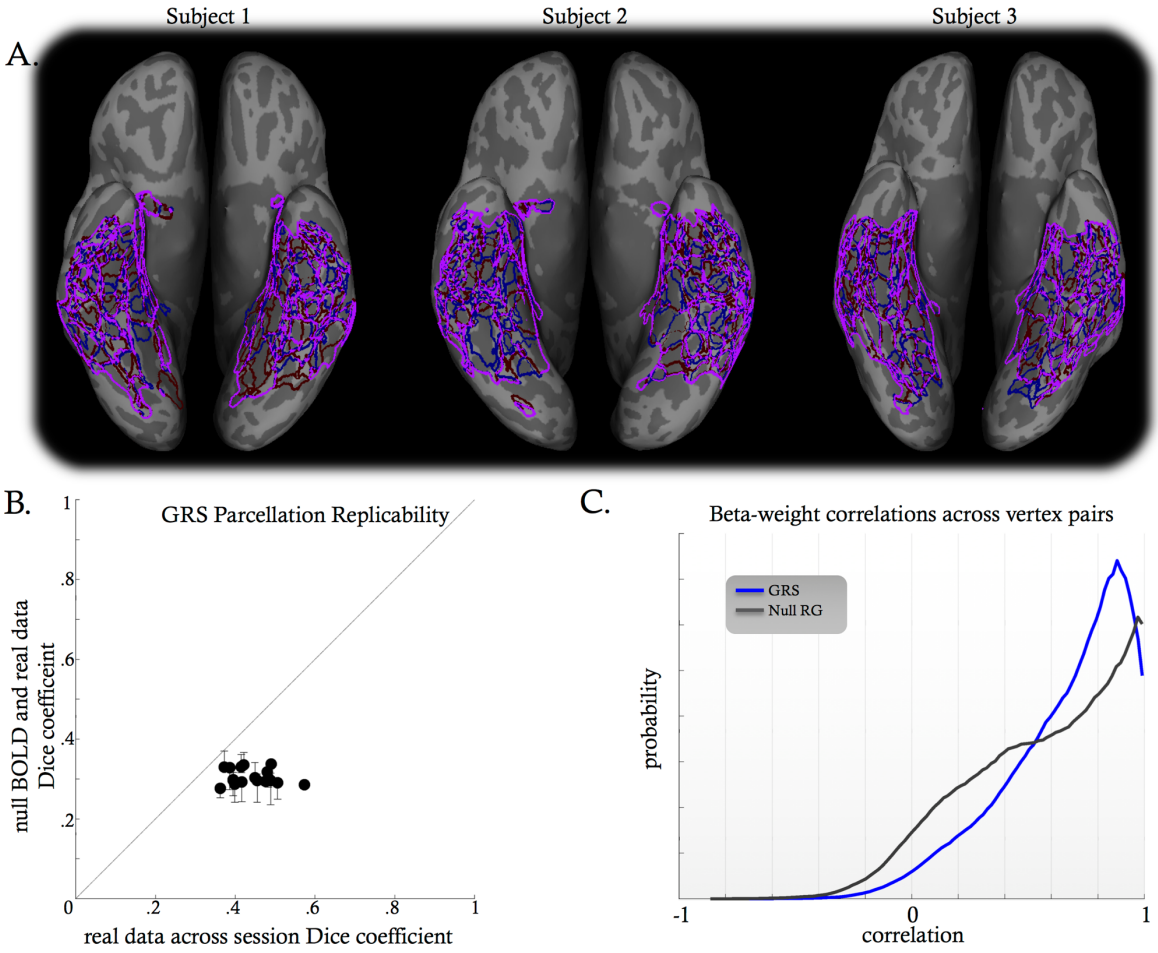

Figure 5.6. Parcellation replicability and null model comparisons

A. Parcellation boundaries identified by GRS across two datasets. Boundaries from Stimulus Set 2 are shown in red, those from Stimulus Set 3 are shown in blue, and borders shared across both datasets are shown in magenta (see Supplementary Figure 5.5 for a comparison of results with and without uniformly colored screens). (B) Parcellation consistency for GRS on the real data plotted against bootstrapped estimation of the 95%CI parcellation similarity of individual hemispheres processed with GRS and the corresponding BOLD null model. Error bars (often smaller than the symbols) represent 95% confidence intervals across approximately 100 permutations per hemisphere bootstrapped 1000 times. (C) Probability distributions of beta-weight correlation values across pairs of vertices in the same parcel. The blue line represents results generated using GRS on real data, the black line represents results generated using the region growing null model. Data are collated across all hemispheres; individual hemisphere data are shown in Supplementary Figure 5.7.

One possible concern was that our stimulus sets were not strictly independent, given the presence of uniformly colored screen stimuli in all three stimulus sets. As described in Supplementary Figure 5.5, we found that parcellations boundaries were very similar when the beta weights associated with the colored screen stimuli were excluded (mean SSCg =0.784, 95% confidence interval 0.770-0.797).

In summary, parcellation boundaries (across different days and stimulus sets) identified by GRS are more replicable than would be expected by chance, and do not reflect non-neural spatial correlations in the BOLD signal.

5.3.4 GRS PARCELLATIONS HAVE COHERENT RESPONSES ACROSS STIMULUS SETS

If GRS parcels are discrete functional units then vertices that fall within the parcel should tend to have more similar stimulus preferences than vertices that fall in different parcels. (However, it should be noted that in clusters that contain a smooth topology of stimulus preferences, similarity preferences between voxels might still fall off as a function of vertex separation, see below, *The nature of clusters*).

Using GRS parcels generated using Stimulus Set 2, we calculated beta-weight correlations for Stimulus Set 3, across all vertex pairs that fell in the same cluster, blue line of Figure 5.6C. The gray line of Figure 5.6C shows the same calculation, but using parcels generated by the region growing model. (This metric was not computed for the BOLD model since the much larger parcel sizes generated by this model were expected to produce dramatically lower within-parcel vertex-wise correlations.) Correlation values were higher for the GRS parcellations than for the region-growing model for every subject and hemisphere (Individual subject data are shown in Supplementary Figure 5.7); two-sample Kolmogorov-Smirnov tests were all significant at $p<0.001$. Thus, GRS parcellations contain vertices with more coherent stimulus responses than predicted by the null BOLD model.

5.3.5 KNOWN CATEGORY-SELECTIVE AREAS ARE RELIABLY IDENTIFIED BY GRS

To validate our technique, we compared the GRS results to conventional localizer contrasts (Saxe, Brett, & Kanwisher, 2006) using the categorical data from Stimulus Set 1. The top rows of Figures 7-9 show conventional localizer contrasts for Faces vs. Objects (Figure 5.7), Bodies vs. Objects (Figure 5.8), and Scenes vs. Objects (Figure 5.9). The second row of each figure shows clusters identified using GRS using the same data. The bottom two rows show these areas as identified using GRS, using Stimulus Sets 2 and 3.

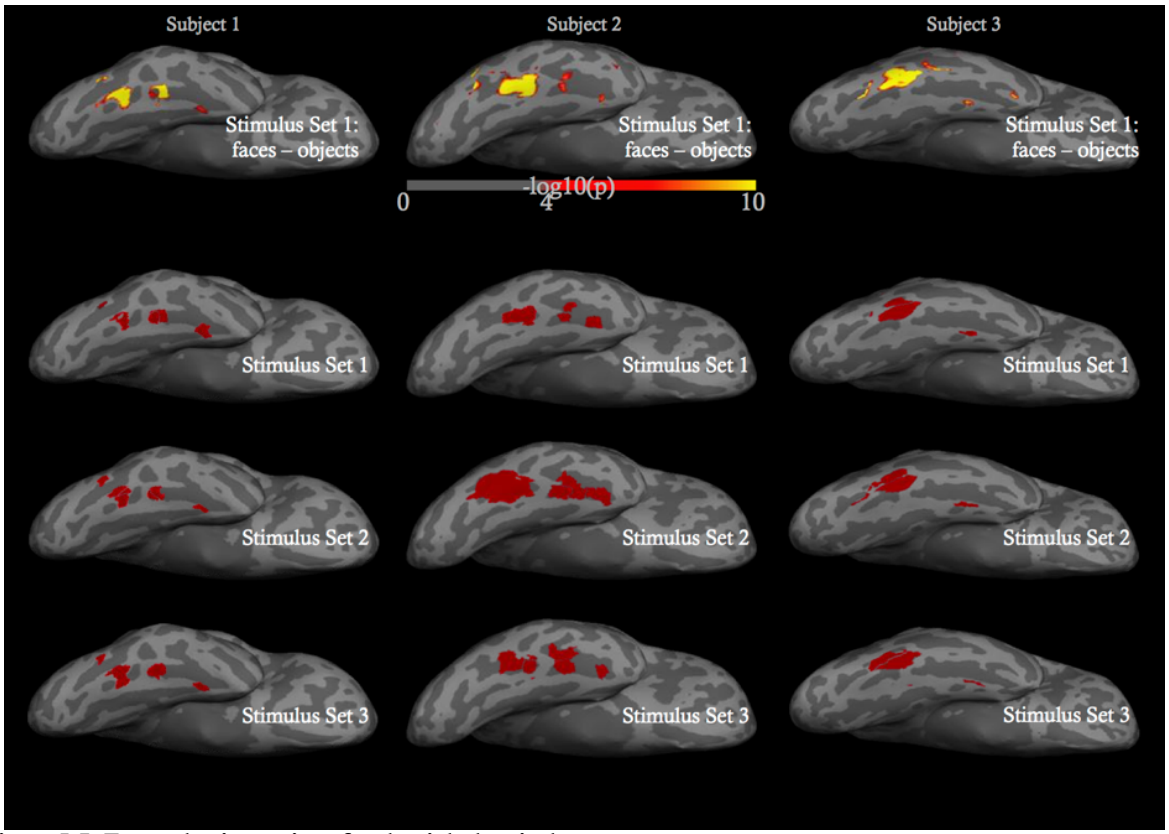

Figure 5.7. Face-selective regions for the right hemisphere.

The upper row shows responses from the categorical Stimulus Set 1 analyzed using the typical Faces vs. Objects statistical contrast used to identify face-selective regions, thresholded at $p < 0.0001$. The lower rows show parcels corresponding to face (red) selective areas, identified from either the same categorical dataset using GRS or naturalistic stimuli from Stimulus Sets 2 and 3.

Face-selective regions are shown in Figure 5.7 (the more lateral occipital face areas were mostly outside our VTC ROI). In S1, the localizer paradigm identified posterior fusiform, mid fusiform, and anterior face patches, as well as a small lateral region on the boundary of the VTC ROI. The GRS method identified all of these face-selective regions across all three stimulus sets. In S2, the localizer paradigm once again identified posterior, mid, and anterior face patches. The mid fusiform face area formed two patches at our conservative threshold. For Stimulus Sets 1 and 3, these three face-selective areas were identified, with the two patches of the mid fusiform face area similarly being identified as separate parcels. For Stimulus Set 2, the GRS algorithm again generated separate GRS parcels for the two mid-fusiform and the anterior patches, but these regions were expanded, to collectively form a contiguous region on the cortical surface. In S3, the posterior and mid fusiform face patches merged into a single ROI using the localizer paradigm. With the GRS paradigm, this contiguous region corresponding to the posterior and mid fusiform areas separated into two contiguous parcels, suggesting that GRS was sensitive to differences in stimulus selectivity between the two adjacent regions. This GRS segregation was supported by the Body vs. Objects contrast, where these two regions were identified as separate parcels, see below.

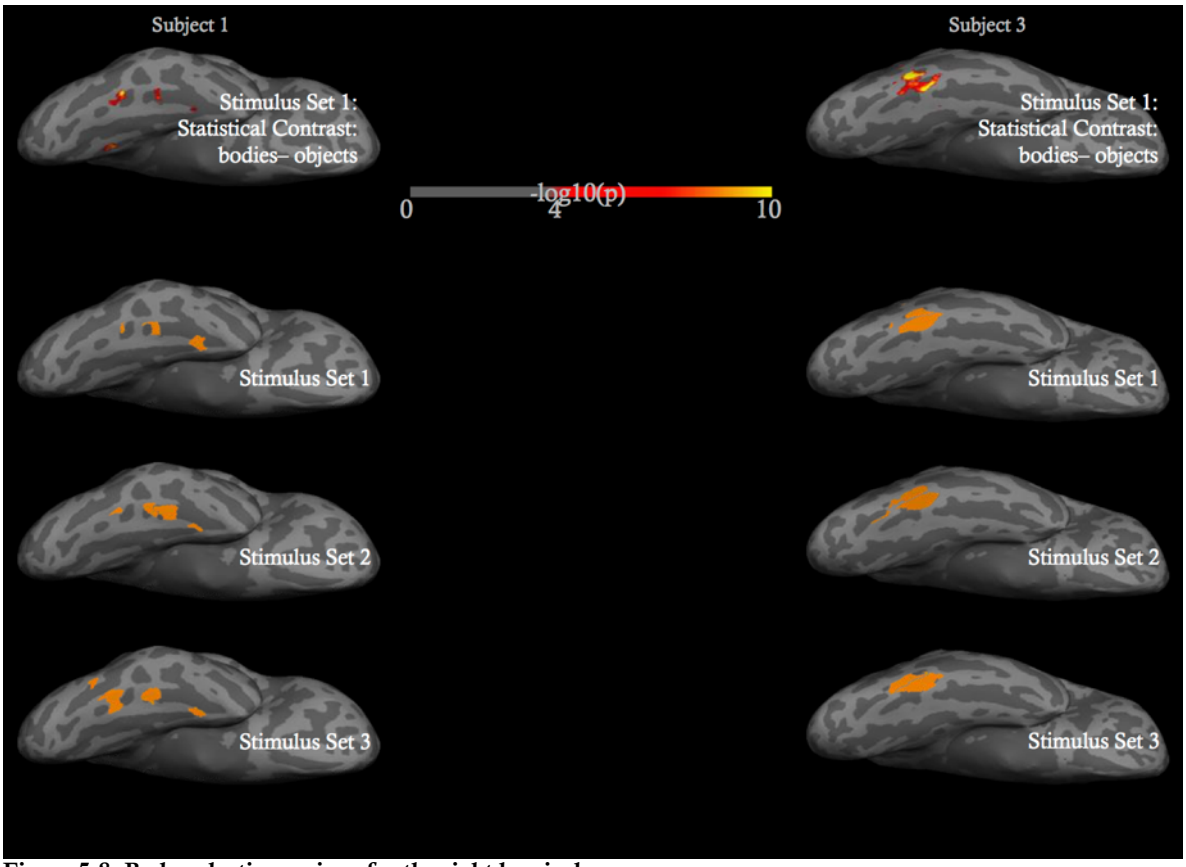

Figure 5.8. Body-selective regions for the right hemisphere.

Right hemisphere is shown (data from left hemisphere are similar and are not shown). The upper row shows responses from the categorical Stimulus Set 1 analyzed using the typical Bodies vs. Objects statistical contrast, thresholded at $p < 0.0001$. The lower rows show parcels corresponding to body (red) selective areas, identified from either the same categorical dataset using GRS or naturalistic stimuli from Stimulus Sets 2 and 3.

Body-selective regions are shown in Figure 5.8. In S1 the Bodies vs. Objects contrast in the localizer paradigm identified body-selective regions which largely overlapped the posterior, mid, and anterior face patches (Figure 5.7). Similar patches were identified using the GRS algorithm for Stimulus Sets 1-3. In S2 the localizer could not identify body-selective areas, so data are not shown. In S3 the localizer identified two body-selective areas; both were contained within the single ROI identified using the Face vs. Object contrast. These two body-selective areas corresponded closely with the two parcellations of this area produced by the GRS algorithm across all three Stimulus Sets.

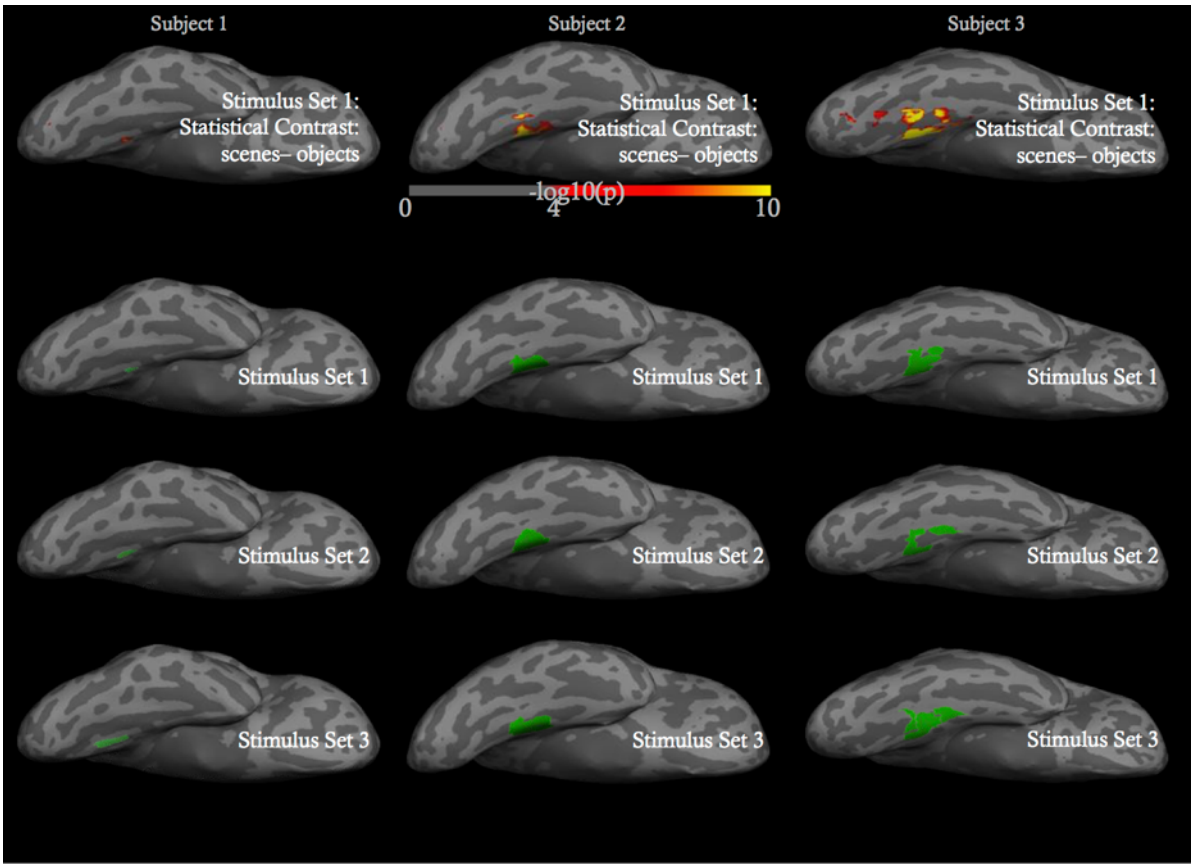

Figure 5.9. Scene-selective regions for the right hemisphere.

Right hemisphere is shown (data from left hemisphere are similar and are not shown). The upper row shows responses from the categorical Stimulus Set 1 analyzed using the typical Places vs. Objects statistical contrast, thresholded at $p < 0.0001$. The lower rows show parcels corresponding to scene (red) selective areas, identified from either the same categorical dataset using GRS or naturalistic stimuli from Stimulus Sets 2 and 3.

Scene-selective regions are shown in Figure 5.9. In S1 the localizer paradigm identified a scene selective region on the medial wall of the temporal lobe. A very similar patch was identified using the GRS method using Stimulus Set 1. Similar parcels were found for Stimulus Sets 2 and 3, though these were larger. In S2 the localizer paradigm identified two scene selective patches on the medial wall of the temporal lobe. For the GRS algorithm, these were merged into a single patch for all three Stimulus Sets. In S3, the localizer paradigm identified three scene selective areas. Using the GRS approach, for Stimulus Sets 1 and 2, two of these patches were merged. In Stimulus Set 3, one parcel corresponded to the most anterior patch. The two posterior patches overlapped with two GRS parcels, but without corresponding tightly with the localizer ROIs.

As might be expected, parcels corresponding to face areas responded most strongly to video clips that contained faces (see below). Similarly, parcels corresponding to body and scene-selective area showed the largest beta-weights for clips of people and scenery (data not shown). In summary, the GRS algorithm reliably discovers clusters corresponding to known category-selective regions using both categorical and naturalistic stimuli.

We quantified the agreement between binary spatial maps generated using traditional statistical contrasts and our GRS technique using uncentered correlation (Lashkari et al., 2008). For comparison, split-half reliability for the localizer approach and results from a previous data-driven method for identifying category-selective areas are also shown (Lashkari et al., 2008).

Table 5.2. Uncentered correlation between spatial maps constructed with the GRS method and the localizer.

In the case of the clustering approach of Lashkari et al, mean correlations averaged across 9 subjects are shown, for clustering with standard errors representing variance across subjects. Lashkari et al. reported results for a variable number of clusters, we show here K=7, where their model performance was highest.

	Split-half localizer				GRS				Clustering
	S1	S2	S3	mean	S1	S2	S3	mean	Lashkari et al.
Face	0.816	0.755	0.828	0.800	0.653	0.652	0.693	0.666	0.37±0.09
Body	0.543	NaN	0.673	0.608	0.340	NaN	0.653	0.497	0.51±0.07
Scene	0.440	0.360	0.407	0.402	0.45	0.642	0.619	0.570	0.31±0.14

5.4 RESULTS: CODING WITHIN THE VENTRAL TEMPORAL CORTEX

5.4.1. FACE AREAS HAVE SIMILAR STIMULUS SELECTIVITIES, BUT CODE ALONG DIFFERENT DIMENSIONS

Figure 5.10 compares responses in posterior, middle, and anterior face areas in S1 right hemisphere. Each column represents a different face-selective area and each row represents a different stimulus set. The matrix of images beneath each parcel show the 9 clips that elicited the highest beta-weight values for that parcel. Unsurprisingly, across all three areas the clips that produced strong beta weights almost always contained faces and there was substantial overlap in which clips elicited the strongest beta-weights across the three face areas.

Figure 5.10. Preferred stimuli in three face-selective areas.

Each column represents a different face-selective area and each row contains data from a different stimulus set. Each hemisphere shows parcels as defined using that dataset. The panel below each hemisphere shows the 9 clips that elicited the highest beta-weight values for that parcel.

Why were these three face areas reliably identified by GRS as being distinct parcels given that the algorithm is blind to the spatial location of vertices and the three regions showed very similar stimulus preferences? Figure 5.11 shows the representational dissimilarity matrix (RDM) for each face-selective area from Figure 5.10. Each RDM was calculated as the correlation distance (1-*r*) of stimulus response patterns within the parcel, for each pair of stimuli (Kriegeskorte et al., 2008). Thus, each row/column of the RDM represents one of the 72 movie clips.

To maintain consistency in stimulus ordering, RDMs for Stimulus Set 1 are ordered by category (see right bar: Faces [red], Bodies [yellow], Scenes [green], Objects [light blue], Grid-Scrambled Objects [dark blue], and

Colored Screens [magenta]) while those for stimulus sets 2 and 3 are sorted based on the rank ordering of the mean beta-weights within the most posterior face area. Given the high beta-weight correlations reported above, it is unsurprising that the three face areas have highly similar stimulus preferences, such that the values along beta weight vector at the bottom of each figures goes from light to dark.

Table 5.3 shows the correlation between the RDMs generated by each pair of face patches. Simulations (see Methods) were used to estimate 95% confidence for two null models. In the first (italic underlined), the spatial location of beta weights were shuffled, providing an estimate of the expected correlation between RDMs if there were no spatial pattern in functional response preferences within each face patch. Correlations across RDMs were *higher* than the 95% confidence interval for this null model, showing that face patches do contain spatial structure in their response properties.

In the second simulation (italic) we calculated the expected correlations between RDMs if all three face patches had identical representational content, and differences across RDMs were simply due to sampling subsets of vertices and noise in beta weight estimates. Correlations across RDMs were *lower* than these 95% confidence intervals, demonstrating that face patches do indeed contain distinct representational content.

Table 5.3. Correlations between each of the RDM matrices of the face patches of Figure 5.11.

Underlined italic text shows 95% confidence intervals based on a simulation that randomized the vertex-wise location of beta weights. Italic text shows 95% confidence intervals based on a simulation that assumed that face patches had identical representational content, and differences across RDMs were due to voxel sampling and noise in beta weight estimates.

	FFA2/mFus	Anterior face patch
FFA1/pFus	0.279 (-0.030-0.033) (0.92-0.942)	0.152 (-0.031-0.032) (0.921-0.941)
FFA2/mFus		0.116 (-0.034-0.034) (0.840-0.894)

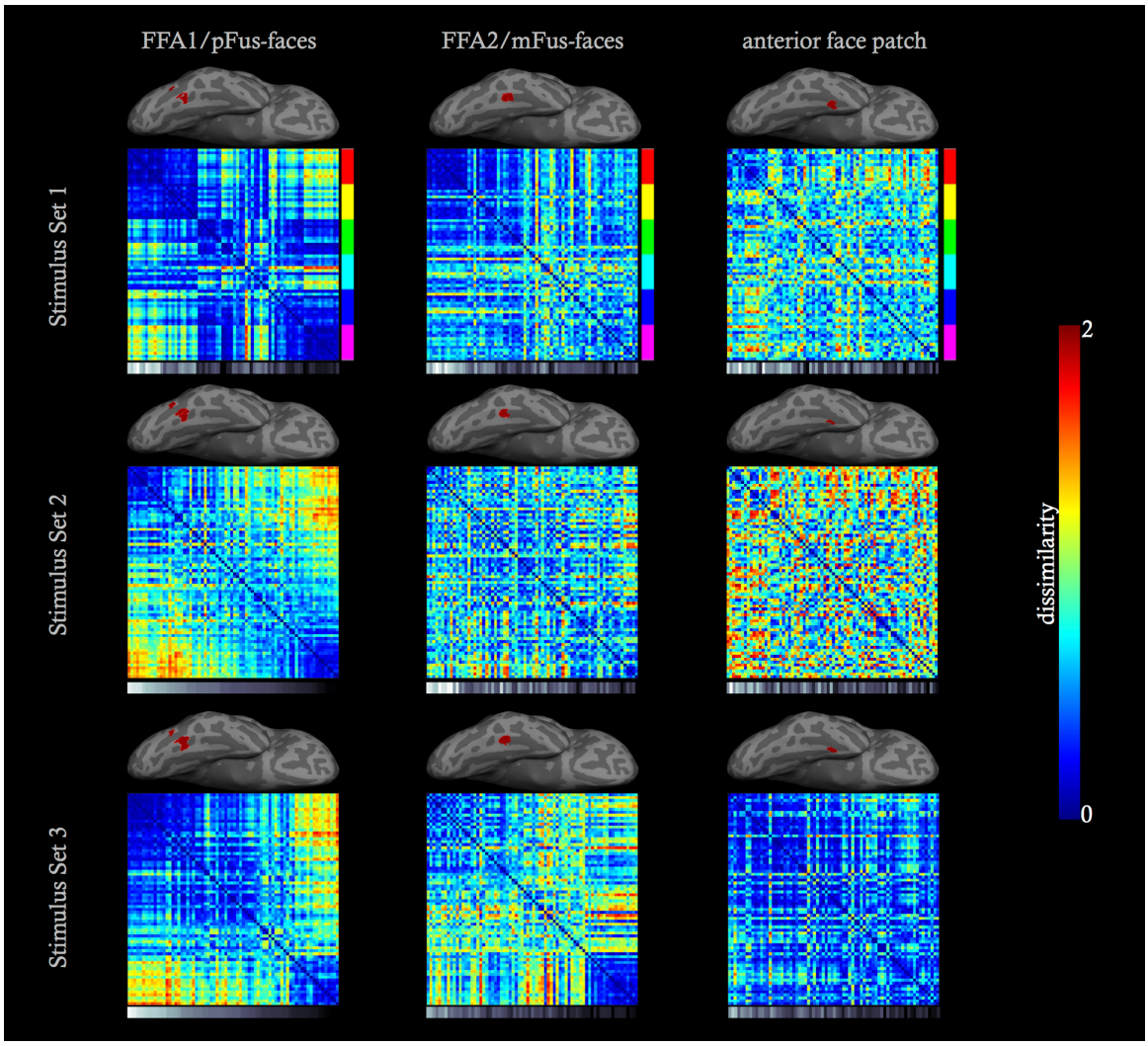

Figure 5.11. Representational dissimilarity matrices of face areas differ.

Each column represents a different face-selective area and each row contains data from a different stimulus set. Each face parcel is shown with the corresponding representational dissimilarity matrix. Below each RDM is a bar representing the average beta-weight for each stimulus within the RDM, where light values represent positive beta-weights and dark values represent negative beta-weights. See **Error! Reference source not found.** for the stimulus orderings for the RDMs in the first column.

We begin by considering the FFA1 (also known as pFus-faces), shown in the leftmost column. The top-left panel, showing responses in the FFA to the categorical stimuli of Stimulus Set 1, replicates previous findings. As shown by the average beta weight vector below the figure, BOLD responses to faces are high, responses to bodies are moderate, and the response to stimuli from all other categories are low. Stimuli falling within certain categories (faces, bodies, scenes, colored screens) elicit very similar response patterns across the cortical surface, while objects and scrambled objects produce less homogenous response profiles. When using naturalistic stimuli (1st column, 2nd and 3rd rows), the spatial response profiles to clips containing faces (top left) are similar to each other

and are dissimilar to the colored screen video clips (bottom right). The remaining clips fall along a continuum of dissimilarity between these extremes.

When comparing RDMs within the FFA1/pFus-faces to the more anterior face patches it is immediately apparent that the RDMs for the two more anterior face patches are distinct from FFA1/pFus-faces and from each other. The most noticeable difference is that face stimuli no longer seem to produce highly similar responses, although these regions as a whole respond strongly to faces, the spatial profile of responses within these areas is not well described by a face/non-face distinction: two face-containing stimuli that elicit a very similar spatial pattern of responses in the posterior fusiform gyrus may produce very different spatial patterns in the other two areas, despite producing a similar overall mean response. Each of these face patches, despite similar overall stimulus preferences, code the stimulus space differently. It is for this reason that the GRS algorithm (unlike other algorithms Vul et al., 2012, discussed further below) identifies each face area as a distinct parcel.

5.4.2 VTC CONTAINS DISTINCT REGIONS WHICH VARY SIGNIFICANTLY IN THEIR FUNCTIONAL REPRESENTATIONS

Figure 5.12A shows the GRS matrix for the right hemisphere VTC of S1 with squares indicating the boundaries of three example clusters. Figure 5.12B shows the parcels corresponding to each of these clusters on the subject's inflated right hemisphere. As mentioned previously, these parcels form discrete patches on the cortical surface. These three clusters were selected based on five criteria: they were (1) well-formed and of reasonable and roughly equal size, (2) were not identified as face, scene or body-selective areas, (3) did not spatially overlap, (4) were identified as clusters for both stimulus sets 2 and 3, and (5) were within posterior ventral cortex, which had high split-half reliability across repeated stimuli (Figure 5.4).

The left-most column of Figure 5.12C shows zoomed insets of the GRS matrix for each of the three clusters. Correlations values fall off as a function of distance from the diagonal, with a somewhat 'boxy' structure (the implications of this in terms of likely underlying cortical topographies are described below).

The middle and right-most columns of Figure 5.12C show the middle frame from the video clips that elicited the 9 highest and lowest beta-weights respectively. These response preferences do not obviously correspond to simple stimulus properties (e.g. curvature, color), features (e.g. shape, size, or eccentricity), or categories (e.g. fruit, cars, or house plants). However, these parcels generally had low responses to uniformly colored screens. For example, parcel 3 shows the largest BOLD responses to person walking through a nightclub, a close up of flowers, leaves blowing on a sidewalk and a cotton-top tamarind on a branch. This was typical; outside of previously identified categorical regions we could not find any parcels with obvious 'word model' selectivity. Although these responses preferences are not easily interpretable, all three parcels fall within the region of VTC that showed high beta-weight correlations across stimulus repeats (Figure 5.4), showing that, while not easily interpretable, these stimulus preferences were highly replicable.

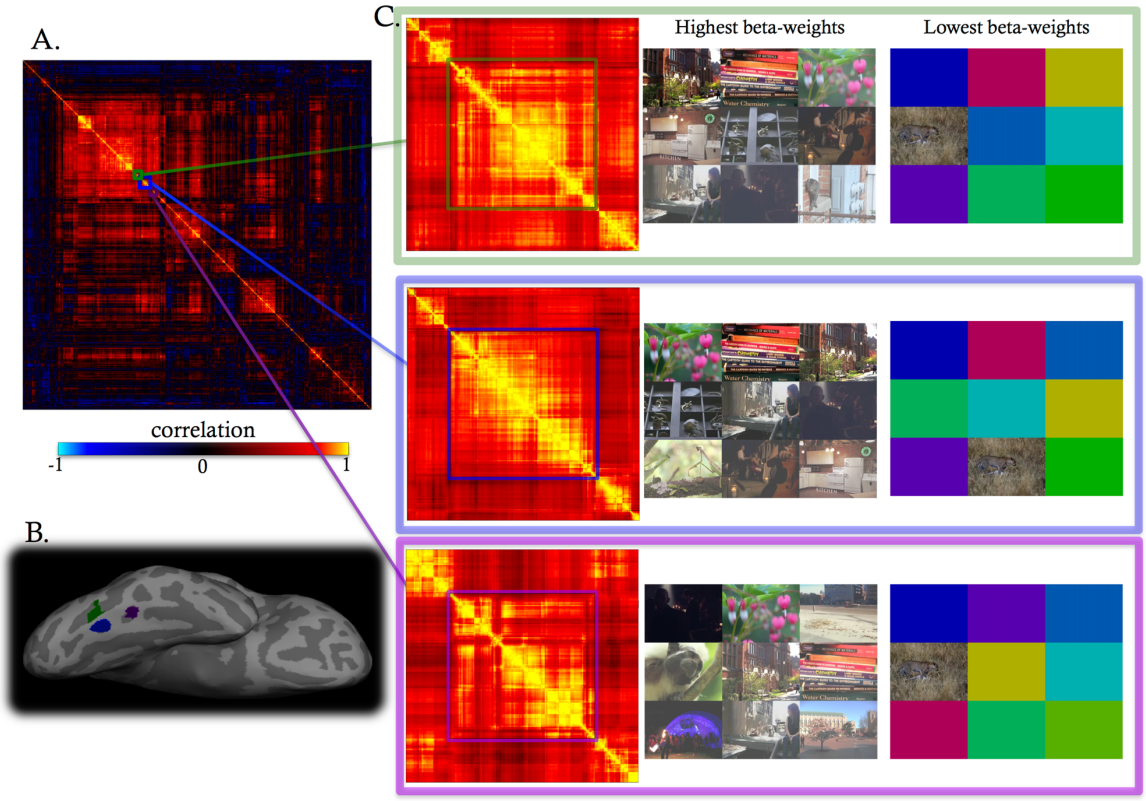

Figure 5.12. Responses in three novel parcels.

(A) The GRS matrix for the right VTC of S1. (B) Parcels corresponding to three clusters on the inflated right hemisphere. (C) Leftmost column shows zoomed inset of the GRS matrix for each parcel, middle and rightmost columns show the middle frame from the 9 video clips eliciting the highest and lowest average beta weights (averaged across the parcel) respectively.

The top row of Figure 5.13 shows a representational dissimilarity matrix created by combining all three of the parcels of Figure 5.12 into a single ROI. Rows 2-4 show RDMs for each individual parcel. For a representational similarity matrix to be visually interpretable it is necessary to have a meaningful method of ordering stimuli along the rows/columns. To illustrate the importance of re-ordering based on similarity, the inset in the top row shows the RDM matrix for the combined ROI, using an arbitrary row/order column order (the alphabetical order of the file names for the video clips).

For naturalistic stimuli, where it is difficult for the experimenter to code the order, optimal leaf ordering (or an analogous technique) can be used to 'discover' potentially meaningful RDM orderings. Indeed, this reordering of dissimilarity matrices can be considered as another example of GRS, though in this case it is the *stimuli* rather than the vertices that are being reordered. In Figure 5.13, the first column of RDMs have been reordered using the permutation obtained from the upper combined ROI (see Supplementary Table 5.2). The RDM for the combined ROI differs visually from the RDMs of each individual parcel, suggesting that each of these three parcels encode different representations of the stimulus space. This is quantified in Table 5.4. Correlations across RDMs were *higher* than the 95% confidence interval for the null model that assumed no spatial structure,

showing that individual parcels contain spatial structure in their response properties. Correlations across RDMs were *lower* than the 95% confidence intervals generated by assuming that all three parcels had identical representational content, demonstrating that these three VTC parcels contain distinct representations of the stimulus space. Thus, parcels not only have different stimulus preferences, but also encode different representations.

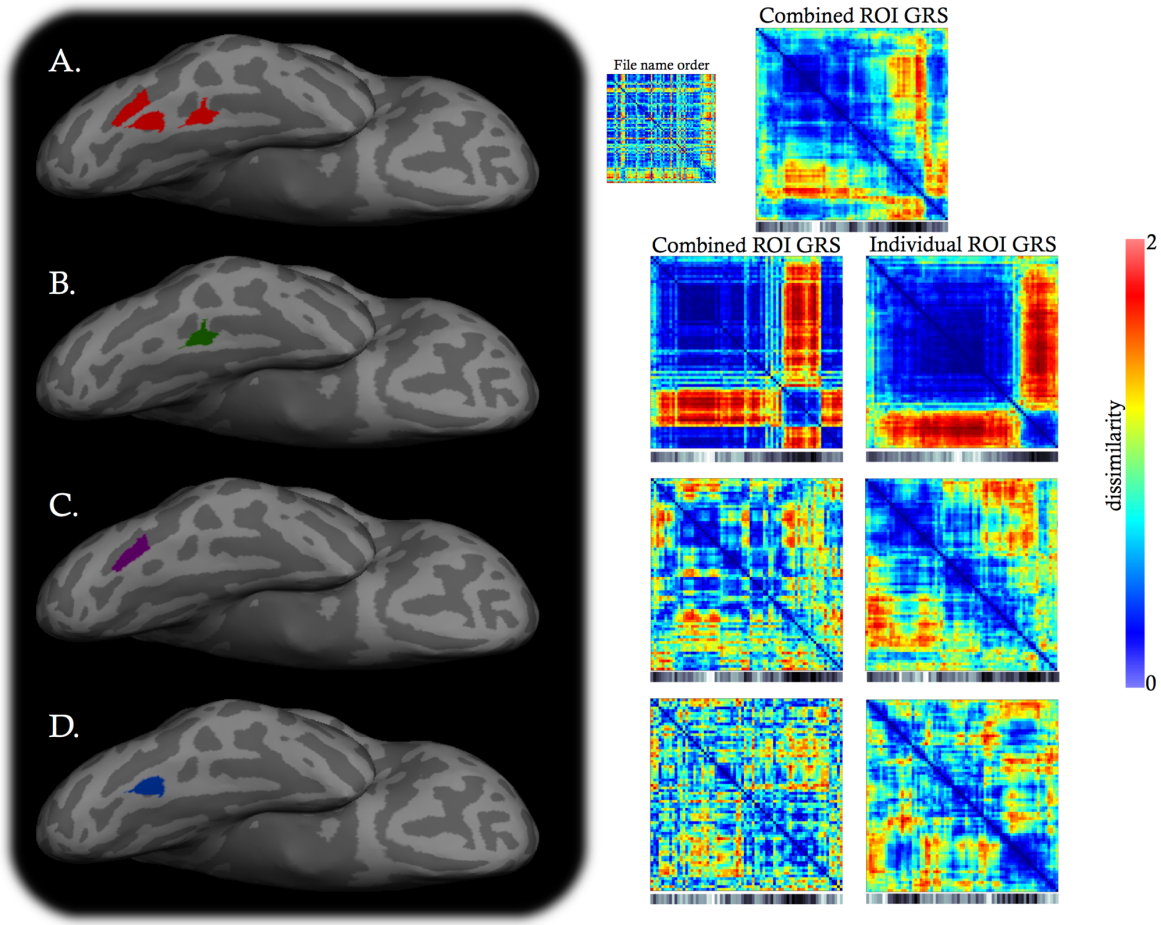

Figure 5.13. Representational dissimilarity matrices for the parcels from Figure 5.12.

The leftmost column shows the locations of each parcel on the inflated right hemisphere. Row A shows data for all three parcels combined into a single ROI. The inset shows the RDM matrix when 'randomly' ordered (based on the alphabetical order of the file names of the video clips). Rows B, C and D show data for each of the individual parcels. The first column of RDMs are ordered based on the permutation vector of the combined ROI. The second column shows each RDM reordered using its own permutation vector (see **Error! Reference source not found.**). Below each RDM is a bar representing the average beta-weight for each stimulus within the RDM, where light values represent positive beta-weights and dark values represent negative beta-weights.

Table 5.4. Correlations between each of the RDM matrices of Figure 5.12.

Underlined italic text shows 95% confidence intervals based on a simulation that randomized the vertex-wise location of beta weights. Italic text shows 95% confidence intervals based on a simulation that assumed that face patches had identical representational content, and differences across RDMs were due to voxel sampling and noise in beta weight estimates.

	Panel B parcel	Panel C parcel	Panel D parcel
Panel A Combined ROI	0.8 (-0.033-0.035) (0.968-0.974)	0.643 (-0.032-0.034) (0.968-0.974)	0.419 (-0.031-0.031) (0.968-0.974)
Panel B parcel		0.411 (-0.031-0.032) (0.782-0.906)	0.213 (-0.032-0.032) (0.776-0.906)
Panel C parcel			0.314 (-0.035-0.034) (0.916-0.952)

The second column of RDMs separately reorders the RDM of each individual parcel (see **Error! Reference source not found.**); a unique structure becomes visible for all three parcels. This ability to order stimuli that cannot easily be coded a priori may provide a potentially useful exploratory tool for visualizing and comparing representational differences across RDMs.

5.5.3. Simulation: The nature of clusters

Figure 5.14 shows simulations of vertex similarity matrices for three types of one dimensional cortical topography. In Figure 5.14A, vertices are ordered based on cortical distance. In Figure 5.14B, the vertex ordering of the beta-weights was initially scrambled to remove any spatial information, and clusters were then recovered using GRS. Note that although the clusters appear in a different order along the diagonal, the algorithm successfully recovered all three clusters.

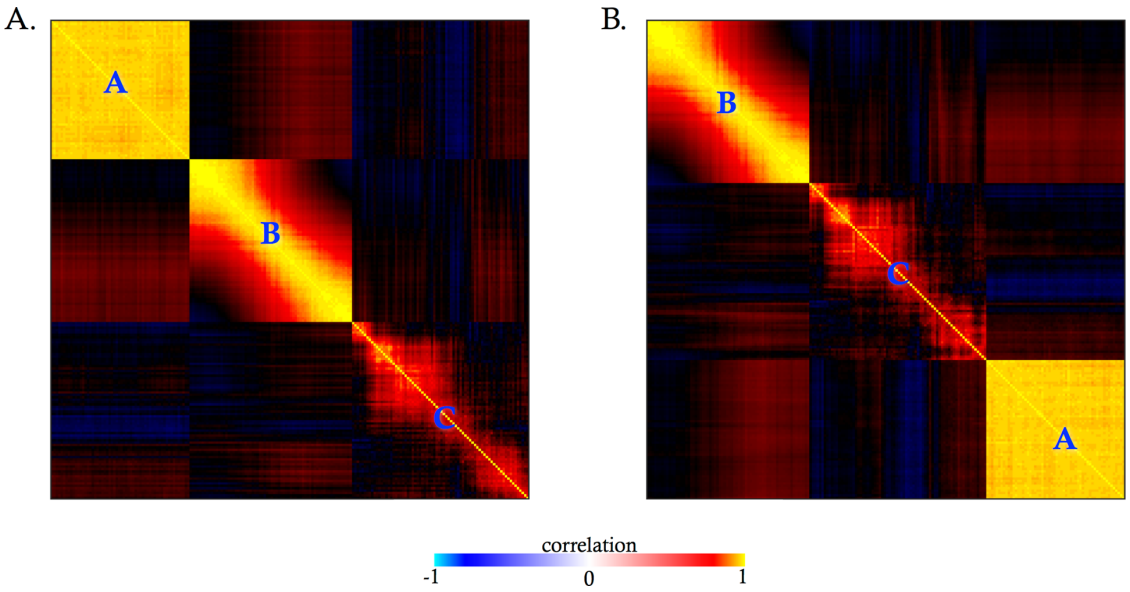

Figure 5.14. Simulated clusters based on three types of cortical topology.

(A) Vertices are ordered based on cortical distance. The top left cluster in A represents a cortical region with a 'spatially uniform' topology, such that every vertex in the cluster varies around a canonical response profile. The middle cluster contains vertices with a complete and smoothly varying topographic representation that is fully sampled by the stimulus space. The bottom right cluster simulates a 'feature space' topographic representation in which each stimulus traverses multiple discrete regions in feature space, and each vertex represents a discrete region in feature space with a Gaussian tuning profile, with the constraint that neighboring vertices have similar response profiles. (B) Vertex ordering of the beta-weights in Panel A were scrambled to remove any spatial information and clusters were then recovered using GRS.

Cluster A in Figure 5.14A represents a cortical region with a 'spatially uniform' response profile, such that every vertex in the cluster has the same pattern of beta-weights across the range of presented stimuli plus additive independent and identically distributed noise (every vertex in the cluster varies around a canonical response profile, Vul et al., 2012). This region appears as a square uniform cluster in both correlation matrices.

Cluster B contains vertices that smoothly vary in their response profile between two uncorrelated response vectors. Neighboring voxels are highly correlated, but the correlation between voxels decreases as a function of distance on a one dimensional cortical surface, creating a complete and smoothly varying topographic representation. This reduction in correlation as a function of cortical distance can be seen in both the original and reordered similarity matrices; neighboring vertex pairs are highly correlated and vertex pairings become progressively less strongly correlated with distance from the diagonal.

Cluster C simulates a more complex topographic representation. Each vertex represents a discrete region in feature space with a Gaussian tuning profile. Vertices are arranged in a topographic map such that nearby locations have similar tuning preferences. The distribution of Gaussian centers is unevenly distributed across the feature space, and tuning widths were randomized. Each stimulus can traverse multiple discrete regions in

feature space, not all stimuli are represented within the feature space, and not all of the feature space is sampled by the stimuli. Once again correlation values fall off as a function of distance from the diagonal, but an additional 'boxy' structure is apparent.

As can be seen in Figure 5.2D and Figure 5.12 the vast majority of clusters that we find in the real data resemble the third, more complex, topology, though we cannot exclude the possibility that other types of organization exist that would produce a similar result.

One important point is that this boxy structure can result in spurious boundaries in cases where not all the feature space is sampled by the stimuli. These 'feature gaps' would cause a parcel to be subdivided into smaller parcels. This would serve to increase variability in parcellation boundaries, but response homogeneity within each sub-parcel would remain high. If this is the case, it is possible that parcellation reliability might increase with a larger stimulus set.

5.6 SUMMARY

Our goal was to develop a method to identify cortical regions with coherent response properties, even in cases where the regions contained spatially non-homogenous responses, were spatially non-contiguous, or had non-obvious stimulus selectivities. We provided three lines of support for the use of our approach. First, GRS parcellations were more replicable than would be expected by chance and differed significantly from the parcellations that would be produced by non-neural spatial correlations in the BOLD data. Second, GRS parcels contain vertices with more coherent stimulus preferences than would be expected by chance. Finally, GRS successfully identifies regions corresponding to known category-selective areas, even when using unconstrained naturalistic stimuli.

5.6.1 STIMULUS PREFERENCES WITHIN NOVEL VTC REGIONS

Although some neurons express categorical selectivity (Bell et al., 2011), heterogeneous stimulus preferences are seen at the cellular and columnar level across much of ventral visual cortex (Sato et al., 2013; Sato, Uchida, & Tanifuji, 2009). For example, in macaques, Sato et al. (2009) report a not atypical inferotemporal cell which responds most strongly to images of a tape dispenser, silly putty, a padlock , a corn cob, and a bird. These single cell responses seem to be characterized by a combination of cell-specific response properties and response components shared across cells in a columnar region (Kreiman et al., 2006; Sato et al., 2013; Sato et al., 2009). Our results suggest that these functional columns are situated within larger-scale functional 'parcels' that span many millimeters of cortex. Despite our finding of seemingly similarly heterogenous stimulus preferences across much of VTC, the selectivities we find at the macro-scale are unlikely to be directly inherited from those seen at the single cell or columnar levels, given the massive size discrepancy between neural columns and fMRI regions.

5.6.2. Comparison with other parcellation methods

Most current fMRI parcellation approaches forgo stimuli altogether, using instead resting-state data. A diversity of clustering approaches are being explored, including edge-detection methods (Cohen et al., 2008), spatially-constrained hierarchical clustering (Blumensath et al., 2013), spatially-constrained spectral clustering (Craddock et al., 2012), and resting-state-functional-connectivity (RSFC)-snowballing (Wig et al., 2014). The goal of these parcellations has generally been to provide seed regions for connectomics and/or nodes for functional connectivity analysis. We do not know of any attempt to compare these parcellations to well characterized functionally-defined areas within the VTC, such as face or scene areas. Our approach was designed to emphasize the stimulus-driven component of the BOLD response by using a naturalistic, stimulus-driven paradigm and estimating responses using a GLM that accounted for the hemodynamic response, repeated stimulus presentations, and nuisance regressors. It is an interesting question how well resting-state parcellations within the VTC will correspond with parcellations based on functional preferences given that resting-state analyses evaluate very low frequency (< .08 Hz) BOLD fluctuations (Power et al., 2014) which likely contain components not driven by task-related neuronal responses (Tong et al., 2015).

Despite the GRS algorithm being 'blind' to spatial information (clusters were defined as coherently varying response profiles across *stimulus* space), our clusters almost always corresponded to discrete parcels in *physical* space – complete and contiguous patches on the cortical surface. While this pattern of results is consistent with the parcellations produced by gene-expression (Hawrylycz et al., 2012), neurotransmitter receptor distribution (Zilles & Amunts, 2009), and cytoarchitecture (Schleicher et al., 2009), it differs strikingly from the 'networks' revealed by resting-state data when using algorithms that do not include explicit spatial constraints.

One other line of research has attempted to identify functional regions by clustering locations (in their case voxels) based on beta-weight estimates to individual stimuli (Lashkari, Sridharan, & Golland, 2010; Lashkari, Sridharan, Vul, et al., 2010; Lashkari et al., 2012; Lashkari et al., 2008; Vul et al., 2012) and compare their results to category-selective regions identified using the localizer method (Lashkari et al., 2008) (see also Table 5.2). One significant difference from our approach is that their research to date has been restricted to categorical stimuli. It is unclear how well their approach will generalize to the diverse naturalistic stimuli that are likely needed to understand the representational content of uncharacterized regions of VTC. A second important difference is that their algorithm characterizes voxel responses as hyper-dimensional clusters in a response space (Lashkari et al., 2008; Vul et al., 2012); assuming that voxels can be described either as mixtures of (independently and identically distributed) activation profiles for pre-specified categories, or as a circular Gaussian around a 'canonical selectivity profile'. Generalization to more diverse representational topologies would significantly add to the complexity of their algorithm, which is already quite complex. A critical limitation of these assumptions is that the algorithm cannot individuate regions which do not differ in their univariate responses. For example, their approach characterizes the three ventral face areas (see Figure 5.7) as a single 'face

system' (e.g. Lashkari et al., 2008; Vul et al., 2012). In contrast, despite no access to spatial information, the GRS approach identifies the three face regions of Figure 5.7 as separate parcels.

5.6.3. Synergy with other methods for examining representational content

Although dimensionality reduction, representational similarity analysis (RSA), and related approaches (Kriegeskorte et al., 2008; McIntosh & Misic, 2013; Mur, 2011) are powerful ways of exploring complex representational content, the logic of these approaches requires selecting an ROI containing a unitary, complete representation. In the absence of a region of interest with coherent response properties, the underlying structure revealed by these algorithms becomes less informative and more difficult to interpret. Choosing an ROI that contains multiple regions that differ in their representational content will produce results that are at best partially obscured (see Figure 5.13) and at worst (e.g. including all of VTC) severely degraded (Mur, 2011). As demonstrated by Figure 5.6C, and Table 5.4, GRS is capable of discovering VTC parcels with distinct and coherent response properties for further analysis.

Specifically, with respect to representational similarity analysis, GRS not only provides a means of identifying functionally coherent ROIs, but also offers a useful alternative to multidimensional scaling (Kriegeskorte et al., 2008) as a tool for exploratory visualization. The visual interpretability of RDMs depends critically on the row/column ordering (as shown by the inset of Figure 5.13). Grouping by response similarity can reorder RDMs such that stimuli that produce similar response patterns are nearby in the RDM.

5.6.4. Conclusions and future directions

Progress in understanding the function of ventral temporal cortex has been impeded by the lack of exploratory methods for investigating cortical function in regions where functional boundaries, stimulus preferences, and representational topology are unclear. While the localizer approach provides a powerful means for testing explicit hypotheses, it requires that the experimenter propose features for which a cortical area might be selective, generate otherwise similar stimuli that explicitly contain/lack those features, and determine contrasts between sets of stimuli. In contrast, GRS does not require the experimenter to anticipate functional preferences, does not require the experimenter to pre-categorize or label stimuli, and does not constrain the stimulus space. Indeed, GRS is likely to be most effective when the stimulus space is sampled as widely as possible. GRS provides a general framework for discovering discrete cortical areas with coherent response properties within enigmatic cortical regions for which regional boundaries and the topology of stimulus preferences have yet to be identified. Identifying such regions is likely to be critical for understanding how VTC represents the visual world.

One obvious future direction includes further functional characterization of individual GRS parcels. One promising approach would be to carry out RSA or related approaches on the responses of individual parcels using labelled naturalistic stimuli. Another would be to investigate how parcels relate to various proposed

superareal organizational patterns such as eccentricity (Hasson et al., 2002), animacy (Anzellotti, Mahon, Schwarzbach, & Caramazza, 2011), real-world size (Konkle & Caramazza, 2013), nested spatial hierarchies (Grill-Spector & Weiner, 2014), and increasing individuation (Tyler et al., 2004). The relationship between parcels and functional organization on the columnar or neural scale also merits further investigation.

Examining consistency of parcellations across different subjects is another a critical next step. Given the anatomical variability of VTC this will be a significant undertaking. However, the consistent patterns of response selectivities to novel shapes in juvenile monkeys (Srihasam et al., 2014) suggests that a large-scale proto-organization for high-level visual properties, which is likely driven by anatomical constraints (Saygin et al., 2016), may exist.

Finally, comparing GRS parcellations with the results from other methodologies such as cortical folding, histology, connectivity, cytoarchitecture, myeloarchitecture, and receptor architecture will be necessary to determine whether or not GRS parcels correspond to cortical areas (David C Van Essen, 2004).

6. Supplementary Figures & Tables

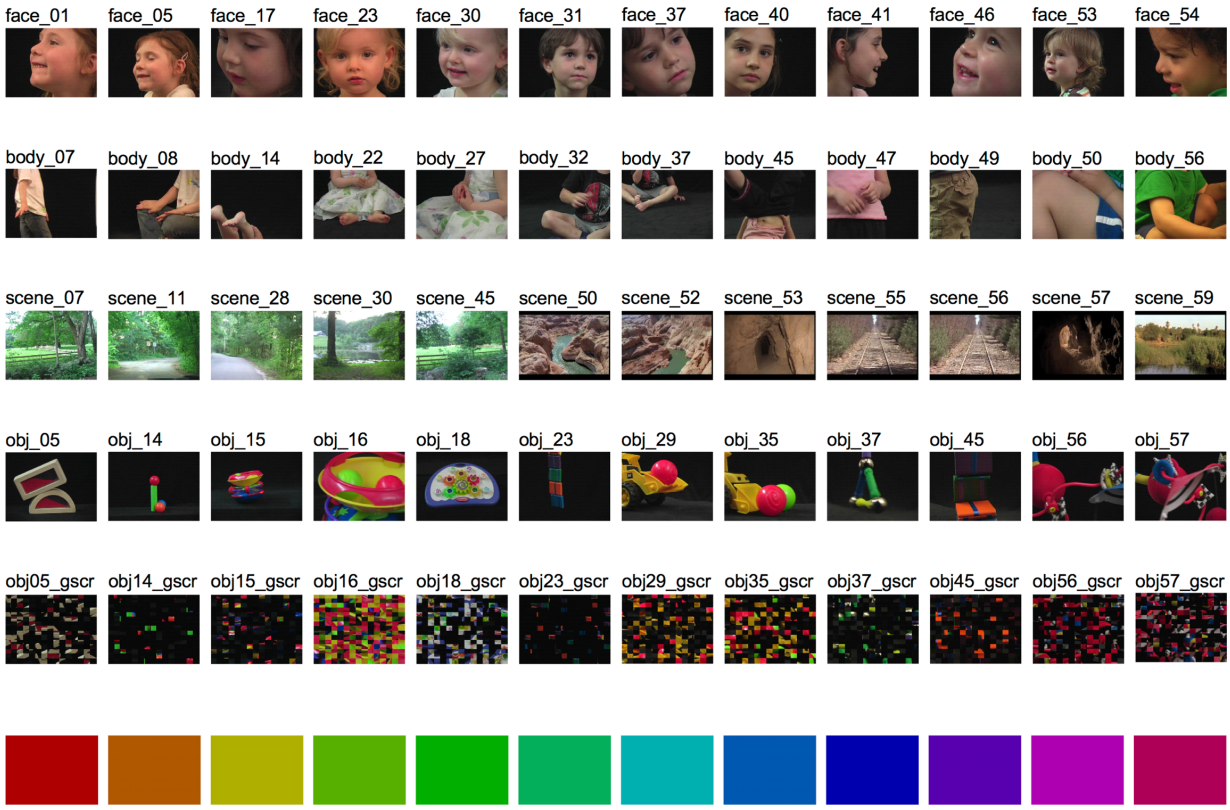

Supplementary Figure 5.1. Stimuli from Stimulus Set 1.

Middle frames from the video clips of faces, bodies, scenes, objects, and scrambled objects used in Stimulus Set 1.

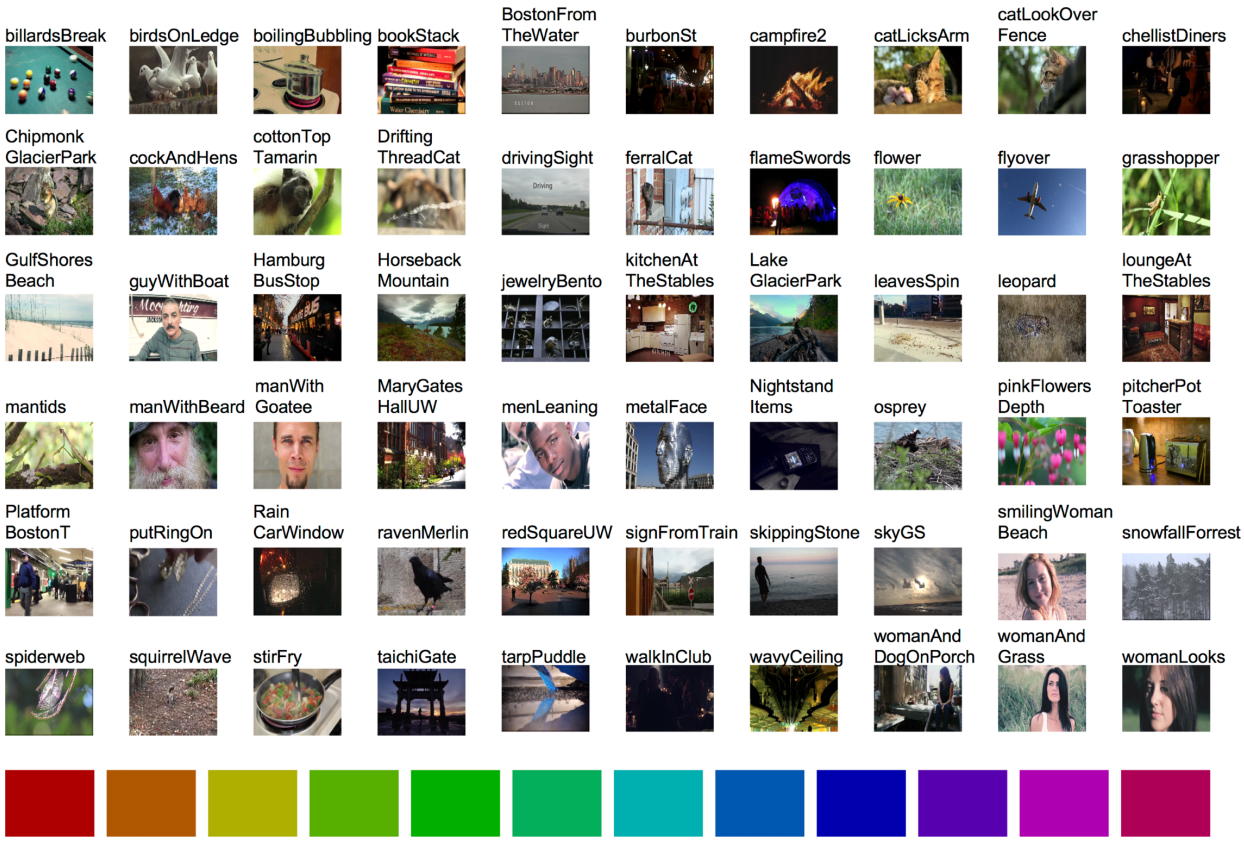

Supplementary Figure 5.2. Stimuli from Stimulus Set 2.

Middle frames from the naturalistic video clips used in naturalistic Stimulus Set 2.

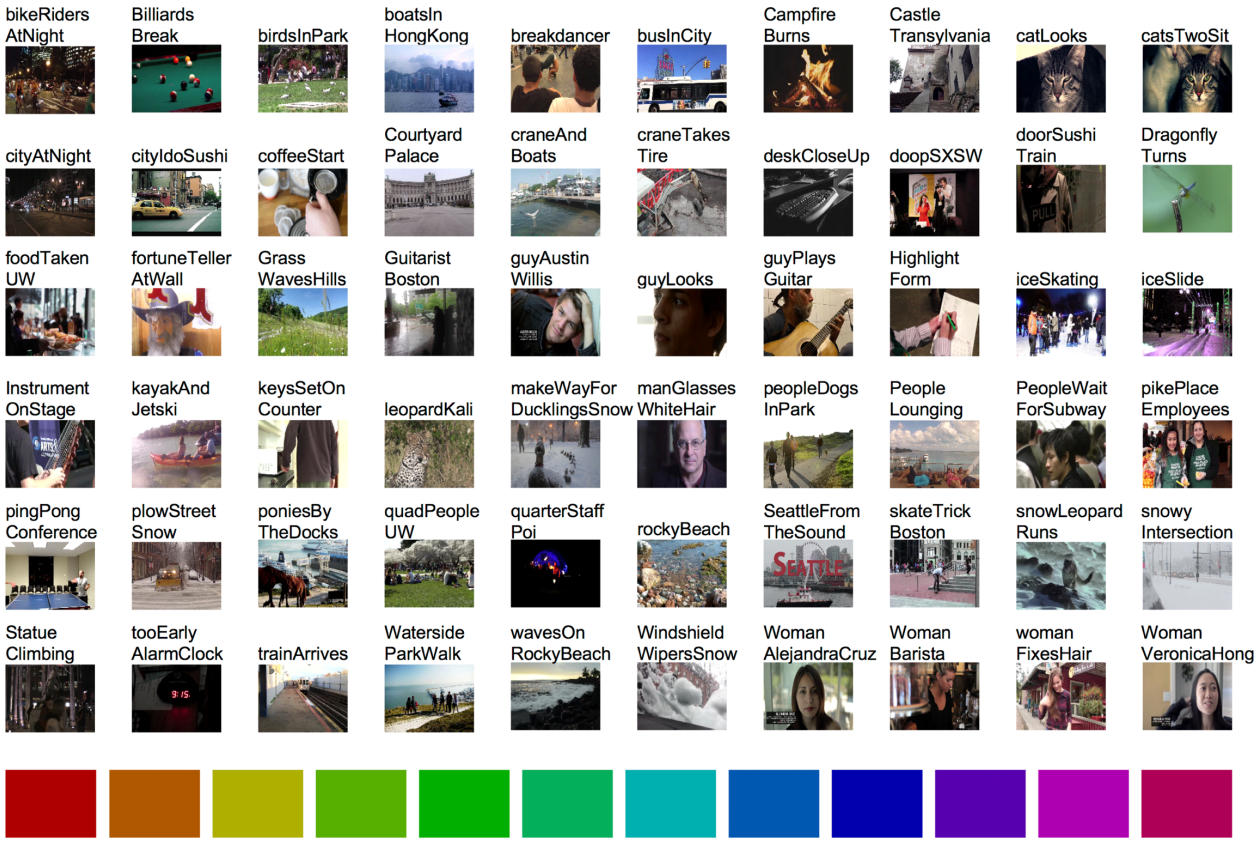

Supplementary Figure 5.3. Stimuli from Stimulus Set 3.

Middle frames from the naturalistic video clips used in naturalistic Stimulus Set 3.

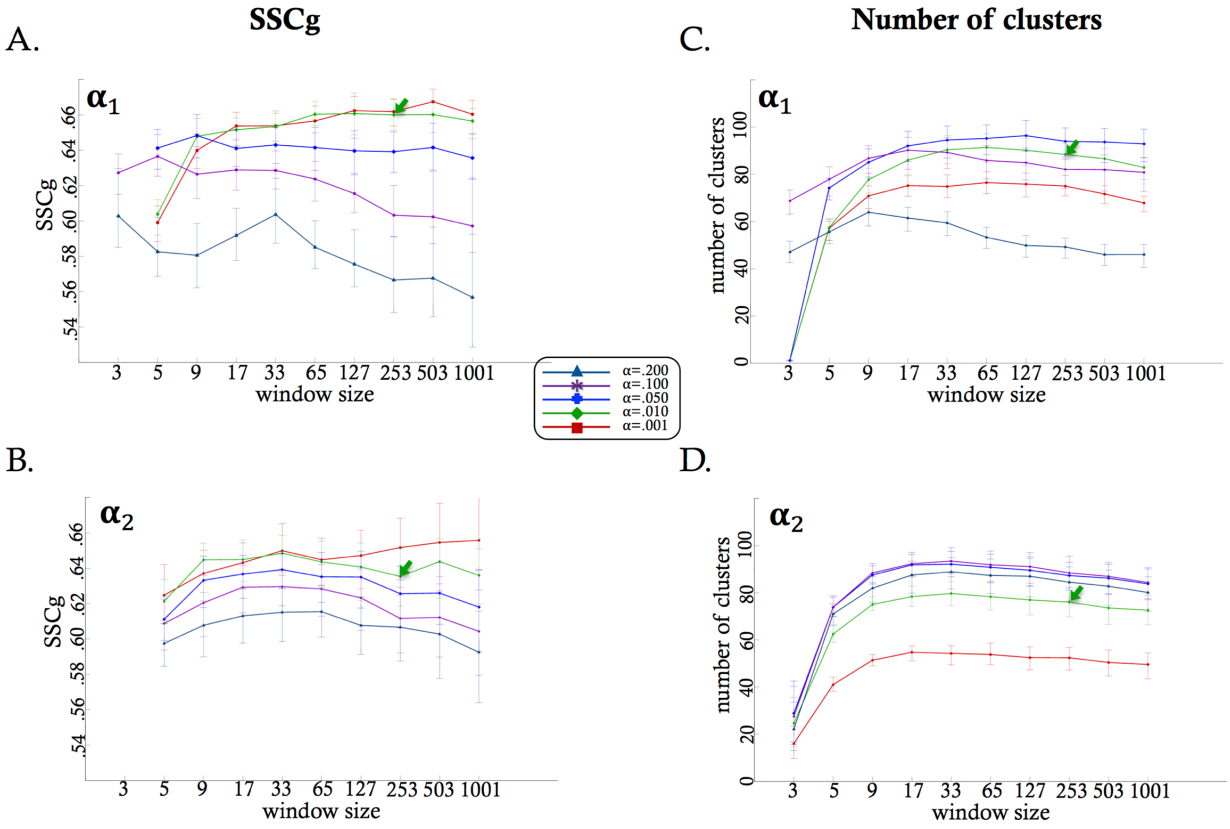

Supplementary Figure 5.4. Parameter analysis.

Parcellation consistency (A, B) and the number of clusters (C, D) were examined as a function of parameter values. The following range of values was examined: w=3-1001, α_1 = 0.001-0.2, α_2 = 0.001-0.2. SSCg values represent parcellation similarity across paired datasets (e.g. Stimulus Sets 1 and 2), using all possible pairwise comparisons. We chose final parameter values that reliably produced a reasonable number of clusters with a high mean SSC, w=253, α_1 = 0.01, α_2 = 0.01, indicated by a green arrow in each panel. Both the number of clusters, and parcellation consistency was reasonably robust to a wide range of parameter values: w=17-1001, α_1 = 0.001-0.05, α_2 = 0.01-0.2. Within this range interactions between α_1 and α_2 were not large (data not shown). In Panels A and C mean values and error bars represent 95% confidence intervals calculated over subject, hemisphere, pairwise Stimulus Set comparisons, and the full parameter range of α_2. In Panels B and D mean values and error bars are calculated over subject, hemisphere, pairwise Stimulus Set comparisons, and the full parameter range of α_1.

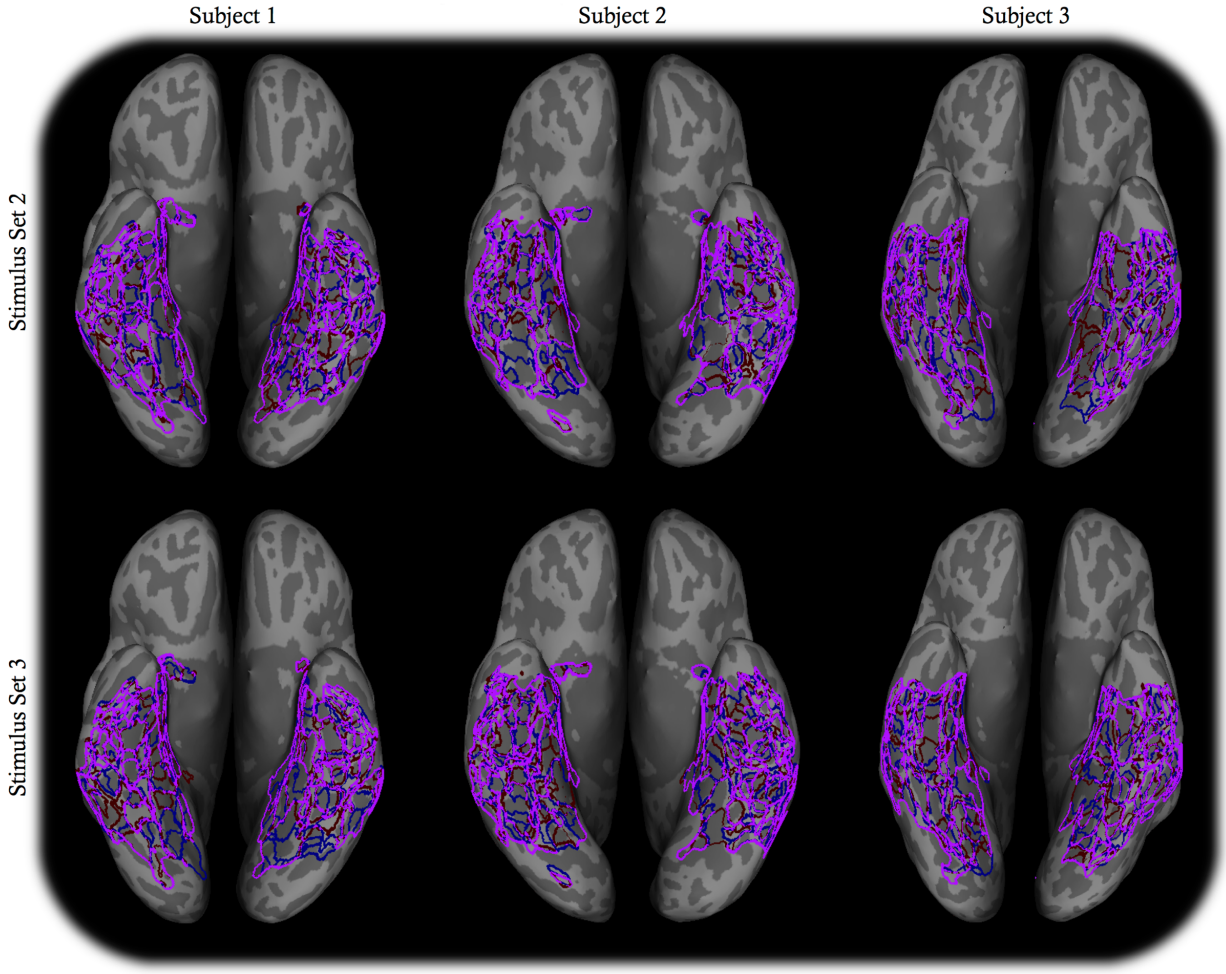

Supplementary Figure 5.5. Parcellation boundaries with and without inclusion of the beta-weights for uniformly colored screens.

Boundaries when colored screens were included are shown in red, boundaries when colored screens were excluded are shown in blue, borders shared across both datasets are shown in magenta.

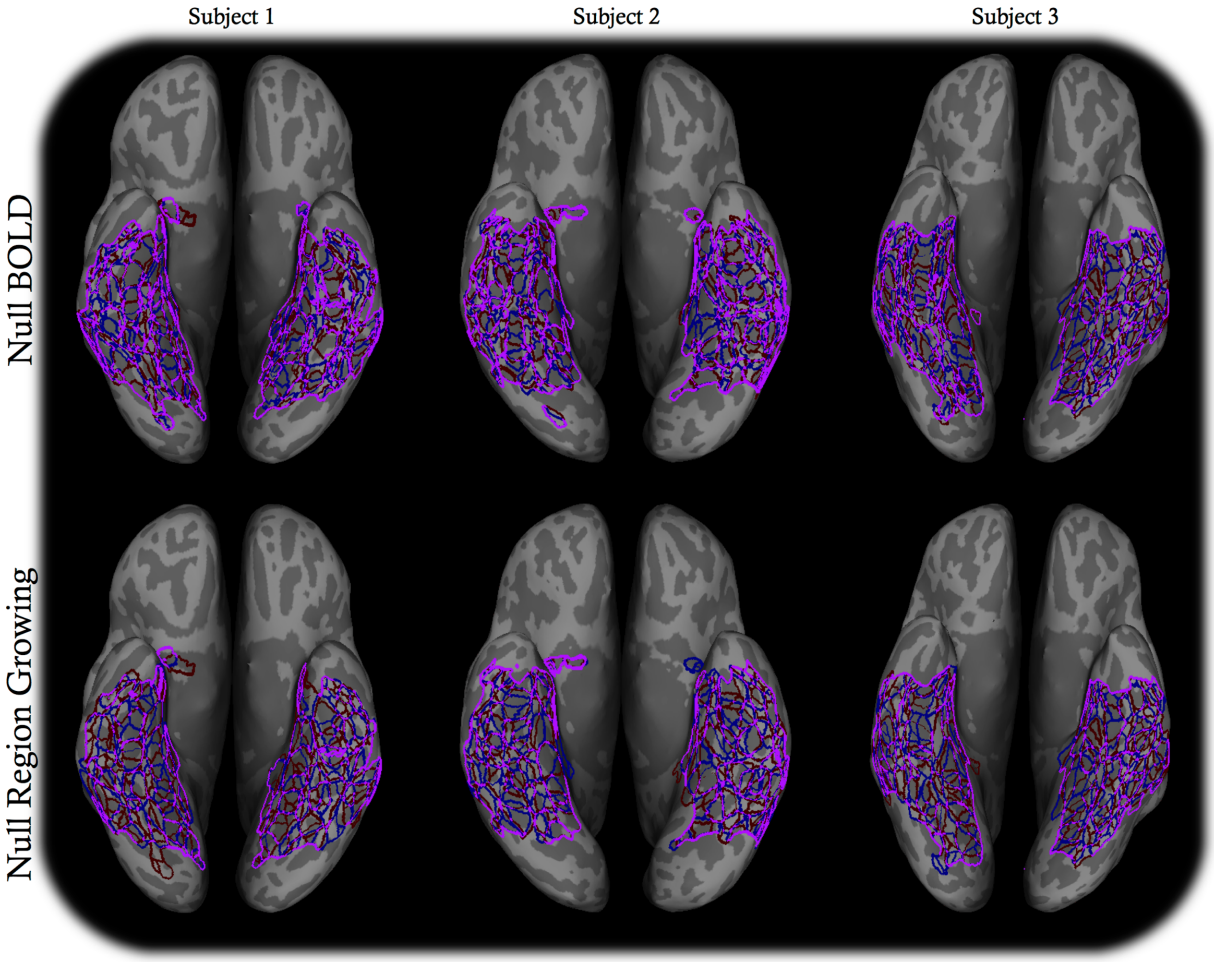

Supplementary Figure 5.6. Parcellation boundaries for the two null models.

For the null BOLD model boundaries from stimulus set 2 are shown in red, those from stimulus set 3 are shown in blue, and borders shared across both datasets are shown in magenta. For the Null region growing model boundaries are calculated across two iterations of the region growing algorithm.

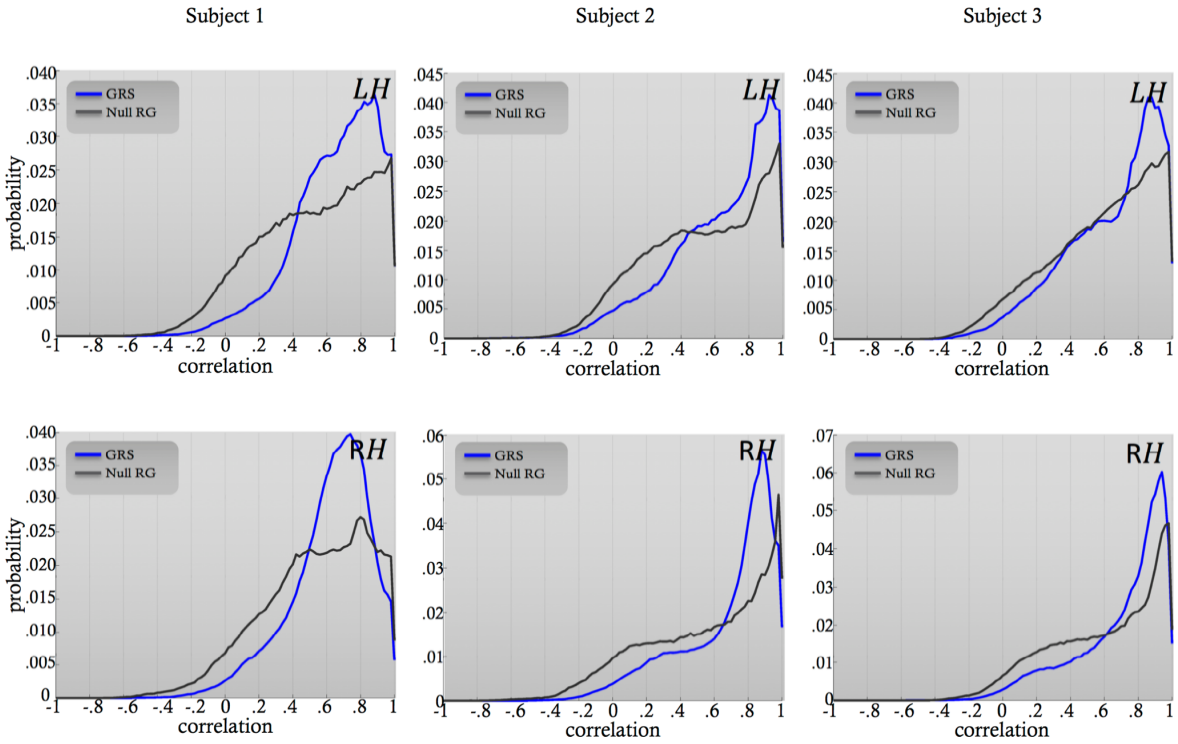

Supplementary Figure 5.7. Probability distributions of beta-weight correlation values across pair of vertices in the same parcel, individual hemisphere data.

The blue line represents results generated using parcels from GRS of real data, the black line represents results generated using parcels from the region growing null model.

Supplementary Table 5.1. List of the stimulus orderings for the RDMs of Figure 5.11.

The images corresponding to each stimulus can be found in Supplementary Figures 1-3. Numerical values represent RGB values for the uniformly colored screens.

Stimulus Set 1	Stimulus Set 2	Stimulus Set 3
face_01	cottonTopTamarin	doopSXSW
face_05	womanAndDogOnPorch	womanBarista
face_17	manWithGoatee	womanFixesHair
face_23	womanLooks	pikePlaceEmployees
face_30	menLeaning	peopleLounging
face_31	womanAndGrass	womanVeronicaHong
face_37	manWithBeard	manAustinWillis
face_40	chellistDiners	peopleWaitForSubway
face_41	walkInClub	womanAlejandraCruz
face_46	smilingWomanBeach	kayakAndJetski
face_53	ferralCat	manLooks
face_54	chipmonkGlacierPark	fortuneTellerAtWall
body_07	mantids	leopardKali
body_08	ravenMerlin	dragonflyTurns
body_14	catLookOverFence	catLooks
body_22	grasshopper	iceSkating
body_27	pinkFlowersDepth	birdsInPark
body_32	jewelryBento	catsTwoSit
body_37	putRingOn	quadPeopleUW
body_45	birdsOnLedge	peopleDogsInPark
body_47	cockAndHens	manGlassesWhiteHair
body_49	boilingBubbling	poniesByTheDocks
body_50	manWithBoat	makeWayForDucklingsSnow
body_56	flyover	pingPongConference
scene_07	squirrelWave	snowLeopardRuns
scene_11	platformBostonT	bikeRidersAtNight
scene_28	bookStack	keysSetOnCounter
scene_30	MaryGatesHallUW	foodTakenUW
scene_45	osprey	manPlaysGuitar
scene_50	catLicksArm	breakdancer
scene_52	metalFace	highlightForm
scene_53	leavesSpin	doorSushiTrain
scene_55	stirFry	quarterStaffPoi
scene_56	spiderweb	snowyIntersection
scene_57	flower	statueClimbing
scene_59	flameSwords	iceSlide
obj_05	pitcherPotToaster	watersideParkWalk
obj_14	kitchenAtTheStables	plowStreetSnow
obj_15	burbonSt	coffeeStart
obj_16	HamburgBusStop	instrumentOnStage
obj_18	drivingSight	cityIdoSushi
obj_23	loungeAtTheStables	guitaristBoston
obj_29	signFromTrain	skateTrickBoston
obj_35	wavyCeiling	wavesOnRockyBeach
obj_37	billardsBreak	windshieldWipersSnow
obj_45	skippingStone	tooEarlyAlarmClock
obj_56	BostonFromTheWater	castleTransylvania
obj_57	redSquareUW	busInCity
obj05_gscr	horsebackMountain	billiardsBreak
obj14_gscr	driftingThreadCat	SeattleFromTheSound
obj15_gscr	leopard	craneTakesTire
obj16_gscr	skyGS	0 0 175
obj18_gscr	175 0 0	craneAndBoats
obj23_gscr	GulfShoresBeach	trainArrives
obj29_gscr	tarpPuddle	boatsInHongKong
obj35_gscr	snowfallForrest	0 175 0
obj37_gscr	175 0 175	courtyardPalace
obj45_gscr	lakeGlacierPark	rockyBeach
obj56_gscr	175 87.5 0	grassWavesHills
obj57_gscr	nightstandItems	175 0 87.5
0 103 31	campfire2	cityAtNight
0 114 158	taichiGate	deskCloseUp
0 124 61	rainCarWindow	campfireBurns
0 174 189	0 175 175	0 175 87.5
0 58 67	0 175 87.5	87.5 0 175
112 0 130	87.5 0 175	0 175 175
189 0 10	0 175 0	175 0 0
24 0 78	87.5 175 0	175 87.5 0
53 27 0	0 87.5 175	175 0 175
8 0 71	175 175 0	175 175 0
88 0 60	175 0 87.5	87.5 175 0
95 51 0	0 0 175	0 87.5 175

Supplementary Table 5.2. List of the stimulus orderings for the RDMs of Figure 5.13.

The images corresponding to each stimulus can be found in Supplementary Figures 1-3. Numerical values represent RGB values for the uniformly colored screens.

Panel A Combined ROI and leftmost column	Panel B Individual ROI	Panel C Individual ROI	Panel D Individual ROI
skippingStone	chipmonkGlacierPark	stirFry	BostonFromTheWater
175 0 175	175 0 175	lakeGlacierPark	bookStack
metalFace	squirrelWave	spiderweb	skyGS
manWithGoatee	driftingThreadCat	nightstandItems	pitcherPotToaster
manWithBeard	skippingStone	skyGS	loungeAtTheStables
womanLooks	metalFace	GulfShoresBeach	kitchenAtTheStables
menLeaning	flyover	wavyCeiling	pinkFlowersDepth
womanAndGrass	birdsOnLedge	loungeAtTheStables	jewelryBento
cottonTopTamarin	womanAndGrass	birdsOnLedge	catLicksArm
driftingThreadCat	manWithGoatee	pitcherPotToaster	womanAndGrass
putRingOn	menLeaning	taichiGate	taichiGate
redSquareUW	platformBostonT	redSquareUW	0 175 87.5
loungeAtTheStables	walkInClub	bookStack	175 87.5 0
wavyCeiling	taichiGate	BostonFromTheWater	catLookOverFence
GulfShoresBeach	spiderweb	drivingSight	0 0 175
nightstandItems	snowfallForrest	grasshopper	175 0 175
pitcherPotToaster	tarpPuddle	flower	tarpPuddle
signFromTrain	manWithBoat	flyover	175 0 0
MaryGatesHallUW	boilingBubbling	mantids	87.5 0 175
BostonFromTheWater	ravenMerlin	kitchenAtTheStables	smilingWomanBeach
kitchenAtTheStables	grasshopper	signFromTrain	womanLooks
bookStack	drivingSight	jewelryBento	menLeaning
jewelryBento	ferralCat	pinkFlowersDepth	cockAndHens
pinkFlowersDepth	wavyCeiling	billardsBreak	MaryGatesHallUW
billardsBreak	flameSwords	MaryGatesHallUW	snowfallForrest
leavesSpin	cockAndHens	leavesSpin	cottonTopTamarin
burbonSt	chellistDiners	snowfallForrest	lakeGlacierPark
walkInClub	womanAndDogOnPorch	driftingThreadCat	manWithBeard
platformBostonT	mantids	flameSwords	flower
manWithBoat	stirFry	burbonSt	stirFry
womanAndDogOnPorch	HamburgBusStop	HamburgBusStop	grasshopper
chellistDiners	GulfShoresBeach	chipmonkGlacierPark	mantids
cockAndHens	signFromTrain	womanLooks	ravenMerlin
HamburgBusStop	jewelryBento	horsebackMountain	chipmonkGlacierPark
ferralCat	bookStack	platformBostonT	manWithBoat
175 87.5 0	MaryGatesHallUW	walkInClub	manWithGoatee
175 0 0	nightstandItems	chellistDiners	chellistDiners
taichiGate	leavesSpin	manWithBoat	womanAndDogOnPorch
drivingSight	BostonFromTheWater	womanAndDogOnPorch	ferralCat
grasshopper	loungeAtTheStables	cockAndHens	billardsBreak
mantids	pinkFlowersDepth	cottonTopTamarin	GulfShoresBeach
flyover	pitcherPotToaster	ravenMerlin	driftingThreadCat
ravenMerlin	kitchenAtTheStables	osprey	signFromTrain
osprey	redSquareUW	0 175 87.5	nightstandItems
birdsOnLedge	putRingOn	175 87.5 0	HamburgBusStop
87.5 175 0	womanLooks	87.5 0 175	leavesSpin
flower	manWithBeard	leopard	flameSwords
chipmonkGlacierPark	cottonTopTamarin	squirrelWave	burbonSt
horsebackMountain	burbonSt	ferralCat	walkInClub
squirrelWave	billardsBreak	menLeaning	platformBostonT
smilingWomanBeach	lakeGlacierPark	manWithGoatee	horsebackMountain
87.5 0 175	skyGS	womanAndGrass	87.5 175 0
catLookOverFence	horsebackMountain	smilingWomanBeach	campfire2
0 87.5 175	175 0 0	175 0 0	175 175 0
0 175 87.5	flower	catLookOverFence	drivingSight
0 175 175	87.5 175 0	manWithBeard	0 175 0
leopard	175 87.5 0	skippingStone	0 87.5 175
175 175 0	osprey	175 175 0	osprey
0 175 0	rainCarWindow	0 175 0	175 0 87.5
catLicksArm	0 175 0	metalFace	metalFace
0 0 175	campfire2	0 87.5 175	leopard
175 0 87.5	87.5 0 175	0 0 175	birdsOnLedge
campfire2	0 0 175	0 175 175	squirrelWave
rainCarWindow	0 175 87.5	175 0 175	0 175 175
boilingBubbling	175 0 87.5	175 0 87.5	skippingStone
spiderweb	0 87.5 175	87.5 175 0	putRingOn
tarpPuddle	0 175 175	tarpPuddle	flyover
snowfallForrest	leopard	putRingOn	wavyCeiling
lakeGlacierPark	175 175 0	catLicksArm	boilingBubbling
stirFry	catLicksArm	rainCarWindow	spiderweb
flameSwords	catLookOverFence	campfire2	rainCarWindow
skyGS	smilingWomanBeach	boilingBubbling	redSquareUW

ToC

CONCLUSIONS

Developing an understanding of the ventral temporal cortex will require a multidisciplinary effort combining information including anatomy, cytoarchitecture, myeloarchitecture, receptor architecture, white matter pathways, functional responses, and topographic organization. **Chapter 1** discusses the contribution of each of these methodologies to understanding of cortical organization. Cortical areas are functionally distinct regions of the brain which differ on a number of these properties. Emerging data, including the results reported in **Chapter 5**, suggest that the ventral temporal cortex contains a series of functionally coherent regions which tile the surface of the ventral temporal cortex. Due to the idiosyncratic anatomy and location of functional regions in the VTC, other methodologies will likely need to be applied in the same subjects to determine if these regions are indicative of cortical areas. Even if the entire VTC is tessellated with cortical areas, VTC may still contain aspects of large-scale and distributed organization. Evidence for large-scale gradients of function responses across the VTC is not inconsistent with a parcellation into distinct areas, and developmental research suggests that these response biases in combination with experience might be what gives rise to functionally distinct visual areas. Large-scale organizations may also organize areas into clusters similar to the retinotopic map clusters in the early- and mid-visual cortex. The representation of visual stimuli may be distributed within or across areas.

It will also be essential to understand how aspects of cortical organization arise with developmental processes, to what extent they change throughout normal life, and how much they can reorganize in the event of dramatic perturbations. Chapters 2 and 3 address the role of neural plasticity for the category-selective regions of the VTC, specifically as revealed by the particular developmental history of subject M.M., who was blinded from the ages of 3.5 to 46 years and subsequently had more than a decade of recovered sight. **Chapter 2** describes developmental and adult plasticity, as well as cortical reorganization. The implications of the amount of experience-dependent plasticity we might expect to see in M.M. for each section are described. **Chapter 3** reports the results of empirical work which suggests the architecture of the category-selective regions requires extensive-visual input to develop normally and has only limited plasticity in adulthood.

The next two chapters addressed cortical parcellation. In **Chapter 4**, parcellation approaches are described for each aspect of cortical organization. Where possible, the performance of these approaches on the VTC was mentioned. Very few articles from the parcellation literature contain figures with results from the VTC, and only one series of studies have used the category-selective regions to attempt to demonstrate validity.

Finally, **Chapter 5** introduces a novel data-driven method for exploration of functional organization. This method, Grouping by Response Similarity, finds a series of functionally coherent regions tiling the surface of the ventral temporal cortex. GRS does not require the experimenter to code information about stimuli or stimulus relationships, which makes the approach amenable to using naturalistic stimuli. In turn, the naturalistic

stimuli facilitate differentially engaging more of the regions in the VTC. GRS also does not have access to any information about the spatial locations of the data, so the finding that functional clusters correspond to discrete, fully-filled patches on the cortical surface is purely a result of the coherent responses within the cluster. Simulation results also demonstrate that GRS can perform successfully on a range of different topographical organization. As a result, GRS separately identifies the VTC face-selective regions which had previously only been identified as a homogenous face 'system' by previous data-driven methods that make more conventional and implausible statistical assumptions. In addition to recovering the known category-selective regions, GRS also identified a large number of other regions tiling the remainder of the VTC. Examining both amplitude and pattern of stimulus-driven responses suggests that these regions do not have any obvious category-selective responses, though the responses within these regions were largely replicable.

In attempting to understand the biological function of any part of an organism requires not only an evolutionary perspective but an ethological one as well. Situated between the early visual cortex and hippocampus, the ventral visual pathway has often been regarded solely as an image recognition system. Some approaches to understanding the function of the ventral temporal cortex could be read as regarding the problem as equivalent to understanding how the brain solves visual object recognition. However, there are many complex problems that the human visual systems have evolved to solve. Developing a full understanding of VTC function will likely require understanding its multifaceted roles in an array of ethologically valid tasks (Peelen & Downing, 2017). One way to begin to move toward this goal is to use unconstrained naturalistic stimuli and allow subjects to freely view the screen rather than enforcing fixation. It has already been demonstrated that free viewing has little impact on form response of Macaque IT neurons (DiCarlo & Maunsell, 2000), and there seems to be comparably little effect on human ventral temporal cortex responses (unpublished observations).

Methods to study and relate topographic organizations should continue to be developed. Simulation results suggest that the GRS method can identify regions with a topographic organization (see Section 5.5.3. Simulation: The nature of clusters), and most clusters from the real data resembled the simulated topographic clusters. These functional properties are in turn likely to be the result of distinctive long-range connectivity and local microanatomical properties. Topographic organizations are partially established by chemical gradients during development (McLaughlin & O'Leary, 2005) and are later refined through experience (Bock et al., 2015; Wiesel & Hubel, 1963, 1965). The white matter bundles that form region-to-region and cross-hemisphere connections in these areas are themselves topographically organized (Bock et al., 2013; Cang & Feldheim, 2013; O'Leary & McLaughlin, 2005). Thus methods that can detect, quantify, and compare topographic organizations are will apply to both function and connectivity (Jbabdi et al., 2013).

If these speculations are correct, then we are well on the way establishing a parcellation of the ventral temporal cortex into a series of cortical areas on par with well-established maps of the early visual areas. However, to stretch the metaphor, having a completed map only serves to facilitate more targeted exploration, and it would

be through something more akin to ecology than cartography that will be required to begin to understand the functional roles of the ventral temporal cortex.

REFERENCES

Ackman, J. B., & Crair, M. C. (2014). Role of emergent neural activity in visual map development. *Current Opinion in Neurobiology, 24*(1), 166-175. doi:10.1016/j.conb.2013.11.011

Adelson, E. H., & Movshon, J. A. (1982). Phenomenal coherence of moving visual patterns. *Nature, 300*(5892), 523-525. URL: https://www.ncbi.nlm.nih.gov/pubmed/7144903

Ahissar, M., & Hochstein, S. (1997). Task difficulty and the specificity of perceptual learning. *Nature, 387*(6631), 401-406. doi:10.1038/387401a0

Amunts, K., Lepage, C., Borgeat, L., Mohlberg, H., Dickscheid, T., Rousseau, M. E., . . . Evans, A. C. (2013). BigBrain: an ultrahigh-resolution 3D human brain model. *Science, 340*(6139), 1472-1475. doi:10.1126/science.1235381

Anderson, M. L., & Finlay, B. L. (2014). Allocating structure to function: the strong links between neuroplasticity and natural selection. *Frontiers in Human Neuroscience, 7*, 918. doi:10.3389/fnhum.2013.00918

Anzellotti, S., Mahon, B. Z., Schwarzbach, J., & Caramazza, A. (2011). Differential activity for animals and manipulable objects in the anterior temporal lobes. *Journal of Cognitive Neuroscience, 23*(8), 2059-2067. doi:10.1162/jocn.2010.21567

Arcaro, M. J., McMains, S. A., Singer, B. D., & Kastner, S. (2009). Retinotopic organization of human ventral visual cortex. *Journal of Neuroscience, 29*(34), 10638-10652. doi:10.1523/JNEUROSCI.2807-09.2009

Arcaro, M. J., Schade, P. F., Vincent, J. L., Ponce, C. R., & Livingstone, M. S. (2017). Seeing faces is necessary for face-domain formation. *Nature Neuroscience, 20*(10), 1404-1412. doi:10.1038/nn.4635

Axelrod, V., & Yovel, G. (2013). The challenge of localizing the anterior temporal face area: a possible solution. *Neuroimage, 81*, 371-380. doi:10.1016/j.neuroimage.2013.05.015

Axelrod, V., & Yovel, G. (2015). Successful decoding of famous faces in the fusiform face area. *PloS One, 10*(2), e0117126. doi:10.1371/journal.pone.0117126

Baggio, H. C., Segura, B., & Junque, C. (2015). Resting-state functional brain networks in Parkinson's disease. *CNS Neuroscience & Therapeutics, 21*(10), 793-801. doi:10.1111/cns.12417

Baker, C. I., Liu, J., Wald, L. L., Kwong, K. K., Benner, T., & Kanwisher, N. (2007). Visual word processing and experiential origins of functional selectivity in human extrastriate cortex. *Proceedings of the National Academy of Sciences of the United States of America, 104*(21), 9087-9092. doi:10.1073/pnas.0703300104

Baldassano, C., Beck, D. M., & Fei-Fei, L. (2013). Differential connectivity within the Parahippocampal Place Area. *Neuroimage, 75*, 228-237. doi:10.1016/j.neuroimage.2013.02.073

Baldassano, C., Beck, D. M., & Fei-Fei, L. (2015). Parcellating connectivity in spatial maps. *PeerJ, 3*, e784. doi:10.7717/peerj.784

Baldassi, C., Alemi-Neissi, A., Pagan, M., Dicarlo, J. J., Zecchina, R., & Zoccolan, D. (2013). Shape similarity, better than semantic membership, accounts for the structure of visual object representations in a population of monkey inferotemporal neurons. *PLoS Computational Biology, 9*(8), e1003167. doi:10.1371/journal.pcbi.1003167

Bar-Joseph, Z., Gifford, D. K., & Jaakkola, T. S. (2001). Fast optimal leaf ordering for hierarchical clustering. *Bioinformatics, 17 Suppl 1*, S22-29. URL: http://www.ncbi.nlm.nih.gov/pubmed/11472989

Behrmann, M., & Plaut, D. C. (2015). A vision of graded hemispheric specialization. *Annals of the New York Academy of Sciences*. doi:10.1111/nyas.12833

Bell, A. H., Malecek, N. J., Morin, E. L., Hadj-Bouziane, F., Tootell, R. B., & Ungerleider, L. G. (2011). Relationship between functional magnetic resonance imaging-identified regions and neuronal category selectivity. *Journal of Neuroscience, 31*(34), 12229-12240. doi:10.1523/JNEUROSCI.5865-10.2011

Beyeler, M., Rokem, A., Boynton, G. M., & Fine, I. (2017). Learning to see again: Biological constraints on cortical plasticity and the implications for sight restoration technologies. *Journal of neural engineering, 14*(5), 051003.

Biederman, I., & Vessel, E. A. (2006). Perceptual pleasure and the brain: A novel theory explains why the brain craves information and seeks it through the senses. *American Scientist, 94*(3), 247-253.

Biswal, B., Yetkin, F. Z., Haughton, V. M., & Hyde, J. S. (1995). Functional connectivity in the motor cortex of resting human brain using echo-planar MRI. *Magnetic Resonance in Medicine, 34*(4), 537-541. URL: http://www.ncbi.nlm.nih.gov/pubmed/8524021

Blumensath, T., Jbabdi, S., Glasser, M. F., Van Essen, D. C., Ugurbil, K., Behrens, T. E., & Smith, S. M. (2013). Spatially constrained hierarchical parcellation of the brain with resting-state fMRI. *Neuroimage, 76*, 313-324. doi:10.1016/j.neuroimage.2013.03.024

Bock, A. S., Binda, P., Benson, N. C., Bridge, H., Watkins, K. E., & Fine, I. (2015). Resting-State Retinotopic Organization in the Absence of Retinal Input and Visual Experience. *Journal of Neuroscience, 35*(36), 12366-12382. doi:10.1523/JNEUROSCI.4715-14.2015

Bock, A. S., Saenz, M., Tungaraza, R., Boynton, G. M., Bridge, H., & Fine, I. (2013). Visual callosal topography in the absence of retinal input. *Neuroimage, 81*, 325-334. doi:10.1016/j.neuroimage.2013.05.038

Bohland, J. W., Bokil, H., Allen, C. B., & Mitra, P. P. (2009). The brain atlas concordance problem: quantitative comparison of anatomical parcellations. *PloS One, 4*(9), e7200. doi:10.1371/journal.pone.0007200

Born, R. T., & Bradley, D. C. (2005). Structure and function of visual area MT. *Annual Review of Neuroscience, 28*, 157-189. doi:10.1146/annurev.neuro.26.041002.131052

Bracci, S., & Op de Beeck, H. (2016). Dissociations and Associations between Shape and Category Representations in the Two Visual Pathways. *Journal of Neuroscience, 36*(2), 432-444. doi:10.1523/JNEUROSCI.2314-15.2016

Bradley, D. C., & Andersen, R. A. (1998). Center-surround antagonism based on disparity in primate area MT. *Journal of Neuroscience, 18*(18), 7552-7565. URL: https://www.ncbi.nlm.nih.gov/pubmed/9736673

Bridge, H., Clare, S., & Krug, K. (2014). Delineating extrastriate visual area MT(V5) using cortical myeloarchitecture. *Neuroimage, 93 Pt 2*, 231-236. doi:10.1016/j.neuroimage.2013.03.034

Brodmann, K. (1909). *Vergleichende Lokalisationslehre der Grosshirnrinde in ihren Prinzipien dargestellt auf Grund des Zellenbaues*: Barth.

Bruce, D. (2001). Fifty years since Lashley's In search of the Engram: refutations and conjectures. *Journal of the History of the Neurosciences, 10*(3), 308-318. doi:10.1076/jhin.10.3.308.9086

Bruce, V., & Young, A. (1986). Understanding face recognition. *British Journal of Psychology, 77*(3), 305-327. doi:10.1111/j.2044-8295.1986.tb02199.x

Buckner, R. L., Krienen, F. M., & Yeo, B. T. (2013). Opportunities and limitations of intrinsic functional connectivity MRI. *Nature Neuroscience, 16*(7), 832-837. doi:10.1038/nn.3423

Buckner, R. L., & Yeo, B. T. (2014). Borders, map clusters, and supra-areal organization in visual cortex. *Neuroimage, 93 Pt 2*, 292-297. doi:10.1016/j.neuroimage.2013.12.036

Byrne, J. H., & Kandel, E. R. (1996). Presynaptic facilitation revisited: state and time dependence. *Journal of Neuroscience, 16*(2), 425-435. URL: https://www.ncbi.nlm.nih.gov/pubmed/8551327

Cahalane, D. J., Charvet, C. J., & Finlay, B. L. (2012). Systematic, balancing gradients in neuron density and number across the primate isocortex. *Frontiers in Neuroanatomy, 6*, 28. doi:10.3389/fnana.2012.00028

Cang, J., & Feldheim, D. A. (2013). Developmental mechanisms of topographic map formation and alignment. *Annual Review of Neuroscience, 36*, 51-77. doi:10.1146/annurev-neuro-062012-170341

Caspers, J., Palomero-Gallagher, N., Caspers, S., Schleicher, A., Amunts, K., & Zilles, K. (2015). Receptor architecture of visual areas in the face and word-form recognition region of the posterior fusiform gyrus. *Brain Struct Funct, 220*(1), 205-219. doi:10.1007/s00429-013-0646-z

Caspers, J., Zilles, K., Amunts, K., Laird, A. R., Fox, P. T., & Eickhoff, S. B. (2014). Functional characterization and differential coactivation patterns of two cytoarchitectonic visual areas on the human posterior fusiform gyrus. *Human Brain Mapping, 35*(6), 2754-2767. doi:10.1002/hbm.22364

Caspers, J., Zilles, K., Eickhoff, S. B., Schleicher, A., Mohlberg, H., & Amunts, K. (2013). Cytoarchitectonical analysis and probabilistic mapping of two extrastriate areas of the human posterior fusiform gyrus. *Brain Struct Funct, 218*(2), 511-526. doi:10.1007/s00429-012-0411-8

Christova, P., & Georgopoulos, A. P. (2018). Invariant and heritable local cortical organization as revealed by fMRI. *Journal of Neurophysiology*. doi:10.1152/jn.00137.2018

Citri, A., & Malenka, R. C. (2008). Synaptic plasticity: multiple forms, functions, and mechanisms. *Neuropsychopharmacology, 33*(1), 18-41. doi:10.1038/sj.npp.1301559

Clancy, B., Finlay, B. L., Darlington, R. B., & Anand, K. J. (2007). Extrapolating brain development from experimental species to humans. *Neurotoxicology, 28*(5), 931-937. doi:10.1016/j.neuro.2007.01.014

Cohen, A. L., Fair, D. A., Dosenbach, N. U., Miezin, F. M., Dierker, D., Van Essen, D. C., . . . Petersen, S. E. (2008). Defining functional areas in individual human brains using resting functional connectivity MRI. *Neuroimage, 41*(1), 45-57. doi:10.1016/j.neuroimage.2008.01.066

Collins, C. E., Airey, D. C., Young, N. A., Leitch, D. B., & Kaas, J. H. (2010). Neuron densities vary across and within cortical areas in primates. *Proceedings of the National Academy of Sciences of the United States of America, 107*(36), 15927-15932. doi:10.1073/pnas.1010356107

Collins, J. A., & Olson, I. R. (2014). Beyond the FFA: The role of the ventral anterior temporal lobes in face processing. *Neuropsychologia, 61*, 65-79. doi:10.1016/j.neuropsychologia.2014.06.005

Craddock, R. C., James, G. A., Holtzheimer, P. E., 3rd, Hu, X. P., & Mayberg, H. S. (2012). A whole brain fMRI atlas generated via spatially constrained spectral clustering. *Human Brain Mapping, 33*(8), 1914-1928. doi:10.1002/hbm.21333

Da Costa, S., van der Zwaag, W., Marques, J. P., Frackowiak, R. S., Clarke, S., & Saenz, M. (2011). Human primary auditory cortex follows the shape of Heschl's gyrus. *Journal of Neuroscience, 31*(40), 14067-14075. doi:10.1523/JNEUROSCI.2000-11.2011

Dahl, C. D., Logothetis, N. K., & Kayser, C. (2009). Spatial organization of multisensory responses in temporal association cortex. *Journal of Neuroscience, 29*(38), 11924-11932. doi:10.1523/JNEUROSCI.3437-09.2009

Dale, A. M., Fischl, B., & Sereno, M. I. (1999). Cortical surface-based analysis. I. Segmentation and surface reconstruction. *Neuroimage, 9*(2), 179-194. doi:10.1006/nimg.1998.0395

Damoiseaux, J. S., Rombouts, S. A., Barkhof, F., Scheltens, P., Stam, C. J., Smith, S. M., & Beckmann, C. F. (2006). Consistent resting-state networks across healthy subjects. *Proceedings of the National Academy of Sciences of the United States of America, 103*(37), 13848-13853. doi:10.1073/pnas.0601417103

DeAngelis, G. C., & Newsome, W. T. (1999). Organization of disparity-selective neurons in macaque area MT. *Journal of Neuroscience, 19*(4), 1398-1415. URL: https://www.ncbi.nlm.nih.gov/pubmed/9952417

Desikan, R. S., Segonne, F., Fischl, B., Quinn, B. T., Dickerson, B. C., Blacker, D., . . . Killiany, R. J. (2006). An automated labeling system for subdividing the human cerebral cortex on MRI scans into gyral based regions of interest. *Neuroimage, 31*(3), 968-980. doi:10.1016/j.neuroimage.2006.01.021

Desimone, R., Albright, T. D., Gross, C. G., & Bruce, C. (1984). Stimulus-selective properties of inferior temporal neurons in the macaque. *Journal of Neuroscience, 4*(8), 2051-2062. URL: https://www.ncbi.nlm.nih.gov/pubmed/6470767

Destrieux, C., Fischl, B., Dale, A., & Halgren, E. (2010). Automatic parcellation of human cortical gyri and sulci using standard anatomical nomenclature. *Neuroimage, 53*(1), 1-15. doi:10.1016/j.neuroimage.2010.06.010

DiCarlo, J. J., & Cox, D. D. (2007). Untangling invariant object recognition. *Trends Cogn Sci, 11*(8), 333-341. doi:10.1016/j.tics.2007.06.010

DiCarlo, J. J., & Maunsell, J. H. (2000). Form representation in monkey inferotemporal cortex is virtually unaltered by free viewing. *Nature Neuroscience, 3*(8), 814-821. doi:10.1038/77722

DiCarlo, J. J., Zoccolan, D., & Rust, N. C. (2012). How does the brain solve visual object recognition? *Neuron, 73*(3), 415-434. doi:10.1016/j.neuron.2012.01.010

Dilks, D. D., Julian, J. B., Paunov, A. M., & Kanwisher, N. (2013). The occipital place area is causally and selectively involved in scene perception. *Journal of Neuroscience, 33*(4), 1331-1336a. doi:10.1523/JNEUROSCI.4081-12.2013

Ding, S. L., Royall, J. J., Sunkin, S. M., Ng, L., Facer, B. A., Lesnar, P., . . . Lein, E. S. (2016). Comprehensive cellular-resolution atlas of the adult human brain. *Journal of Comparative Neurology, 524*(16), 3127-3481. doi:10.1002/cne.24080

Dinse, J., Hartwich, N., Waehnert, M. D., Tardif, C. L., Schafer, A., Geyer, S., . . . Bazin, P. L. (2015). A cytoarchitecture-driven myelin model reveals area-specific signatures in human primary and secondary areas using ultra-high resolution in-vivo brain MRI. *Neuroimage, 114*, 71-87. doi:10.1016/j.neuroimage.2015.04.023

Dornas, J. V., & Braun, J. (2018). Finer parcellation reveals detailed correlational structure of resting-state fMRI signals. *Journal of Neuroscience Methods, 294*, 15-33. doi:10.1016/j.jneumeth.2017.10.020
Downing, P. E., Jiang, Y., Shuman, M., & Kanwisher, N. (2001). A cortical area selective for visual processing of the human body. *Science, 293*(5539), 2470-2473. doi:10.1126/science.1063414
Dubner, R., & Zeki, S. M. (1971). Response properties and receptive fields of cells in an anatomically defined region of the superior temporal sulcus in the monkey. *Brain Research, 35*(2), 528-532. URL: https://www.ncbi.nlm.nih.gov/pubmed/5002708
Dubois, J., de Berker, A. O., & Tsao, D. Y. (2015). Single-unit recordings in the macaque face patch system reveal limitations of fMRI MVPA. *Journal of Neuroscience, 35*(6), 2791-2802. doi:10.1523/JNEUROSCI.4037-14.2015
Duchaine, B., & Yovel, G. (2015). A Revised Neural Framework for Face Processing. *Annual Review of Vision Science, 1*(1), 393-416. doi:doi:10.1146/annurev-vision-082114-035518
Duvernoy, H. (1991). The human brain: surface, blood supply, and three-dimensional anatomy: New York: Springer-Verlag.
Eickhoff, S. B., Constable, R. T., & Yeo, B. T. (2017). Topographic organization of the cerebral cortex and brain cartography. *Neuroimage*. doi:10.1016/j.neuroimage.2017.02.018
Eickhoff, S. B., Thirion, B., Varoquaux, G., & Bzdok, D. (2015). Connectivity-based parcellation: Critique and implications. *Human Brain Mapping, 36*(12), 4771-4792. doi:10.1002/hbm.22933
Eifuku, S., Nakata, R., Sugimori, M., Ono, T., & Tamura, R. (2010). Neural correlates of associative face memory in the anterior inferior temporal cortex of monkeys. *Journal of Neuroscience, 30*(45), 15085-15096. doi:10.1523/JNEUROSCI.0471-10.2010
Engel, S. A., Glover, G. H., & Wandell, B. A. (1997). Retinotopic organization in human visual cortex and the spatial precision of functional MRI. *Cerebral Cortex, 7*(2), 181-192. URL: https://www.ncbi.nlm.nih.gov/pubmed/9087826
Engel, S. A., Rumelhart, D. E., Wandell, B. A., Lee, A. T., Glover, G. H., Chichilnisky, E. J., & Shadlen, M. N. (1994). fMRI of human visual cortex. *Nature, 369*(6481), 525. doi:10.1038/369525a0
Epstein, R., Graham, K. S., & Downing, P. E. (2003). Viewpoint-specific scene representations in human parahippocampal cortex. *Neuron, 37*(5), 865-876. URL: http://www.ncbi.nlm.nih.gov/pubmed/12628176
Epstein, R., & Kanwisher, N. (1998). A cortical representation of the local visual environment. *Nature, 392*(6676), 598-601. doi:10.1038/33402
Epstein, R. A. (2008). Parahippocampal and retrosplenial contributions to human spatial navigation. *Trends Cogn Sci, 12*(10), 388-396. doi:10.1016/j.tics.2008.07.004
Fahle, M. (1994). Human pattern recognition: parallel processing and perceptual learning. *Perception, 23*(4), 411-427. doi:10.1068/p230411
Fedorenko, E., Duncan, J., & Kanwisher, N. (2012). Language-selective and domain-general regions lie side by side within Broca's area. *Current Biology, 22*(21), 2059-2062. doi:10.1016/j.cub.2012.09.011
Felleman, D. J., & Van Essen, D. C. (1991). Distributed hierarchical processing in the primate cerebral cortex. *Cerebral Cortex, 1*(1), 1-47. URL: http://www.ncbi.nlm.nih.gov/pubmed/1822724
Filippi, M., Agosta, F., Spinelli, E. G., & Rocca, M. A. (2013). Imaging resting state brain function in multiple sclerosis. *Journal of Neurology, 260*(7), 1709-1713. doi:10.1007/s00415-012-6695-z
Fine, I., & Jacobs, R. A. (2002). Comparing perceptual learning tasks: a review. *J Vis, 2*(2), 190-203. doi:10.1167/2.2.5
Fine, I., Wade, A. R., Brewer, A. A., May, M. G., Goodman, D. F., Boynton, G. M., . . . MacLeod, D. I. (2003). Long-term deprivation affects visual perception and cortex. *Nature Neuroscience, 6*(9), 915-916. doi:10.1038/nn1102
Finlay, B. L., & Darlington, R. B. (1995). Linked regularities in the development and evolution of mammalian brains. *Science, 268*(5217), 1578-1584. URL: https://www.ncbi.nlm.nih.gov/pubmed/7777856
Fischl, B., Rajendran, N., Busa, E., Augustinack, J., Hinds, O., Yeo, B. T., . . . Zilles, K. (2008). Cortical folding patterns and predicting cytoarchitecture. *Cerebral Cortex, 18*(8), 1973-1980. doi:10.1093/cercor/bhm225
Fischl, B., Sereno, M. I., & Dale, A. M. (1999). Cortical surface-based analysis. II: Inflation, flattening, and a surface-based coordinate system. *Neuroimage, 9*(2), 195-207. doi:10.1006/nimg.1998.0396

Fischl, B., van der Kouwe, A., Destrieux, C., Halgren, E., Segonne, F., Salat, D. H., . . . Dale, A. M. (2004). Automatically parcellating the human cerebral cortex. *Cerebral Cortex, 14*(1), 11-22. URL: https://www.ncbi.nlm.nih.gov/pubmed/14654453

Flanagan, J. G. (2006). Neural map specification by gradients. *Current Opinion in Neurobiology, 16*(1), 59-66. doi:10.1016/j.conb.2006.01.010

Freiwald, W. A., Tsao, D. Y., & Livingstone, M. S. (2009). A face feature space in the macaque temporal lobe. *Nature Neuroscience, 12*(9), 1187-1196. doi:10.1038/nn.2363

Geary, W. A., & Wooten, G. F. (1989). Receptor Autoradiography. In L. Heimer & L. Záborszky (Eds.), *Neuroanatomical Tract-Tracing Methods 2*. Boston, MA: Springer.

Gibbs, R. A., Rogers, J., Katze, M. G., Bumgarner, R., Weinstock, G. M., Mardis, E. R., . . . Zwieg, A. S. (2007). Evolutionary and biomedical insights from the rhesus macaque genome. *Science, 316*(5822), 222-234. doi:10.1126/science.1139247

Glasser, M. F., & Van Essen, D. C. (2011). Mapping human cortical areas in vivo based on myelin content as revealed by T1- and T2-weighted MRI. *Journal of Neuroscience, 31*(32), 11597-11616. doi:10.1523/JNEUROSCI.2180-11.2011

Goldstone, R. L. (2000). Unitization during category learning. *Journal of Experimental Psychology: Human Perception and Performance, 26*(1), 86-112. URL: https://www.ncbi.nlm.nih.gov/pubmed/10696607

Granger, A. J., & Nicoll, R. A. (2014). Expression mechanisms underlying long-term potentiation: a postsynaptic view, 10 years on. *Philosophical Transactions of the Royal Society of London. Series B: Biological Sciences, 369*(1633), 20130136. doi:10.1098/rstb.2013.0136

Greve, D. N., & Fischl, B. (2009). Accurate and robust brain image alignment using boundary-based registration. *Neuroimage, 48*(1), 63-72. doi:10.1016/j.neuroimage.2009.06.060

Grill-Spector, K. (2003). The neural basis of object perception. *Current Opinion in Neurobiology, 13*(2), 159-166. URL: https://www.ncbi.nlm.nih.gov/pubmed/12744968

Grill-Spector, K., Kushnir, T., Edelman, S., Avidan, G., Itzchak, Y., & Malach, R. (1999). Differential processing of objects under various viewing conditions in the human lateral occipital complex. *Neuron, 24*(1), 187-203. URL: http://www.ncbi.nlm.nih.gov/pubmed/10677037

Grill-Spector, K., & Weiner, K. S. (2014). The functional architecture of the ventral temporal cortex and its role in categorization. *Nature Reviews: Neuroscience, 15*(8), 536-548. doi:10.1038/nrn3747

Grimaldi, P., Saleem, K. S., & Tsao, D. (2016). Anatomical Connections of the Functionally Defined "Face Patches" in the Macaque Monkey. *Neuron, 90*(6), 1325-1342. doi:10.1016/j.neuron.2016.05.009

Gross, C. (2013). Some revolutions in neuroscience. *Journal of Cognitive Neuroscience, 25*(1), 4-13. doi:10.1162/jocn_a_00308

Grossberg, S. (1968). Some physiological and biochemical consequences of psychological postulates. *Proceedings of the National Academy of Sciences, 60*(3), 758-765.

Grossberg, S. (1974). Classical and instrumental learning by neural networks. *Progress in theoretical biology, 3*(51-141), 42-47.

Guclu, U., & van Gerven, M. A. (2015). Deep Neural Networks Reveal a Gradient in the Complexity of Neural Representations across the Ventral Stream. *Journal of Neuroscience, 35*(27), 10005-10014. doi:10.1523/JNEUROSCI.5023-14.2015

Hafkemeijer, A., van der Grond, J., & Rombouts, S. A. (2012). Imaging the default mode network in aging and dementia. *Biochimica et Biophysica Acta, 1822*(3), 431-441. doi:10.1016/j.bbadis.2011.07.008

Hartshorne, J. K., Tenenbaum, J. B., & Pinker, S. (2018). A critical period for second language acquisition: evidence from 2/3 million English speakers. *Cognition*.

Hasson, U., Hendler, T., Ben Bashat, D., & Malach, R. (2001). Vase or face? A neural correlate of shape-selective grouping processes in the human brain. *Journal of Cognitive Neuroscience, 13*(6), 744-753. doi:10.1162/08989290152541412

Hasson, U., Levy, I., Behrmann, M., Hendler, T., & Malach, R. (2002). Eccentricity bias as an organizing principle for human high-order object areas. *Neuron, 34*(3), 479-490. URL: http://www.ncbi.nlm.nih.gov/pubmed/11988177

Hawrylycz, M. J., Lein, E. S., Guillozet-Bongaarts, A. L., Shen, E. H., Ng, L., Miller, J. A., . . . Jones, A. R. (2012). An anatomically comprehensive atlas of the adult human brain transcriptome. *Nature, 489*(7416), 391-399. doi:10.1038/nature11405

Haxby, J. V., Gobbini, M. I., Furey, M. L., Ishai, A., Schouten, J. L., & Pietrini, P. (2001). Distributed and overlapping representations of faces and objects in ventral temporal cortex. *Science, 293*(5539), 2425-2430. doi:10.1126/science.1063736

Haxby, J. V., Hoffman, E. A., & Gobbini, M. I. (2000). The distributed human neural system for face perception. *Trends Cogn Sci, 4*(6), 223-233. URL: http://www.ncbi.nlm.nih.gov/pubmed/10827445

Henriksson, L., Khaligh-Razavi, S. M., Kay, K., & Kriegeskorte, N. (2015). Visual representations are dominated by intrinsic fluctuations correlated between areas. *Neuroimage, 114*, 275-286. doi:10.1016/j.neuroimage.2015.04.026

Henriksson, L., Mur, M., & Kriegeskorte, N. Faciotopy—A face-feature map with face-like topology in the human occipital face area. *Cortex*. doi:http://dx.doi.org/10.1016/j.cortex.2015.06.030

Hensch, T. K. (2005). Critical period plasticity in local cortical circuits. *Nature Reviews: Neuroscience, 6*(11), 877-888. doi:10.1038/nrn1787

Heywood, C. A., Gadotti, A., & Cowey, A. (1992). Cortical area V4 and its role in the perception of color. *Journal of Neuroscience, 12*(10), 4056-4065. URL: https://www.ncbi.nlm.nih.gov/pubmed/1403100

Hinds, O., Polimeni, J. R., Rajendran, N., Balasubramanian, M., Amunts, K., Zilles, K., . . . Triantafyllou, C. (2009). Locating the functional and anatomical boundaries of human primary visual cortex. *Neuroimage, 46*(4), 915-922. doi:10.1016/j.neuroimage.2009.03.036

Hinton, G. E., McClelland, J. L., & Rumelhart, D. E. (1986). Distributed representations. *Parallel distributed processing: Explorations in the microstructure of cognition, 1*(3), 77-109.

Honnorat, N., Eavani, H., Satterthwaite, T. D., Gur, R. E., Gur, R. C., & Davatzikos, C. (2015). GraSP: Geodesic Graph-based Segmentation with Shape Priors for the functional parcellation of the cortex. *Neuroimage, 106*, 207-221. doi:10.1016/j.neuroimage.2014.11.008

Hooks, B. M., & Chen, C. (2007). Critical periods in the visual system: changing views for a model of experience-dependent plasticity. *Neuron, 56*(2), 312-326. doi:10.1016/j.neuron.2007.10.003

Hubel, D. H., & Wiesel, T. N. (1959). Receptive fields of single neurones in the cat's striate cortex. *Journal of Physiology, 148*, 574-591. URL: https://www.ncbi.nlm.nih.gov/pubmed/14403679

Hubel, D. H., & Wiesel, T. N. (1998). Early exploration of the visual cortex. *Neuron, 20*(3), 401-412. URL: http://www.ncbi.nlm.nih.gov/pubmed/9539118

Huberman, A. D., Feller, M. B., & Chapman, B. (2008). Mechanisms underlying development of visual maps and receptive fields. *Annual Review of Neuroscience, 31*, 479-509. doi:10.1146/annurev.neuro.31.060407.125533

Huntenburg, J. M., Bazin, P. L., & Margulies, D. S. (2018). Large-Scale Gradients in Human Cortical Organization. *Trends Cogn Sci, 22*(1), 21-31. doi:10.1016/j.tics.2017.11.002

Ishai, A., Ungerleider, L. G., Martin, A., Schouten, J. L., & Haxby, J. V. (1999). Distributed representation of objects in the human ventral visual pathway. *Proceedings of the National Academy of Sciences of the United States of America, 96*(16), 9379-9384. URL: https://www.ncbi.nlm.nih.gov/pubmed/10430951

Issa, E. B., Papanastassiou, A. M., & DiCarlo, J. J. (2013). Large-scale, high-resolution neurophysiological maps underlying FMRI of macaque temporal lobe. *Journal of Neuroscience, 33*(38), 15207-15219. doi:10.1523/JNEUROSCI.1248-13.2013

Itti, L., & Koch, C. (2001). Computational modelling of visual attention. *Nature Reviews: Neuroscience, 2*(3), 194-203. doi:10.1038/35058500

Jain, R., Millin, R., & Mel, B. W. (2015). Multimap formation in visual cortex. *J Vis, 15*(16), 3. doi:10.1167/15.16.3

Jbabdi, S., Sotiropoulos, S. N., & Behrens, T. E. (2013). The topographic connectome. *Current Opinion in Neurobiology, 23*(2), 207-215. doi:10.1016/j.conb.2012.12.004

Jenkins, W. M., Merzenich, M. M., Ochs, M. T., Allard, T., & Guic-Robles, E. (1990). Functional reorganization of primary somatosensory cortex in adult owl monkeys after behaviorally controlled tactile stimulation. *Journal of Neurophysiology, 63*(1), 82-104. doi:10.1152/jn.1990.63.1.82

Johansen-Berg, H., Behrens, T. E., Robson, M. D., Drobnjak, I., Rushworth, M. F., Brady, J. M., . . . Matthews, P. M. (2004). Changes in connectivity profiles define functionally distinct regions in human medial frontal cortex. *Proceedings of the National Academy of Sciences of the United States of America, 101*(36), 13335-13340. doi:10.1073/pnas.0403743101

Julian, J. B., Fedorenko, E., Webster, J., & Kanwisher, N. (2012). An algorithmic method for functionally defining regions of interest in the ventral visual pathway. *Neuroimage, 60*(4), 2357-2364. doi:10.1016/j.neuroimage.2012.02.055

Kaler, S. R., & Freeman, B. J. (1994). Analysis of environmental deprivation: cognitive and social development in Romanian orphans. *Journal of Child Psychology and Psychiatry and Allied Disciplines, 35*(4), 769-781. URL: https://www.ncbi.nlm.nih.gov/pubmed/7518826

Kamps, F. S., Julian, J. B., Kubilius, J., Kanwisher, N., & Dilks, D. D. (2016). The occipital place area represents the local elements of scenes. *Neuroimage, 132*, 417-424. doi:10.1016/j.neuroimage.2016.02.062

Kanwisher, N., & Dilks, D. D. (2013). The Functional organization of the ventral visual pathway in humans. In J. S. Werner & L. M. Chalupa (Eds.), *The New Visual Neurosciences* (pp. 733-748): MIT Press.

Kanwisher, N., McDermott, J., & Chun, M. M. (1997). The fusiform face area: a module in human extrastriate cortex specialized for face perception. *Journal of Neuroscience, 17*(11), 4302-4311. URL: http://www.ncbi.nlm.nih.gov/pubmed/9151747

Kappeler, P. M., & van Schaik, C. P. (2002). Evolution of primate social systems. *International journal of primatology, 23*(4), 707-740.

Karbasforoushan, H., & Woodward, N. D. (2012). Resting-state networks in schizophrenia. *Current Topics in Medicinal Chemistry, 12*(21), 2404-2414. URL: http://www.ncbi.nlm.nih.gov/pubmed/23279179

Khaligh-Razavi, S. M., & Kriegeskorte, N. (2014). Deep supervised, but not unsupervised, models may explain IT cortical representation. *PLoS Computational Biology, 10*(11), e1003915. doi:10.1371/journal.pcbi.1003915

Kiani, R., Esteky, H., Mirpour, K., & Tanaka, K. (2007). Object category structure in response patterns of neuronal population in monkey inferior temporal cortex. *Journal of Neurophysiology, 97*(6), 4296-4309. doi:10.1152/jn.00024.2007

Knudsen, E. I. (1985). Experience alters the spatial tuning of auditory units in the optic tectum during a sensitive period in the barn owl. *Journal of Neuroscience, 5*(11), 3094-3109. URL: https://www.ncbi.nlm.nih.gov/pubmed/4056865

Konkle, T., & Caramazza, A. (2013). Tripartite organization of the ventral stream by animacy and object size. *Journal of Neuroscience, 33*(25), 10235-10242. doi:10.1523/JNEUROSCI.0983-13.2013

Konkle, T., & Oliva, A. (2012). A real-world size organization of object responses in occipitotemporal cortex. *Neuron, 74*(6), 1114-1124. doi:10.1016/j.neuron.2012.04.036

Kravitz, D. J., Saleem, K. S., Baker, C. I., Ungerleider, L. G., & Mishkin, M. (2013). The ventral visual pathway: an expanded neural framework for the processing of object quality. *Trends Cogn Sci, 17*(1), 26-49. doi:10.1016/j.tics.2012.10.011

Kreiman, G., Hung, C. P., Kraskov, A., Quiroga, R. Q., Poggio, T., & DiCarlo, J. J. (2006). Object selectivity of local field potentials and spikes in the macaque inferior temporal cortex. *Neuron, 49*(3), 433-445. doi:10.1016/j.neuron.2005.12.019

Kriegeskorte, N. (2015). Deep Neural Networks: A New Framework for Modeling Biological Vision and Brain Information Processing. *Annu Rev Vis Sci, 1*, 417-446. doi:10.1146/annurev-vision-082114-035447

Kriegeskorte, N., Cusack, R., & Bandettini, P. (2010). How does an fMRI voxel sample the neuronal activity pattern: compact-kernel or complex spatiotemporal filter? *Neuroimage, 49*(3), 1965-1976. doi:10.1016/j.neuroimage.2009.09.059

Kriegeskorte, N., Mur, M., & Bandettini, P. (2008). Representational similarity analysis - connecting the branches of systems neuroscience. *Frontiers in Systems Neuroscience, 2*, 4. doi:10.3389/neuro.06.004.2008

Krizhevsky, A., Sutskever, I., & Hinton, G. E. (2012). *Imagenet classification with deep convolutional neural networks.* Paper presented at the Advances in Neural Information Processing Systems.

Krubitzer, L. (2009). In search of a unifying theory of complex brain evolution. *Annals of the New York Academy of Sciences, 1156*, 44-67. doi:10.1111/j.1749-6632.2009.04421.x

Krubitzer, L., & Kaas, J. (2005). The evolution of the neocortex in mammals: how is phenotypic diversity generated? *Current Opinion in Neurobiology, 15*(4), 444-453. doi:10.1016/j.conb.2005.07.003

Lafer-Sousa, R., & Conway, B. R. (2013). Parallel, multi-stage processing of colors, faces and shapes in macaque inferior temporal cortex. *Nature Neuroscience, 16*(12), 1870-1878. doi:10.1038/nn.3555

Lafer-Sousa, R., Conway, B. R., & Kanwisher, N. G. (2016). Color-Biased Regions of the Ventral Visual Pathway Lie between Face-and Place-Selective Regions in Humans, as in Macaques. *The Journal of Neuroscience, 36*(5), 1682-1697.

Lashkari, D., Sridharan, R., & Golland, P. (2010). Categories and Functional Units: An Infinite Hierarchical Model for Brain Activations. *Advances in Neural Information Processing Systems, 23*, 1252-1260. URL: http://www.ncbi.nlm.nih.gov/pubmed/24839377

Lashkari, D., Sridharan, R., Vul, E., Hsieh, P. J., Kanwisher, N., & Golland, P. (2010). Nonparametric Hierarchical Bayesian Model for Functional Brain Parcellation. *Conf Comput Vis Pattern Recognit Workshops*, 15-22. doi:10.1109/CVPRW.2010.5543434

Lashkari, D., Sridharan, R., Vul, E., Hsieh, P. J., Kanwisher, N., & Golland, P. (2012). Search for patterns of functional specificity in the brain: a nonparametric hierarchical Bayesian model for group fMRI data. *Neuroimage, 59*(2), 1348-1368. doi:10.1016/j.neuroimage.2011.08.031

Lashkari, D., Vul, E., Kanwisher, N., & Golland, P. (2008). Discovering structure in the space of activation profiles in fMRI. *Medical Image Computing and Computer-Assisted Intervention, 11*(Pt 1), 1016-1024. URL: http://www.ncbi.nlm.nih.gov/pubmed/18979845

Laumann, T. O., Gordon, E. M., Adeyemo, B., Snyder, A. Z., Joo, S. J., Chen, M. Y., . . . Petersen, S. E. (2015). Functional System and Areal Organization of a Highly Sampled Individual Human Brain. *Neuron, 87*(3), 657-670. doi:10.1016/j.neuron.2015.06.037

Lee, Y., Duchaine, B., Wilson, H. R., & Nakayama, K. (2010). Three cases of developmental prosopagnosia from one family: detailed neuropsychological and psychophysical investigation of face processing. *Cortex, 46*(8), 949-964. doi:10.1016/j.cortex.2009.07.012

Levy, I., Hasson, U., Avidan, G., Hendler, T., & Malach, R. (2001). Center-periphery organization of human object areas. *Nature Neuroscience, 4*(5), 533-539. doi:10.1038/87490

Levy, I., Hasson, U., & Malach, R. (2004). One Picture Is Worth at Least a Million Neurons. *Current Biology, 14*(11), 996-1001. doi:10.1016/j.cub.2004.05.045

Lewis, T. L., & Maurer, D. (2005). Multiple sensitive periods in human visual development: evidence from visually deprived children. *Developmental Psychobiology, 46*(3), 163-183. doi:10.1002/dev.20055

Li, H. J., Hou, X. H., Liu, H. H., Yue, C. L., He, Y., & Zuo, X. N. (2015). Toward systems neuroscience in mild cognitive impairment and Alzheimer's disease: a meta-analysis of 75 fMRI studies. *Human Brain Mapping, 36*(3), 1217-1232. doi:10.1002/hbm.22689

Liu, N., Kriegeskorte, N., Mur, M., Hadj-Bouziane, F., Luh, W. M., Tootell, R. B., & Ungerleider, L. G. (2013). Intrinsic structure of visual exemplar and category representations in macaque brain. *Journal of Neuroscience, 33*(28), 11346-11360. doi:10.1523/JNEUROSCI.4180-12.2013

Lorenz, S., Weiner, K. S., Caspers, J., Mohlberg, H., Schleicher, A., Bludau, S., . . . Amunts, K. (2017). Two New Cytoarchitectonic Areas on the Human Mid-Fusiform Gyrus. *Cerebral Cortex, 27*(1), 373-385. doi:10.1093/cercor/bhv225

Luo, S., Qi, R. F., Wen, J. Q., Zhong, J. H., Kong, X., Liang, X., . . . Lu, G. M. (2015). Abnormal Intrinsic Brain Activity Patterns in Patients with End-Stage Renal Disease Undergoing Peritoneal Dialysis: A Resting-State Functional MR Imaging Study. *Radiology*, 141913. doi:10.1148/radiol.2015141913

Madhyastha, T. M., Askren, M. K., Boord, P., & Grabowski, T. J. (2015). Dynamic connectivity at rest predicts attention task performance. *Brain Connect, 5*(1), 45-59. doi:10.1089/brain.2014.0248

Mahon, B. Z., Anzellotti, S., Schwarzbach, J., Zampini, M., & Caramazza, A. (2009). Category-specific organization in the human brain does not require visual experience. *Neuron, 63*(3), 397-405. doi:10.1016/j.neuron.2009.07.012

Mahon, B. Z., & Caramazza, A. (2011). What drives the organization of object knowledge in the brain? *Trends Cogn Sci, 15*(3), 97-103. doi:10.1016/j.tics.2011.01.004

Malach, R., Levy, I., & Hasson, U. (2002). The topography of high-order human object areas. *Trends Cogn Sci, 6*(4), 176-184. URL: http://www.ncbi.nlm.nih.gov/pubmed/11912041

Malach, R., Reppas, J. B., Benson, R. R., Kwong, K. K., Jiang, H., Kennedy, W. A., . . . Tootell, R. B. (1995). Object-related activity revealed by functional magnetic resonance imaging in human occipital cortex. *Proceedings of the National Academy of Sciences of the United States of America, 92*(18), 8135-8139. URL: http://www.ncbi.nlm.nih.gov/pubmed/7667258

Marchetti, I., Koster, E. H., Sonuga-Barke, E. J., & De Raedt, R. (2012). The default mode network and recurrent depression: a neurobiological model of cognitive risk factors. *Neuropsychology Review, 22*(3), 229-251. doi:10.1007/s11065-012-9199-9

McIntosh, A. R., & Misic, B. (2013). Multivariate statistical analyses for neuroimaging data. *Annual Review of Psychology, 64*, 499-525. doi:10.1146/annurev-psych-113011-143804

McKinney, S. (2017). Cochlear implantation in children under 12 months of age. *Current Opinion in Otolaryngology & Head and Neck Surgery, 25*(5), 400-404. doi:10.1097/MOO.0000000000000400

McKone, E., Crookes, K., Jeffery, L., & Dilks, D. D. (2012). A critical review of the development of face recognition: experience is less important than previously believed. *Cognitive Neuropsychology, 29*(1-2), 174-212. doi:10.1080/02643294.2012.660138

McLaughlin, T., & O'Leary, D. D. (2005). Molecular gradients and development of retinotopic maps. *Annual Review of Neuroscience, 28*, 327-355. doi:10.1146/annurev.neuro.28.061604.135714

Meadows, J. C. (1974). Disturbed perception of colours associated with localized cerebral lesions. *Brain, 97*(4), 615-632. URL: https://www.ncbi.nlm.nih.gov/pubmed/4547992

Merzenich, M. M., Kaas, J. H., Wall, J., Nelson, R. J., Sur, M., & Felleman, D. (1983). Topographic reorganization of somatosensory cortical areas 3b and 1 in adult monkeys following restricted deafferentation. *Neuroscience, 8*(1), 33-55. URL: https://www.ncbi.nlm.nih.gov/pubmed/6835522

Moeller, S., Freiwald, W. A., & Tsao, D. Y. (2008). Patches with links: a unified system for processing faces in the macaque temporal lobe. *Science, 320*(5881), 1355-1359. doi:10.1126/science.1157436

Mondloch, C. J., Le Grand, R., & Maurer, D. (2003). Early visual experience is necessary for the development of some—but not all—aspects of face processing. *The development of face processing in infancy and early childhood: Current perspectives*, 99-117.

Moser, E. I., Kropff, E., & Moser, M. B. (2008). Place cells, grid cells, and the brain's spatial representation system. *Annual Review of Neuroscience, 31*, 69-89. doi:10.1146/annurev.neuro.31.061307.090723

Movshon, J. A., & Newsome, W. T. (1996). Visual response properties of striate cortical neurons projecting to area MT in macaque monkeys. *Journal of Neuroscience, 16*(23), 7733-7741. URL: https://www.ncbi.nlm.nih.gov/pubmed/8922429

Movshon, J. A., & Van Sluyters, R. C. (1981). Visual neural development. *Annual Review of Psychology, 32*, 477-522. doi:10.1146/annurev.ps.32.020181.002401

Mur, M. C. (2011). *High-level visual object representations in inferior temporal cortex.* (Doctorial Dissertation), Datawyse/Universitaire Pers Maastricht, Maastricht, The Netherlands.

Naselaris, T., Bassett, D. S., Fletcher, A. K., Kording, K., Kriegeskorte, N., Nienborg, H., . . . Kay, K. (2018). Cognitive Computational Neuroscience: A New Conference for an Emerging Discipline. *Trends Cogn Sci*. doi:10.1016/j.tics.2018.02.008

Naselaris, T., Stansbury, D. E., & Gallant, J. L. (2012). Cortical representation of animate and inanimate objects in complex natural scenes. *Journal of Physiology, Paris, 106*(5-6), 239-249. doi:10.1016/j.jphysparis.2012.02.001

Nasr, S., Liu, N., Devaney, K. J., Yue, X., Rajimehr, R., Ungerleider, L. G., & Tootell, R. B. (2011). Scene-selective cortical regions in human and nonhuman primates. *Journal of Neuroscience, 31*(39), 13771-13785. doi:10.1523/JNEUROSCI.2792-11.2011

Nasr, S., & Tootell, R. B. (2012). Role of fusiform and anterior temporal cortical areas in facial recognition. *Neuroimage, 63*(3), 1743-1753. doi:10.1016/j.neuroimage.2012.08.031

Nitsche, M. A., Roth, A., Kuo, M.-F., Fischer, A. K., Liebetanz, D., Lang, N., . . . Paulus, W. (2007). Timing-Dependent Modulation of Associative Plasticity by General Network Excitability in the Human Motor Cortex. *The Journal of Neuroscience, 27*(14), 3807-3812. doi:10.1523/jneurosci.5348-06.2007

O'Leary, D. D., Chou, S. J., & Sahara, S. (2007). Area patterning of the mammalian cortex. *Neuron, 56*(2), 252-269. doi:10.1016/j.neuron.2007.10.010

O'Leary, D. D., & McLaughlin, T. (2005). Mechanisms of retinotopic map development: Ephs, ephrins, and spontaneous correlated retinal activity. *Progress in Brain Research, 147*, 43-65. doi:10.1016/S0079-6123(04)47005-8

O'Neil, E. B., Hutchison, R. M., McLean, D. A., & Kohler, S. (2014). Resting-state fMRI reveals functional connectivity between face-selective perirhinal cortex and the fusiform face area related to face inversion. *Neuroimage, 92*, 349-355. doi:10.1016/j.neuroimage.2014.02.005

O'Toole, A. J., Jiang, F., Abdi, H., & Haxby, J. V. (2005). Partially distributed representations of objects and faces in ventral temporal cortex. *Journal of Cognitive Neuroscience, 17*(4), 580-590. doi:10.1162/0898929053467550

Ohki, K., Chung, S., Ch'ng, Y. H., Kara, P., & Reid, R. C. (2005). Functional imaging with cellular resolution reveals precise micro-architecture in visual cortex. *Nature, 433*(7026), 597-603. doi:10.1038/nature03274

Op de Beeck, H. P., Deutsch, J. A., Vanduffel, W., Kanwisher, N. G., & DiCarlo, J. J. (2008). A stable topography of selectivity for unfamiliar shape classes in monkey inferior temporal cortex. *Cerebral Cortex, 18*(7), 1676-1694. doi:10.1093/cercor/bhm196

Op de Beeck, H. P., Dicarlo, J. J., Goense, J. B., Grill-Spector, K., Papanastassiou, A., Tanifuji, M., & Tsao, D. Y. (2008). Fine-scale spatial organization of face and object selectivity in the temporal lobe: do functional magnetic resonance imaging, optical imaging, and electrophysiology agree? *Journal of Neuroscience, 28*(46), 11796-11801. doi:10.1523/JNEUROSCI.3799-08.2008

Orban, G. A., Van Essen, D., & Vanduffel, W. (2004). Comparative mapping of higher visual areas in monkeys and humans. *Trends Cogn Sci, 8*(7), 315-324. doi:10.1016/j.tics.2004.05.009

Osher, D. E., Saxe, R. R., Koldewyn, K., Gabrieli, J. D. E., Kanwisher, N., & Saygin, Z. M. (2015). Structural Connectivity Fingerprints Predict Cortical Selectivity for Multiple Visual Categories across Cortex. *Cerebral Cortex*. doi:10.1093/cercor/bhu303

Parkes, L. M., Schwarzbach, J. V., Bouts, A. A., Deckers, R. H., Pullens, P., Kerskens, C. M., & Norris, D. G. (2005). Quantifying the spatial resolution of the gradient echo and spin echo BOLD response at 3 Tesla. *Magnetic Resonance in Medicine, 54*(6), 1465-1472. doi:10.1002/mrm.20712

Patel, G. H., Kaplan, D. M., & Snyder, L. H. (2014). Topographic organization in the brain: searching for general principles. *Trends Cogn Sci*. doi:10.1016/j.tics.2014.03.008

Peelen, M. V., & Downing, P. E. (2005). Selectivity for the human body in the fusiform gyrus. *Journal of Neurophysiology, 93*(1), 603-608. doi:10.1152/jn.00513.2004

Peelen, M. V., & Downing, P. E. (2017). Category selectivity in human visual cortex: Beyond visual object recognition. *Neuropsychologia, 105*, 177-183. doi:10.1016/j.neuropsychologia.2017.03.033

Poston, K. L., & Eidelberg, D. (2012). Functional brain networks and abnormal connectivity in the movement disorders. *Neuroimage, 62*(4), 2261-2270. doi:10.1016/j.neuroimage.2011.12.021

Power, Jonathan D., Schlaggar, Bradley L., & Petersen, Steven E. (2014). Studying Brain Organization via Spontaneous fMRI Signal. *Neuron, 84*(4), 681-696. doi:http://dx.doi.org/10.1016/j.neuron.2014.09.007

Pribram, K. H. (1961). Regional Physiology of the Central Nervous System. *Progresss in Neurology and Psychiatry*, 45.

Pribram, K. H. (1982). Localization and distribution of function in the brain. *Neuropsychology after Lashley*, 273-296.

Prince, S. J., Pointon, A. D., Cumming, B. G., & Parker, A. J. (2000). The precision of single neuron responses in cortical area V1 during stereoscopic depth judgments. *Journal of Neuroscience, 20*(9), 3387-3400. URL: https://www.ncbi.nlm.nih.gov/pubmed/10777801

Raichle, M. E. (2009). A paradigm shift in functional brain imaging. *Journal of Neuroscience, 29*(41), 12729-12734. doi:10.1523/JNEUROSCI.4366-09.2009

Rajimehr, R., Devaney, K. J., Bilenko, N. Y., Young, J. C., & Tootell, R. B. (2011). The "parahippocampal place area" responds preferentially to high spatial frequencies in humans and monkeys. *PLoS Biology, 9*(4), e1000608. doi:10.1371/journal.pbio.1000608

Rajimehr, R., Young, J. C., & Tootell, R. B. (2009). An anterior temporal face patch in human cortex, predicted by macaque maps. *Proceedings of the National Academy of Sciences of the United States of America, 106*(6), 1995-2000. doi:10.1073/pnas.0807304106

Raviola, E., & Wiesel, T. N. (1978). Effect of dark-rearing on experimental myopia in monkeys. *Investigative Ophthalmology and Visual Science, 17*(6), 485-488. URL: https://www.ncbi.nlm.nih.gov/pubmed/566258

Reckfort, J., Wiese, H., Pietrzyk, U., Zilles, K., Amunts, K., & Axer, M. (2015). A multiscale approach for the reconstruction of the fiber architecture of the human brain based on 3D-PLI. *Frontiers in Neuroanatomy, 9*, 118. doi:10.3389/fnana.2015.00118

Rilling, J. K. (2014). Comparative primate neuroimaging: insights into human brain evolution. *Trends Cogn Sci, 18*(1), 46-55. URL: http://www.ncbi.nlm.nih.gov/pubmed/24501779

Roe, A. W., Chelazzi, L., Connor, C. E., Conway, B. R., Fujita, I., Gallant, J. L., . . . Vanduffel, W. (2012). Toward a unified theory of visual area V4. *Neuron, 74*(1), 12-29. doi:10.1016/j.neuron.2012.03.011

Rolls, E. T. (1984). Neurons in the cortex of the temporal lobe and in the amygdala of the monkey with responses selective for faces. *Human Neurobiology, 3*(4), 209-222. URL: http://www.ncbi.nlm.nih.gov/pubmed/6526707

Rust, N. C., & Dicarlo, J. J. (2010). Selectivity and tolerance ("invariance") both increase as visual information propagates from cortical area V4 to IT. *Journal of Neuroscience, 30*(39), 12978-12995. doi:10.1523/JNEUROSCI.0179-10.2010

Sato, T., Uchida, G., Lescroart, M. D., Kitazono, J., Okada, M., & Tanifuji, M. (2013). Object representation in inferior temporal cortex is organized hierarchically in a mosaic-like structure. *Journal of Neuroscience, 33*(42), 16642-16656. doi:10.1523/JNEUROSCI.5557-12.2013

Sato, T., Uchida, G., & Tanifuji, M. (2009). Cortical columnar organization is reconsidered in inferior temporal cortex. *Cerebral Cortex, 19*(8), 1870-1888. doi:10.1093/cercor/bhn218

Saxe, R., Brett, M., & Kanwisher, N. (2006). Divide and conquer: a defense of functional localizers. *Neuroimage, 30*(4), 1088-1096; discussion 1097-1089. doi:10.1016/j.neuroimage.2005.12.062

Saygin, Z. M., Osher, D. E., Koldewyn, K., Reynolds, G., Gabrieli, J. D., & Saxe, R. R. (2012). Anatomical connectivity patterns predict face selectivity in the fusiform gyrus. *Nature Neuroscience, 15*(2), 321-327. doi:10.1038/nn.3001

Saygin, Z. M., Osher, D. E., Norton, E. S., Youssoufian, D. A., Beach, S. D., Feather, J., . . . Kanwisher, N. (2016). Connectivity precedes function in the development of the visual word form area. *Nat Neurosci, 19*(9), 1250-1255. doi:10.1038/nn.4354

Schleicher, A., Morosan, P., Amunts, K., & Zilles, K. (2009). Quantitative architectural analysis: a new approach to cortical mapping. *Journal of Autism and Developmental Disorders, 39*(11), 1568-1581. doi:10.1007/s10803-009-0790-8

Schmidt, A., Diwadkar, V. A., Smieskova, R., Harrisberger, F., Lang, U. E., McGuire, P., . . . Borgwardt, S. (2014). Approaching a network connectivity-driven classification of the psychosis continuum: a selective review and suggestions for future research. *Frontiers in Human Neuroscience, 8*, 1047. doi:10.3389/fnhum.2014.01047

Schwarzlose, R. F., Baker, C. I., & Kanwisher, N. (2005). Separate face and body selectivity on the fusiform gyrus. *Journal of Neuroscience, 25*(47), 11055-11059. doi:10.1523/JNEUROSCI.2621-05.2005

Sha, L., Haxby, J. V., Abdi, H., Guntupalli, J. S., Oosterhof, N. N., Halchenko, Y. O., & Connolly, A. C. (2015). The animacy continuum in the human ventral vision pathway. *Journal of Cognitive Neuroscience, 27*(4), 665-678.

Shakeshaft, N. G., & Plomin, R. (2015). Genetic specificity of face recognition. *Proceedings of the National Academy of Sciences of the United States of America, 112*(41), 12887-12892. doi:10.1073/pnas.1421881112

Shannon, R. V. (2012). Advances in auditory prostheses. *Current Opinion in Neurology, 25*(1), 61-66. doi:10.1097/WCO.0b013e32834ef878

Siless, V., Chang, K., Fischl, B., & Yendiki, A. (2018). AnatomiCuts: Hierarchical clustering of tractography streamlines based on anatomical similarity. *Neuroimage, 166*, 32-45. doi:10.1016/j.neuroimage.2017.10.058

Silver, M. A., & Kastner, S. (2009). Topographic maps in human frontal and parietal cortex. *Trends Cogn Sci, 13*(11), 488-495. doi:10.1016/j.tics.2009.08.005
Smith, T. J. (2013). Watching you watch movies: Using eye tracking to inform film theory.
Sorg, C., Gottler, J., & Zimmer, C. (2015). Imaging Neurodegeneration: Steps Toward Brain Network-Based Pathophysiology and Its Potential for Multi-modal Imaging Diagnostics. *Clinical Neuroradiology, 25 Suppl 2*, 177-181. doi:10.1007/s00062-015-0438-3
Srihasam, K., Sullivan, K., Savage, T., & Livingstone, M. S. (2010). Noninvasive functional MRI in alert monkeys. *Neuroimage, 51*(1), 267-273. doi:10.1016/j.neuroimage.2010.01.082
Srihasam, K., Vincent, J. L., & Livingstone, M. S. (2014). Novel domain formation reveals proto-architecture in inferotemporal cortex. *Nature Neuroscience, 17*(12), 1776-1783. doi:10.1038/nn.3855
Sugita, Y. (2008). Face perception in monkeys reared with no exposure to faces. *Proceedings of the National Academy of Sciences of the United States of America, 105*(1), 394-398. doi:10.1073/pnas.0706079105
Sutherland, M. T., McHugh, M. J., Pariyadath, V., & Stein, E. A. (2012). Resting state functional connectivity in addiction: Lessons learned and a road ahead. *Neuroimage, 62*(4), 2281-2295. doi:10.1016/j.neuroimage.2012.01.117
Tanaka, K. (2003). Columns for complex visual object features in the inferotemporal cortex: clustering of cells with similar but slightly different stimulus selectivities. *Cerebral Cortex, 13*(1), 90-99. URL: https://www.ncbi.nlm.nih.gov/pubmed/12466220
Tanifuji, M., Sato, T., Uchida, G., Yamane, Y., & Tsunoda, K. (2010). How Images of Objects Are Represented in Macaque Inferotemporal Cortex. In A. W. Roe (Ed.), *Imaging the Brain with Optical Methods* (pp. 93-117): Springer New York.
Tanigawa, H., Lu, H. D., & Roe, A. W. (2010). Functional organization for color and orientation in macaque V4. *Nature Neuroscience, 13*(12), 1542-1548. doi:10.1038/nn.2676
Tatler, B. W., Hayhoe, M. M., Land, M. F., & Ballard, D. H. (2011). Eye guidance in natural vision: reinterpreting salience. *J Vis, 11*(5), 5. doi:10.1167/11.5.5
Taylor, J. C., & Downing, P. E. (2011). Division of labor between lateral and ventral extrastriate representations of faces, bodies, and objects. *Journal of Cognitive Neuroscience, 23*(12), 4122-4137. doi:10.1162/jocn_a_00091
Tisch, M. (2017). Implantable hearing devices. *GMC Current Topics in Otorhinolaryngology, Head and Neck Surgery, 16*, Doc06. doi:10.3205/cto000145
Tong, Y., Hocke, L. M., Fan, X., Janes, A. C., & Frederick, B. (2015). Can apparent resting state connectivity arise from systemic fluctuations? *Frontiers in Human Neuroscience, 9*, 285. doi:10.3389/fnhum.2015.00285
Tong, Y., Hocke, L. M., Nickerson, L. D., Licata, S. C., Lindsey, K. P., & Frederick, B. (2013). Evaluating the effects of systemic low frequency oscillations measured in the periphery on the independent component analysis results of resting state networks. *Neuroimage, 76*, 202-215. doi:10.1016/j.neuroimage.2013.03.019
Tootell, R. B., Nelissen, K., Vanduffel, W., & Orban, G. A. (2004). Search for color 'center(s)' in macaque visual cortex. *Cerebral Cortex, 14*(4), 353-363. URL: https://www.ncbi.nlm.nih.gov/pubmed/15028640
Tracy, J. I., & Doucet, G. E. (2015). Resting-state functional connectivity in epilepsy: growing relevance for clinical decision making. *Current Opinion in Neurology, 28*(2), 158-165. doi:10.1097/WCO.0000000000000178
Trampel, R., Bazin, P.-L., Pine, K., & Weiskopf, N. (2017). In-vivo magnetic resonance imaging (MRI) of laminae in the human cortex. *Neuroimage*. doi:10.1016/j.neuroimage.2017.09.037
Tsao, D. Y., Freiwald, W. A., Tootell, R. B., & Livingstone, M. S. (2006). A cortical region consisting entirely of face-selective cells. *Science, 311*(5761), 670-674. doi:10.1126/science.1119983
Tsao, D. Y., Moeller, S., & Freiwald, W. A. (2008). Comparing face patch systems in macaques and humans. *Proceedings of the National Academy of Sciences of the United States of America, 105*(49), 19514-19519. doi:10.1073/pnas.0809662105
Tukey, J. (1977). Exploratory data analysis., Bd. 7616 von Behavioral Science: Quantitative Methods: Addison-Wesley.

Tyler, L. K., Stamatakis, E. A., Bright, P., Acres, K., Abdallah, S., Rodd, J. M., & Moss, H. E. (2004). Processing objects at different levels of specificity. *Journal of Cognitive Neuroscience, 16*(3), 351-362. doi:10.1162/089892904322926692

Van Essen, D. C. (2004). Organization of visual areas in macaque and human cerebral cortex. *The visual neurosciences, 1*, 507-521.

Van Essen, D. C. (2005). Surface-based comparisons of macaque and human cortical organization. *From monkey brain to human brain*, 3-19.

Van Essen, D. C., & Dierker, D. L. (2007). Surface-based and probabilistic atlases of primate cerebral cortex. *Neuron, 56*(2), 209-225. doi:10.1016/j.neuron.2007.10.015

Vul, E., Lashkari, D., Hsieh, P. J., Golland, P., & Kanwisher, N. (2012). Data-driven functional clustering reveals dominance of face, place, and body selectivity in the ventral visual pathway. *Journal of Neurophysiology, 108*(8), 2306-2322. doi:10.1152/jn.00354.2011

Wandell, B. A., Brewer, A. A., & Dougherty, R. F. (2005). Visual field map clusters in human cortex. *Philosophical Transactions of the Royal Society of London. Series B: Biological Sciences, 360*(1456), 693-707. doi:10.1098/rstb.2005.1628

Wandell, B. A., Dumoulin, S. O., & Brewer, A. A. (2007). Visual field maps in human cortex. *Neuron, 56*(2), 366-383. doi:10.1016/j.neuron.2007.10.012

Wandell, B. A., Dumoulin, S. O., & Brewer, A. A. (2009). Visual Cortex in Humans. In L. R. Squire (Ed.), *Encyclopedia of Neuroscience* (pp. 251-257). Oxford: Academic Press.

Wang, D., Buckner, R. L., Fox, M. D., Holt, D. J., Holmes, A. J., Stoecklein, S., . . . Liu, H. (2015). Parcellating cortical functional networks in individuals. *Nature Neuroscience, 18*(12), 1853-1860. doi:10.1038/nn.4164

Wang, G., Tanaka, K., & Tanifuji, M. (1996). Optical imaging of functional organization in the monkey inferotemporal cortex. *Science, 272*(5268), 1665-1668. URL: http://www.ncbi.nlm.nih.gov/pubmed/8658144

Weiner, K. S., Barnett, M. A., Lorenz, S., Caspers, J., Stigliani, A., Amunts, K., . . . Grill-Spector, K. (2017). The Cytoarchitecture of Domain-specific Regions in Human High-level Visual Cortex. *Cerebral Cortex, 27*(1), 146-161. doi:10.1093/cercor/bhw361

Weiner, K. S., Golarai, G., Caspers, J., Chuapoco, M. R., Mohlberg, H., Zilles, K., . . . Grill-Spector, K. (2014). The mid-fusiform sulcus: a landmark identifying both cytoarchitectonic and functional divisions of human ventral temporal cortex. *Neuroimage, 84*, 453-465. doi:10.1016/j.neuroimage.2013.08.068

Weiner, K. S., & Grill-Spector, K. (2011). Not one extrastriate body area: using anatomical landmarks, hMT+, and visual field maps to parcellate limb-selective activations in human lateral occipitotemporal cortex. *Neuroimage, 56*(4), 2183-2199. doi:10.1016/j.neuroimage.2011.03.041

Weiner, K. S., & Grill-Spector, K. (2013). Neural representations of faces and limbs neighbor in human high-level visual cortex: evidence for a new organization principle. *Psychological Research, 77*(1), 74-97. doi:10.1007/s00426-011-0392-x

Weiner, K. S., & Zilles, K. (2015). The anatomical and functional specialization of the fusiform gyrus. *Neuropsychologia*. doi:10.1016/j.neuropsychologia.2015.06.033

Wiesel, T. N., & Hubel, D. H. (1963). Single-Cell Responses in Striate Cortex of Kittens Deprived of Vision in One Eye. *Journal of Neurophysiology, 26*, 1003-1017. doi:10.1152/jn.1963.26.6.1003

Wiesel, T. N., & Hubel, D. H. (1965). Comparison of the effects of unilateral and bilateral eye closure on cortical unit responses in kittens. *Journal of Neurophysiology, 28*(6), 1029-1040. doi:10.1152/jn.1965.28.6.1029

Wig, G. S., Laumann, T. O., Cohen, A. L., Power, J. D., Nelson, S. M., Glasser, M. F., . . . Petersen, S. E. (2014). Parcellating an individual subject's cortical and subcortical brain structures using snowball sampling of resting-state correlations. *Cerebral Cortex, 24*(8), 2036-2054. doi:10.1093/cercor/bht056

Wilmer, J. B., Germine, L., Chabris, C. F., Chatterjee, G., Williams, M., Loken, E., . . . Duchaine, B. (2010). Human face recognition ability is specific and highly heritable. *Proceedings of the National Academy of Sciences of the United States of America, 107*(11), 5238-5241. doi:10.1073/pnas.0913053107

Wittenberg, G. F. (2010). Experience, cortical remapping, and recovery in brain disease. *Neurobiology of Disease, 37*(2), 252-258. doi:10.1016/j.nbd.2009.09.007

Workman, A. D., Charvet, C. J., Clancy, B., Darlington, R. B., & Finlay, B. L. (2013). Modeling transformations of neurodevelopmental sequences across mammalian species. *Journal of Neuroscience, 33*(17), 7368-7383. doi:10.1523/JNEUROSCI.5746-12.2013

Yamins, D. L., & DiCarlo, J. J. (2016a). Eight open questions in the computational modeling of higher sensory cortex. *Current Opinion in Neurobiology, 37*, 114-120. doi:10.1016/j.conb.2016.02.001

Yamins, D. L., & DiCarlo, J. J. (2016b). Using goal-driven deep learning models to understand sensory cortex. *Nature Neuroscience, 19*(3), 356-365. doi:10.1038/nn.4244

Yendiki, A., Panneck, P., Srinivasan, P., Stevens, A., Zollei, L., Augustinack, J., . . . Fischl, B. (2011). Automated probabilistic reconstruction of white-matter pathways in health and disease using an atlas of the underlying anatomy. *Frontiers in Neuroinformatics, 5*, 23. doi:10.3389/fninf.2011.00023

Yeo, B. T., Krienen, F. M., Sepulcre, J., Sabuncu, M. R., Lashkari, D., Hollinshead, M., . . . Buckner, R. L. (2011). The organization of the human cerebral cortex estimated by intrinsic functional connectivity. *Journal of Neurophysiology, 106*(3), 1125-1165. doi:10.1152/jn.00338.2011

Yoon, K. J., Vissers, C., Ming, G. L., & Song, H. (2018). Epigenetics and epitranscriptomics in temporal patterning of cortical neural progenitor competence. *Journal of Cell Biology*. doi:10.1083/jcb.201802117

Zalesky, A., Fornito, A., Harding, I. H., Cocchi, L., Yucel, M., Pantelis, C., & Bullmore, E. T. (2010). Whole-brain anatomical networks: does the choice of nodes matter? *Neuroimage, 50*(3), 970-983. doi:10.1016/j.neuroimage.2009.12.027

Zeiler, M. D., & Fergus, R. (2013). Visualizing and Understanding Convolutional Networks. *arXiv preprint arXiv:1311.2901*.

Zeki, S. (1980). The representation of colours in the cerebral cortex. *Nature, 284*(5755), 412-418. URL: https://www.ncbi.nlm.nih.gov/pubmed/6767195

Zeki, S. M. (1978). Functional specialisation in the visual cortex of the rhesus monkey. *Nature, 274*(5670), 423-428. URL: https://www.ncbi.nlm.nih.gov/pubmed/97565

Zilles, K., & Amunts, K. (2009). Receptor mapping: architecture of the human cerebral cortex. *Current Opinion in Neurology, 22*(4), 331-339. doi:10.1097/WCO.0b013e32832d95db

Zilles, K., & Amunts, K. (2010). Centenary of Brodmann's map--conception and fate. *Nature Reviews: Neuroscience, 11*(2), 139-145. doi:10.1038/nrn2776

Zilles, K., & Palomero-Gallagher, N. (2017). Multiple Transmitter Receptors in Regions and Layers of the Human Cerebral Cortex. *Frontiers in Neuroanatomy, 11*, 78. doi:10.3389/fnana.2017.00078

Zilles, K., Palomero-Gallagher, N., & Schleicher, A. (2004). Transmitter receptors and functional anatomy of the cerebral cortex. *Journal of Anatomy, 205*(6), 417-432. doi:10.1111/j.0021-8782.2004.00357.x

Zola-Morgan, S. (1995). Localization of brain function: the legacy of Franz Joseph Gall (1758-1828). *Annual Review of Neuroscience, 18*, 359-383. doi:10.1146/annurev.ne.18.030195.002043